Creation of Novel Gold-Nanorod-Based Localized Surface Plasmon Resonance Biosensors

A thesis submitted

by

Jie Cao

for the degree of

Doctor of Philosophy

at

City University London

School of Engineering and Mathematical Sciences

September 2013

Table of Contents

List of Figures

List of Tables

Acknowledgements

Foremost, I would like to express my sincere gratitude to my supervisors Prof. Tong Sun and Prof. Kenneth T. V. Grattan for their continuous support of my Ph.D study. Without their patient guidance, enormous encouragement, insightful comments, immense knowledge and persistent help throughout the period of my Ph.D study, this dissertation would not have been possible. No words can express my appreciation to them. I'm very lucky to have two great professors to be my Ph. D supervisors at the same time.

I also would like to give my sincere gratitude to my supervisor at Harbin Institute of Technology – Prof. Jie Zhao. I would not be able to have the opportunity to study abroad without his recommendation. His hard working attitude has been always inspiring me to keep moving forward.

My special thanks go to Dr. Ewan K. Galbraith, who gave me tremendous help for my Ph.D research. Whenever I needed a favour, he was always willing to offer any help he could. Sincerely thank you for the advice, discussions, encouragement, comments and all the support you gave to me.

To my fellow group mates in Optical Fibre Sensor Research Group: Lourdes Shanika Alwis, Shuying Chen, Dr. V.T. Venu, Dr. Weizhong Zhao, Dr. Fredderic Surre, Jacques Oliver, Minh Hieu Tu, Dr. Matthias Fabian, Bochao Zhou and Shuo Yang, thank you all for the support, encouragement, suggestions, lovely chats and the precious memories we shared together.

To my parents, thank you for your infinite love and endless support and encouragement you have been giving to me since you brought me into this world. You are the best parents who make me the luckiest child in the world. I hope I could always make you proud. This dissertation is for you – my dearest father, Yongxin Cao, and my dearest mother, Xiuqin Xu.

Finally, I would like to express deepest appreciation and love to my lovely wife Di Wu, who has been wholeheartedly supporting me in my life, who has been always trying to cheer me up and make me happy whenever I feel sad, who has been suffering the loneliness without any complaints, and who has been waiting for me for these years. Thank you for all the sacrifices you made for me. I would not go this far without you.

Copyright Declaration

Abstract

Starting with a comprehensive review of both surface plasmon resonance (SPR) based and localized surface plasmon resonance (LSPR) based sensors, this thesis reports the studies on the development of a novel sensitive gold nanorod (GNR) based label-free LSPR optical fibre biosensor, and the development of a novel robust method for effectively modifying the surface of cetyl-trimethyl ammonium bromide (CTAB) capped GNRs and their LSPR biosensing applications.

A novel GNR-based LSPR optical fibre sensor was fabricated and evaluated in this work. The sensor probe was prepared by covalently immobilizing GNRs, synthesized using a seed-mediated growth method, on the decladed surface of a piece of multimode optical fibre. In order to operate the LSPR sensor as a reflective sensor, a silver mirror was also coated at one distal end of the sensor probe by a dip coating method. In the refractive index sensitivity test, it was found that the longitudinal plasmon band (LPB) of GNRs is highly sensitive to the refractive index change close to the GNRs surface, and the sensitivity of the LSPR optical fibre sensor increases with the increase of the aspect ratio of GNRs. The results showed that the GNR-based LSPR optical fibre sensors prepared in this work have linear and high refract index sensitivities. For sensors based on GNRs with aspect ratios of 2.6, 3.1, 3.7 and 4.3, their refractive index sensitivities were found to be 269, 401, 506 and 766 nm/RIU (RIU = refractive index unit), respectively, in the refractive index range from 1.34 to 1.41. In order to evaluate the biosensing performance, the GNR-based LSPR optical fibre sensor with aspect ratio of 4.1 and a 2 cm sensing length was further functionalized with human IgG to detect the specific target — anti-human IgG, and a detection limit of 1.6 nM was observed using a wavelength-based interrogation approach.

In another study, in order to overcome the drawbacks of the CTAB-capped GNRs found in biosensing and biomedical applications, a simple yet robust pH-mediated method for effectively modifying the surface of CTAB-capped GNRs synthesized by the seed-mediated growth method was developed. This method allows the complete replacement of the CTAB molecules attached on the GNRs surface with the 11-mercaptoundecaonic acid (MUA) molecules to take place in a total aqueous environment by controlling the pH of the MUA aqueous solution, thus avoiding the irreversible aggregation of GNRs during the complex surface modification process observed in the previous reported methods. The success of the complete replacement of CTAB with MUA was confirmed by the surface elemental analysis using an X-ray photoelectron spectroscopy (XPS), and the MUA-modified GNRs created in this work demonstrated a high stability up to 4 months at least when stored in a buffer solution at pH 9 at 4°C. The MUA-modified GNRs with an aspect ratio of 3.9 were furthered developed as a solution-phase-based label-free LSPR biosensor by functionalizing the GNRs with human IgG. A detection limit as low as 0.4 nM for detecting anti-human IgG was achieved by this sensor.

The achievements of this work are concluded and the directions of future work are also pointed out.

Abbreviations and Symbols

ATR	Attenuated Total Reflection
AR	Aspect Ratio
EW	Evanescent Wave
EBL	Electron Beam Lithography
FBG	Fibre Bragg Grating
GNP	Gold Nanoparticle
GNR	Gold Nanorod
GNS	Gold Nanosphere
LBL	Layer-By-Layer
LOD	Limit of Detection
LPG	Long Period Fibre Grating
LPB	Longitudinal Plasmon Band
LSPR	Localized Surface Plasmon Resonance
MNP	Metallic Nanoparticle
SAM	Self-Assembled Monolayer
SERS	Surface-Enhanced Raman Scattering
SNR	Signal to Noise Ratio
SP	Surface Plasmon
SPR	Surface Plasmon Resonance
SPW	Surface Plasmon Wave
TEM	Transmission Electron Microscope
TIR	Total Internal Reflection
TPB	Transverse Plasmon Band
XPS	X-ray Photoelectron Spectroscopy

APTES	3-Aminopropyltriethoxysilane
BDAC	Benzyldimethylhexadecylammonium Chloride
BaP	Benzo[a]Pyrene
BSA	Bovine serum albumin
CTAB	Cetyl-trimethyl ammonium bromide
DA	Domoic Acid
DI	De-ionized
DNA	Deoxyribonucleic acid
EDC	N-(3-Dimethylaminopropyl)-N′-ethylcarbodiimide hydrochloride
hA	Human Albumin
hCG	Pregnancyshuman Chorionic Gonadotropin
hHBV	Human Hepatitis B Virus
ITO	Indium Tin Oxide
M3G	Morphine-3-Glucuronide
MC-LR	Microcystin-LR
MPTMS	3-Mercaptopropyl trimethoxysilane
MPTES	3-Mercaptopropyl triethoxysilane
MUA	11-Mercaptoundecaonic acid
PAA	Poly(acrylic acid)
PDADMAC	Poly(diallyldimethylammonium chloride)
PEG	Polyethyleneglycol
PMMA	poly(methyl methacrylate)
PSS	Poly(sodium-4-styrenesulfonate)
PSA	Prostate-Specific Antigen
PVP	Polyvinylpyrrolindone
RSV	Respiratory Syncytial Virus

Sulfo-NHS	*N*-hydroxysulfosuccinimide
TCAB	Tetradodecylammonium Bromide
TEOS	Tetraethoxysilane
TNT	2,4,6-trinitrotoluene

c	Speed of light in vacuum
ω	Frequency of light
θ	Incident angle of incident light
λ	Wavelength of light
ε_d	Dielectric constant of dielectric medium
ε_m	Dielectric constant of metal
ε_p	Dielectric constant of prism
ε_r	Real part of the dielectric function of MNP
ε_i	Imaginary part of the dielectric function of MNP
e	Ellipticity
m	Sensitivity factor
N	Electron density
P_j	Depolarization factor
R	Radius of spherical nanoparticle
V	Volume of the particle
k_D	Propagation constant of light in vacuum
k_{EV}	Propagation constant of EW
k_P	Propagation constant of light in prism
k_{SP}	Propagation constant of SPW
S_{RI}	Refractive index sensitivity
$Cext$	Extinction cross-section
ΔY	Change of parameter of SPR sensor
Δn	Change of refractive index
$\Delta\lambda$	LSPR wavelength shift

Au	Gold
Ag	Silver
Br	Bromine
S	Sulphur
Si	Silicon
Pt	Platinum

Chapter 1

Introduction

1.1 Background

As an essential and powerful tool, biosensor has been playing an important role in applications closely related to our lives, such as biochemical research, new medicine development, disease diagnosis and illicit drug detection [1]. Traditional biosensors normally require bulk and expensive instruments, large sample volume, time-consuming detection and laboratory environment. Therefore, there has been a significant demand from the related industry for the development of more advanced biosensors with preferable properties including high sensitivity, fast response, small sample volume requirement, robustness, miniaturization and cost-effectiveness. It is, however, difficult to find an ideal and unique sensing solution to enable such a biosensor to possess all of the above desirable properties, but the advancement in the research in nanotechnology has made it a step closer.

Among various bio-sensing technologies, both surface plasmon resonance (SPR) and localized surface plasmon resonance (LSPR) sensing technologies have been widely explored and reported due to their attractive features such as high sensitivity, label-free detection, fast response and real-time monitoring [2, 3]. SPR is known as a phenomenon that surface conductive electrons oscillate collectively with resonant frequency and propagate with along the metal-dielectric interface [2]. SPR effect normally can be generated at the metal-dielectric interface by evanescent wave. Due to its ultra-high sensitivity to surrounding refractive index change even caused by biomolecular interaction for example as well as other advantages mentioned above, SPR as an advanced and powerful bio-sensing technology has already been applied in many commercial instruments such as the Biacore^{TM}.

The conventional SPR sensors are normally fabricated based on the Kretschmann configuration [4], in which a very thin layer (~ 50 nm) of noble metal film such as gold and silver is coated on the bottom of a glass prism. The evanescent wave induced by the incident light at the prism-metal interface will excite the SPR effect at the metal-dielectric interface to detect any refractive index change close to the metal surface. However, the disadvantages of the prism based SPR sensors are that, the fabrication of the SPR sensors normally involves bulk and expensive components, and a laboratory environment is required for conducting an experiment, all of which limit the prism based SPR sensor to be widely applied.

LSPR, on the other hand, is an optical phenomenon that, when incident light interacts with metallic nanoparticles, the electric field of light can excite the conduction electrons in the metallic nanoparticles to oscillate collectively with a resonant frequency [5]. The properties of LSPR are strongly dependent on the nanoparticles' size, shape and composition as well as the local dielectric environment surrounding nanoparticles [5], therefore their characteristics can be tailored or controlled through the variation of these key parameters. Similar to the SPR-based sensors, LSPR-based sensors are also highly sensitive to the local refractive index change near the surface of nanoparticles coated on the dielectric material, e.g. optical fibres, therefore they are in particular suitable for high sensitive measurements. So far various types of LSPR-based biochemical sensors have been reported with promising results. Compared to the SPR sensors, although SPR sensors provide much higher sensitivity to the change in the bulk refractive index, it was reported that LSPR sensors can offer a comparable sensitivity when measuring a short range change in refractive index caused by the molecular adsorption for instance [6]. Some single-nanoparticle based LSPR sensors have been found to possess higher sensitivities than those of array-nanoparticle based LSPR sensors [7, 8].

The fabrication of the LSPR sensors usually involves the use of noble metal nanoparticles. The metallic nanoparticles are either immobilized on the dielectric material substrate such as glass slide, or suspended in the solution such as water. Gold, among the noble metals, is normally preferable to most of biological applications due to its good biocompatibility and the strong thiol-gold covalent bond for biomolecules immobilization [9]. In addition, the size and shape of nanoparticles influence strongly the LSPR properties, thus LSPR sensors based on the gold nanoparticles (GNPs) with various geometries, such as sphere, rod, cube and pyramid, show significant differences in their corresponding absorption spectra and sensitivities [10], which also offers flexibility when designing LSPR sensors for particular applications. Among these GNPs, gold nanorod (GNR), due to its unique shape and optical

properties that the plasmon band of GNR is tunable with its aspect ratio, has shown potential in the LSPR sensor field and has attracted more and more attention. It was reported that the GNR based LSPR sensor possesses a higher sensitivity compared to the LSPR sensors based on conventionally used spherical GNPs with similar structures [10, 11].

These biosensors become more advantageous when they are integrated into optical fibres. Fibre-optic based sensor devices have shown advantages such as small sample volume requirement, a miniaturized and simplified optical design, immunity to electromagnetic interference and capability for remote sensing. Thus, the optical fibre sensors have been widely applied in many areas such as medical instruments, aerospace, distributed sensing, civil engineering and mine safety monitoring [12]. Combing the advantages of both LSPR sensing technique and optical fibre sensor, LSPR based optical fibre biosensors offer a promising solution to overcome the limitations arising from conventional biosensors discussed above. In 2003, Cheng and Chau reported a LSPR optical fibre biochemical sensor based on self-assembled colloidal GNPs [13]. The simplicity of their sensor system and promising sensitivity of the sensor attracted many attentions. Since then tremendous effort has been made in the field with an aim to develop novel LSPR based optical fibre biosensors.

1.2 Aims and objectives of this work

Compared to the commonly used spherical GNPs, research in developing gold nanorods (GNRs) based LSPR sensors just started recently. Most of the reported optical fibre based LSPR sensors are based on the gold nanoshperes (GNSs) [14, 15]. Despite a few GNRs based LSPR sensor with other constructions have been reported [16, 17], there was limited report on the development of GNR based LSPR optical fibre sensors, which forms the focus of this research reported in this thesis, with an aim to ‘fill in the gaps’ identified. In addition, GNRs used in the fabrication of LSPR sensors are normally synthesized by a seed-mediated chemical method in the presence of cetyltrimethylammoniumbromide (CTAB) surfactant [18], which results in the formation of a dense bilayer of CTAB molecules working as a stabilizer on the surface of GNRs. The main drawback of this technique is that the CTAB bilayer blocks either large biomolecules or functional linkers from approaching the GNRs surface to functionalize GNRs for immunosensing, therefore it affects the overall performance of the LSPR sensors either based on optical fibre or on other substrates.

In light of the above, this work mainly aims to develop a novel and highly sensitive GNRs based LSPR optical fibre sensor for the biosensing applications, and to find a method which can effectively modify the surface of CTAB-capped GNRs in order to improve the performance of GNRs based LSPR sensors.

The major objectives of the work reported in this thesis are:

- To conduct a thorough literature review on the work associated with both SPR and LSPR based sensors, as a background to this research.
- To synthesize GNRs with various aspect ratios prior to the fabrication of GNRs based LSPR optical fibre sensor probes, and to establish a sensor system for further evaluation and calibration.
- To carry out a series of experiments to observe the response of the LSPR optical fibre sensors based on GNRs with various aspect ratios to bulk refractive index change, and make a comparison with the sensors' sensitivities in order to find out the relationship between the aspect ratio of GNRs and the sensitivities of their corresponding LSPR sensors created to refractive index change.
- To functionalise the GNRs based LSPR optical fibre sensor probe in order to make it a biosensor, and carry out experiments to evaluate its performance of being a label-free immunobiosensor.
- To develop an effective surface modification method to modify the surface of CTAB-capped GNRs in order to improve the performance of GNRs based LSPR sensors.
- To summarize the achievements made throughout the project period and outline the directions of future research.
- To report widely the research outcomes obtained at various stages through various means, including peer-reviewed international journal publications and presented at international conferences.

1.3 Structure of the thesis

The thesis is structured encompassing six chapters describing the comprehensive work carried out to achieve the aims and objectives set out above.

Chapter 1 begins with a brief background in relation to both SPR and LSPR based biosensors. After analysing the current issues in the reported LSPR sensors, the aims and objectives of this work are proposed, followed by the structure of the thesis which outlines the whole work carried out.

Chapter 2 focuses on the review of existing technologies surrounding both SPR and LSPR sensors. Firstly, it explains the sensing principle of SPR, followed by an introduction to the configuration and characteristics of the typical SPR sensors and their applications. Secondly, *Chapter 2* also explains the sensing principle of LSPR, and introduces the optical properties and synthesis of GNPs, particularly the GNRs. The characteristics of LSPR sensors based on different configurations are described together with their associated applications. Finally, available surface modification methods for GNRs are introduced and discussed.

Chapter 3 introduces the details of the fabrication of the GNRs based LSPR optical fibre sensors, including the synthesis of GNRs with various aspect ratios via a seed-mediated method, the preparation of multimode optical fibres as a sensor substrate, and the immobilization of GNRs on the unclad surface of optical fibres. The experimental set-up consisting of different instruments is also included in the discussions. In addition, a study on the refractive index sensitivity of the LSPR sensors based on GNRs with different aspect ratios has been carried out and the results have been compared and discussed.

Chapter 4 describes the performance of the LSPR optical fibre sensors prepared in Chapter 3 in the biosensing applications when working as a label-free immunobiosensor. The as-prepared LSPR sensor probe was further functionalized with human IgG before being extensively evaluated through a series of experiments for detecting the anti-human IgG at different concentrations. The results regarding the detection limit and sensitivity were analysed and discussed.

Chapter 5 reports a novel method to modify effectively the surface of CTAB-capped GNRs prior to the fabrication of LSPR biosensors. The detailed procedure with regard to this method was described, and the characteristics of the GNRs before and after the surface modification were compared. A study on evaluating the performance of the surface modified GNRs of being a solution-phase-based LSPR biosensor was also carried out in this chapter.

Chapter 6 concludes the whole work carried out with the results obtained from this research, summarizing the achievements made in relation to the aims and objectives identified in Chapter 1. Suggestions for future work are also included, with an aim to achieve better sensor performance and widen the scope of the research.

1.4 Summary

In this chapter, a brief background related to the work contained in the thesis has been introduced. Additionally, the aims and objectives of the work have been proposed, and the structure of the thesis as an outline of the whole work carried out has also been described in this chapter.

1.5 References

[1] J. Homola, Present and future of surface plasmon resonance biosensors, Analytical And Bioanalytical Chemistry, 377 (2003) 528-539.

[2] J. Homola, S.S. Yee, G. Gauglitz, Surface plasmon resonance sensors: review, Sensors And Actuators B-Chemical, 54 (1999) 3-15.

[3] J.N. Anker, W.P. Hall, O. Lyandres, N.C. Shah, J. Zhao, R.P. Van Duyne, Biosensing with plasmonic nanosensors, Nature Materials, 7 (2008) 442-453.

[4] E. Kretschm, H. Raether, Radiative decay of non radiative surface plasmons excited by light, Zeitschrift Fur Naturforschung Part A-astrophysik Ahysik Und Physikalische Chemie, A 23 (1968) 2135-2136.

[5] K.A. Willets, R.P. Van Duyne, Localized surface plasmon resonance spectroscopy and sensing, Annual Review Of Physical Chemistry, 58 (2007), 267-297.

[6] A.J. Haes, R.P. Van Duyne, A unified view of propagating and localized surface plasmon resonance biosensors, Analytical And Bioanalytical Chemistry, 379 (2004) 920-930.

[7] A.D. McFarland, R.P. Van Duyne, Single silver nanoparticles as real-time optical sensors with zeptomole sensitivity, Nano Letters, 3 (2003) 1057-1062.

[8] G. Raschke, S. Kowarik, T. Franzl, C. Sonnichsen, T.A. Klar, J. Feldmann, A. Nichtl, K. Kurzinger, Biomolecular recognition based on single gold nanoparticle light scattering, Nano Letters, 3 (2003) 935-938.

[9] X.M. Lu, M. Rycenga, S.E. Skrabalak, B. Wiley, Y.N. Xia, Chemical synthesis of novel plasmonic nanoparticles, Annual Review Of Physical Chemistry, 60 (2009)167-192.

[10] H.J. Chen, X.S. Kou, Z. Yang, W.H. Ni, J.F. Wang, Shape- and size-dependent refractive index sensitivity of gold nanoparticles, Langmuir : The ACS Journal Of Surfaces And Colloids, 24 (2008) 5233-5237.

[11] J. Cao, E.K. Galbraith, T. Sun, K.T.V. Grattan, Cross-comparison of surface plasmon resonance-based optical fiber sensors with different coating structures, IEEE Sensors Journal, 12 (2012) 2355-2361.

[12] K.T.V. Grattan, B.T. Meggitt, Optical fiber sensor technology, Chapman & Hall, London, (1995).

[13] S.F. Cheng, L.K. Chau, Colloidal gold-modified optical fiber for chemical and biochemical sensing, Analytical Chemistry, 75 (2003) 16-21.

[14] J.L. Tang, S.F. Cheng, W.T. Hsu, T.Y. Chiang, L.K. Chau, Fiber-optic biochemical sensing with a colloidal gold-modified long period fiber grating, Sensors And Actuators B-Chemical, 119 (2006) 105-109.

[15] V.V.R. Sai, T. Kundu, S. Mukherji, Novel U-bent fiber optic probe for localized surface plasmon resonance based biosensor, Biosensors & Bioelectronics, 24 (2009) 2804-2809.

[16] S.M. Marinakos, S. Chen, A. Chilkoti, Plasmonic detection of a model analyte in serum by a gold nanorod sensor, Analytical Chemistry, 79 (2007) 5278-5283.

[17] C. Wang, J. Irudayaraj, Gold nanorod probes for the detection of multiple pathogens, Small, 4 (2008) 2204-2208.

[18] B. Nikoobakht, M.A. El-Sayed, Preparation and growth mechanism of gold nanorods (NRs) using seed-mediated growth method, Chemstry Of Materials, 15 (2003) 1957-1962.

Chapter 2

Background and review of surface plasmon resonance (SPR) and localized surface plasmon resonance (LSPR) based sensors

2.1 Introduction

Since the first application of surface plasmon resonance (SPR) sensor reported three decades ago, a considerable amount of studies on the development of SPR based sensors for various applications, in particular for biochemical and biological sensing applications, has been carried out. The importance of SPR sensing technology on the biochemistry study as well as other fields has been widely recognized. Instrumentations based on SPR sensing technology have been successfully developed and commercialized and SPR biosensors have become a powerful tool for analysing the biomolecular interactions. On the other hand, the localized surface plasmon resonance (LSPR) sensing technology, as a newly developed biosensing technique compared to SPR, has attracted more and more attentions in recent years. Not only have the LSPR sensors demonstrated a comparable performance on biosensing applications compared to SPR sensors, but also LSPR technology has extended the application scope of SPR, for instance, to the application of LSPR in surface-enhanced Raman scattering (SERS). Although the majority of the work contained in this thesis is based on the LSPR technology, it is also important to understand the differences and similarities between SPR and LSPR, in order to develop a sensor with an optimal design and performance. Therefore, this chapter reviews the major development of both SPR and LSPR technologies, including their sensing principles, sensor configuration and typical applications, especially the biosensing applications.

2.2 Background and development of SPR sensor

2.2.1 Introduction to SPR

The physical phenomenon of SPR was first described in 1902 by Wood [1, 2], who observed a pattern of "anomalous" diffraction in the reflected light when the polarized light was shone on a mirror with a diffraction grating on its surface. After that, many scientists had been trying to explain this intriguing phenomenon for decades, but a comprehensive explanation of SPR could not be given until 1968 when Otto [3] and, in the same year, Kretschmann and Raether [4] reported the excitation of the surface plasmons by the method of attenuated total reflection (ATR) based on a similar prism coupling configuration respectively. The potential use of SPR for sensing purposes started to be recognized in late seventies [5, 6]. And in 1983, the application of SPR based sensor for monitoring the biomolecular interaction was first demonstrated by Liedberg *et al* [7]. By employing the SPR sensing technique, they were able to realize the direct and real-time detection of the biomolecular interaction even without labelling molecules, the technique which was normally used in the traditional techniques. Since then, SPR sensing technology has been drawing a great attention and continuously being developed. In 1990, Pharmacia Biosensor AB launched the first commercial SPR biosensor based on the Kretschmann configuration – the Biacore instrument [8]. The success of Biacore SPR products has attracted many other companies devoting to the development of commercial SPR instruments with their own features. To date, a great deal of work has been done in terms of the development of new SPR based instruments and modification of the SPR sensor designs for various purposes, especially for label-free, real-time biosensing. SPR technology, as a leading sensing technology, has been playing a prominent role in the fields of physical, chemical and biological studies.

2.2.2 SPR theory

Surface plasmon (SP) is a collective electrons oscillation existing at the metal-dielectric interface. The physical phenomenon that surface plasmon wave (SPW) propagating along the metal-dielectric interface is known as surface plasmon resonance (SPR) [9]. SPR can be excited by incident light when the frequency of light photons matches the natural frequency of surface electrons that induces the electrons oscillation with a resonant frequency. By solving Maxwell's equation, it can be found that the SPW is a TM-polarized or p-polarized

electromagnetic wave, the field intensity of which is maximum at the metal-dielectric interface and decays exponentially into both metal and dielectric media as shown in Fig. 2.1.

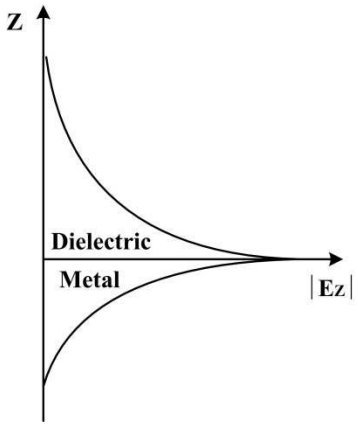

Fig. 2.1. Field intensity of SPW decays exponentially into metal and dielectric media.

According to Maxwell's theory, SPW can propagate along the metal-dielectric interface with propagation constant (k_{SP}) which is given by the following expression:

$$k_{SP} = \frac{\omega}{c}\sqrt{\frac{\varepsilon_m \varepsilon_d}{\varepsilon_m + \varepsilon_d}} \tag{2.1}$$

where ω represents the frequency of the incident light, and c is the speed of light in vacuum; ε_m and ε_d represent the dielectric constant of metal layer and dielectric medium, respectively. It can be concluded from the above equation that the properties of SPW are highly dependent on the both metal and dielectric media. When light travels through the dielectric medium ε_d at frequency ω, the propagation constant of light k_D is given by:

$$k_D = \frac{\omega}{c}\sqrt{\varepsilon_d} \tag{2.2}$$

The dispersion relation for SPW is shown in Fig. 2.2. As shown in Fig. 2.2, the dispersion relation of SPW never intersects with that of light travelling in dielectric medium ε_d (for instance in air), which indicates that the incident light cannot directly excite SPR at the metal-dielectric interface. Therefore, in order to excite SPR, the momentum of incident light in dielectric medium has to be enhanced to match that of SPW.

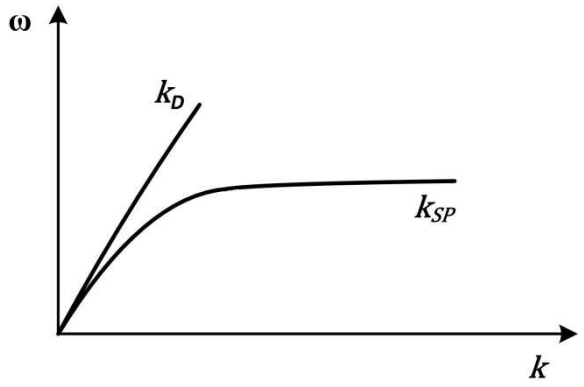

Fig. 2.2. Dispersion relation for SPW (k_{SP}) and light in dielectric medium (k_D). ω and k represent frequency and propagation constant respectively [10].

2.2.3 Excitation of SPR

2.2.3.1 Otto configuration

In 1968, Otto first reported an ATR method to excite SPR by coupling evanescent wave (EW) with SPW at the metal-dielectric interface via a prism based configuration, which is known as the Otto configuration, as shown in Fig. 2.3. The idea behind this configuration is that, since the EW is also an electromagnetic wave with intensity decaying exponentially into the media, the properties of which are similar to those of SPW, there is a strong possibility that SPR could be excited by coupling EW with SPW. As illustrated in Fig. 2.3, a glass prism is used to generate the EW which is formed at the boundary of two media with different refractive indexes due to the total internal reflection (TIR). A metal surface is brought to the bottom of the prism with a very small gap (~200 nm) between them. When the incident angle of a p-polarized incident light launched into the prism is equal to or greater than the critical angle, the phenomenon of TIR occurs, which results in the generation of EW at the prism-air interface. The exponentially decaying evanescent filed then penetrates into the metal close to the prism base to couple with SPW, which excites the SPR at the metal-air interface. As there is a loss of intensity in reflected light due to the energy transfer, this technique that using EW generated by TIR to couple with SPW is called attenuated total reflection (ATR) [2].

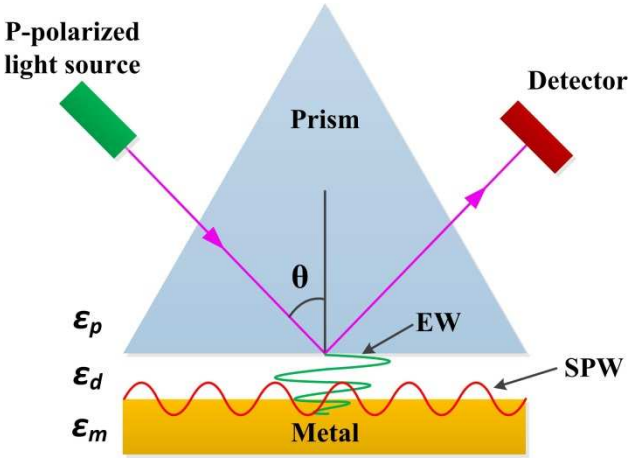

Fig. 2.3. Schematic diagram of Otto configuration.

The propagation constant of EW at the prism-air interface is given by:

$$k_{EV} = \frac{\omega}{c}\sqrt{\varepsilon_p}\sin\theta = k_P \sin\theta \tag{2.3}$$

where ε_p and ε_d represent the dielectric constant of prism and dielectric medium (air in this case), and $\varepsilon_p > \varepsilon_d$. θ represents the incident angle of incident light, k_P represents the propagation constant of light in prism. By adjusting the incident angle, the SPR will be excited when:

$$k_{EV} = k_{SP} \tag{2.4}$$

However, the main disadvantage of the Otto configuration is that, in order to enable the evanescent field to penetrate into the metal layer, the metal layer has to be brought very close to the base of prism, which makes the Otto configuration difficult to be applied in practical applications. Therefore, the Otto configuration has not been widely employed in SPR sensing.

2.2.3.2 Kretschmann Configuration

In the same year, Kretschmann and Raether also reported a prism based SPR configuration, which is well-known as Kretschmann configuration, as shown in Fig. 2.4. Kretschmann and Raether noticed that the EW could also be generated at the prism-metal interface when the metal layer is attached to the prism base. So as long as the thickness of the metal is small

enough, the EW could also excite the SPR at the metal-dielectric interface. Therefore, in order to overcome the limitation caused by the gap between the prism and metal layer in Otto configuration, they coated a very thin metal film (about 50 nm) directly onto the prism base as demonstrated in Fig. 2.4. When the incident angle of the p-polarized light is equal to or greater than the critical angle, the EW will be generated at the prism-metal interface, penetrates into the metal and couples with SPW, which further excites the SPR at the metal-dielectric interface. This configuration allows the target analytes to be conveniently in contact with the metal surface, the layout of which overcomes the drawback of Otto configuration. Since then, the Kretschmann configuration has become the standard configuration of the prism-based SPR sensors and has been widely applied by researchers for various sensing purposes as well as by many companies for fabricating commercial SPR products even to date.

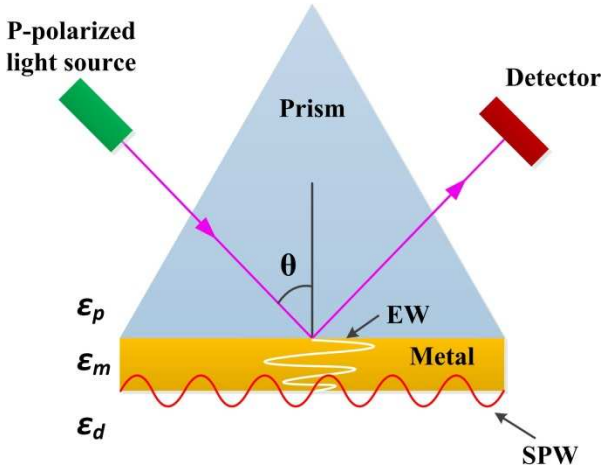

Fig. 2.4. Schematic diagram of Kretschmann configuration.

From the dispersion relations for the incident light and SPW as shown in Fig. 2.5, we can observe that, the dispersion curves of EW (curves b and c) intersect with that of SPW at the metal-dielectric interface (curve d) when the incident angle θ is equal to and greater than the critical angle θ_{TIR}. Thus, the SPR can be exited at the crossing point when $k_{EV} = k_{SP}$. It is also noticed that, the dispersion curve of EW never intersects with that of SPW at the metal-prism interface (curve e) even when the incident angle is equal to 90° (curve c), which indicates that no SPR can be exited at the metal-prism interface.

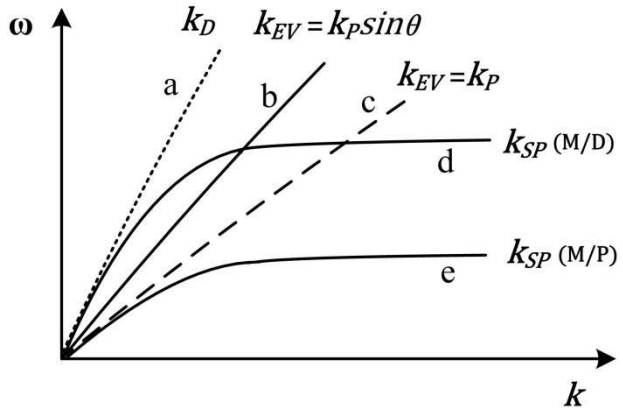

Fig. 2.5. Dispersion curves of: (a) incident light in dielectric medium, (b) EW when incident angle $\theta = \theta_{TIR}$, (c) EW when incident angle $\theta = 90^{\circ}$, (d) SPW at metal-dielectric interface, and (e) SPW at metal-prism interface. k_D, k_{EV}, k_p, $k_{SP\,(M/D)}$, $k_{SP\,(M/P)}$ represent the propagation constants of light in air, EW at metal-prism interface, light in prism, SPW at metal-dielectric interface, SPW at metal-prism interface, respectively [10].

2.2.4 Sensing principle and characteristics of SPR sensor

2.2.4.1 Sensing principle

Briefly, the basic sensing principle of SPR sensor is to detect the refractive index change happened around the sensing area. When the incident light couples with the SPWs (in the form of EW), part of the energy of the incident light will be transferred into the free electrons of the metal, which results in the oscillation of the free electrons at the metal-dielectric interface and the loss in energy of the reflected light. Any change in the refractive index (or dielectric constant) at or close to the metal-dielectric interface, even the small change caused by the biomolecular interaction, will change the condition for the SPR excitation. As a result, the energy transferred from the incident light varies with the refractive index change. Therefore, the refractive index change around the sensing surface can be detected by monitoring the change of the optical parameters of the reflected light.

Fig. 2.6 shows an example of a typical prism based SPR biosensor. As shown in Fig. 2.6 (a), the bio-receptors (or so-called ligands) are immobilized on the sensing surface. By measuring the intensity of reflected light at different incident angles, a dip in the reflectance spectrum of the reflected light can be observed at a particular angle (θ_1). The loss of reflected light intensity is caused by the excitation of SPR when incident light couples with SPs. And

the incident angle corresponding to the maximum loss of reflected light intensity is called resonance angle or SPR angle.

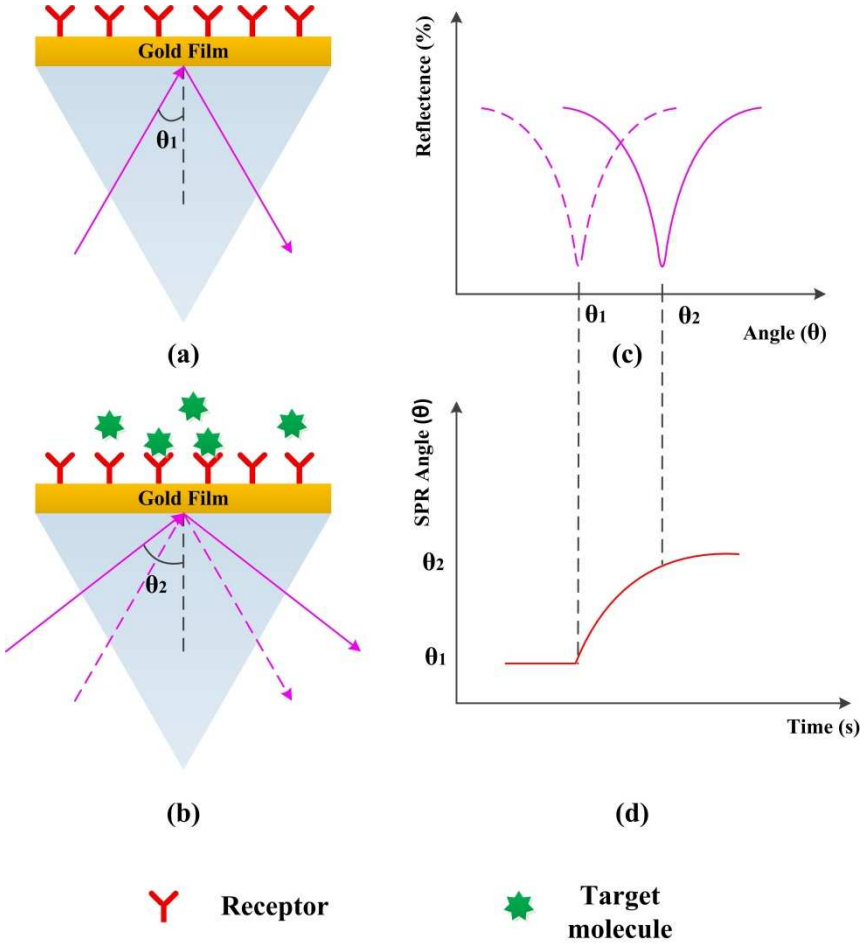

Fig. 2.6. (a) Prism based SPR sensor functionalized with bio-receptors, (b) Target molecules binding to receptors, (c) Resonance angle shift after the binding of target molecules and (d) The change of SPR angle as a function of time.

After the target molecules are bound to the receptors as demonstrated in Fig. 2.6 (b), the capture of target molecules will induce the change of the refractive index at the sensing surface. According to Equation 2.4, the variation in the refractive index will change the condition for excitation of SPR, thereby resulting in the shift of the SPR angle from θ_1 to θ_2 as shown in Fig. 2.6 (c). Fig. 2.6 (d) demonstrates the change of SPR angle as a function of time in the real-time monitoring. It has been found that the SPR angle increases with the increase of refractive index at the sensing surface [10].

The angular interrogation method introduced above is based on the measurement at a fixed wavelength by using a monochromatic light source and this method has been commonly used in SPR sensors [11, 12]. Apart from it, detecting approaches based on intensity measurement at a fixed SPR angle [7, 13, 14] and resonance wavelength interrogation by using polychromatic light source [15-17] also have been often applied in SPR sensors.

2.2.4.2 Characteristics of SPR sensor

When evaluating the performance of a SPR sensor, especially a SPR biosensor, several key characteristics of a SPR sensor are required to be taken into consideration, which include sensitivity, linearity, resolution, limit of detection, regenerability and stability [18-20].

Sensitivity: The sensitivity of a SPR sensor is a key parameter which indicates how sensitive the SPR sensor is to the refractive index change near the sensing surface. It also has an influence on the limit of detection (LOD) for the SPR biosensor. Normally, the higher the refractive index sensitivity, the lower the LOD can be achieved. The sensitivity, $S_{RI,}$ is defined as the ratio between the change of the monitored parameter of SPR sensor (such as SPR angle, wavelength or intensity) and the surrounding refractive index change, and it can be expressed as:

$$S_{RI} = \frac{\Delta Y}{\Delta n} \tag{2.5}$$

where ΔY and Δn denote the change of parameter of SPR sensor and the corresponding change of refractive index respectively. For example, for wavelength based measurement, the sensitivity of a SPR sensor is the ratio of SPR wavelength shift to the corresponding refractive index change, and the unit of sensitivity is nm/RIU (RIU = refractive index unit).

Linearity: Linearity is usually defined as the maximum deviation from the linear transfer function over the specified dynamic range [19]. The sensor linearity demonstrates the linear relationship between measurand and the sensor output over the working range. In SPR sensors, the term linearity usually refers to the linearity of SPR sensitivity over a specific range of refractive index. In the linear fitting of measurand (such as angle or wavelength) shift as a function of refractive index change, R-squared value can reflect the linearity of the SPR sensor. In a specific refractive index range, the closer the R-squared value is to 1, the more linear the sensitivity of SPR sensor is, and such refractive index range is called linear range. SPR sensors with linear sensitivity are desirable, as they require fewer calibration

points to produce a set of accurate sensor calibration data. In addition, when SPR sensor operates in the linear range it is easier to identify the accuracy of the measurements.

Resolution: The resolution of an SPR sensor is defined as the smallest change in the bulk refractive index that produces a detectable change in the sensor output. The resolution of an SPR sensor, R_{RI}, is typically expressed in terms of the standard deviation of noise of the SPR sensor output, δ_{SO}, translated to the refractive index of bulk medium [20],

$$R_{RI} = \frac{\delta_{SO}}{S_{RI}} \tag{2.6}$$

where S_{RI} is the bulk refractive index sensitivity. The unit of the resolution of an SPR sensor system is RIU. The resolution of SPR sensors is mainly dependent on the resolution of the detector (or spectrometer) and the signal to noise ratio (SNR) of the sensor system. Therefore, the resolution of SPR sensor can be improved by employing a detector with a higher resolution and also by enhancing the SNR through the generation of strong and stable sensor signals, using stable light source and appropriate data processing and analysis for instance.

Limit of detection: The limit of detection (LOD) is a key characteristic for the evaluation of a SPR biosensor. The LOD is defined as the lowest detectable concentration of the analyte, with unit such as nM or mg/mL, and it is highly dependent on the sensitivity and resolution of the SPR biosensor as well as its bioaffinity to the analyte. Normally, for the SPR biosensors with the same bioaffinity to the analyte, improving the sensitivity and resolution of the SPR biosensor could improve its LOD accordingly.

Regenerability: Regenerability is an ability of biosensor that, after the analyte is bound to the receptors immobilized on the biosensor, the biosensor can be regenerated by disassociating the analyte from the receptors so that the biosensor can be reused as a new sensor. Because the expensive noble metals such as gold are normally used for the preparation of SPR biosensor, SPR biosensor with regenerability can reduce the cost of experiments when the same sensor is able to be used for several times. However, it is worth noting that, after multiple regenerations, the results of measurement from such sensor might not be reliable, as the condition at the sensing surface could be changed by rinsing during the regeneration process.

Stability: Stability is ability of the sensor to provide the same output when measuring the same value of measurand under the same operating conditions over a period of time. It depends on the robustness of the sensor such as the oxidation resistance.

2.2.5 Optical fibre based SPR sensor

The development of fibre-optic SPR sensors began in the early 1990s [16, 21-24]. Optical fibre can be used to excite SPR due to the fact that the guidance of light in the optical fibre is based on the total internal reflection (TIR). Light propagating through an optical fibre consists of two components: the TIR guided field in the fibre core and the exponentially decaying evanescent field generated at the core-cladding interface. Since in the prism based SPR sensor where the prism is used to obtain the TIR and EW to excite SPR, the optical fibre can also be used for the same purpose to fabricate optical fibre based SPR sensor. Compared to the conventional prism based SPR sensors, the optical fibre based SPR sensors have shown advantages including small sample requirement, simplified and flexible sensor design, miniaturized sensor system, remote sensing capability and resistance to electromagnetic interference. Therefore, more and more studies on the development of various optical fibre based SPR sensors and their applications have been reported in recent years.

The mechanical flexibility and the variety of optical fibres allow many interesting and promising fibre-optic SPR sensors to be realized. According to their typical features, the fibre-optic SPR sensors reported so far can be classified into four categories: decladed optical fibre, side-polished optical fibre, tapered optical fibre and fibre grating based SPR sensors. Table 1 summarises the characteristics of these SPR sensors.

Table 1. Characteristics of optical fibre based SPR sensors with different structures.

Sensor structure	Characteristics	Detection RI range	RI Sensitivity	Ref.
Transmission-based	MMF[a], decladed	1.33 ~ 1.40	~ 2500 ~ 3000 nm/RIU	1
Reflection-based	MMF, decladed, silver end mirror	1.34 ~ 141	~ 3085 nm/RIU	2
U-shaped	MMF, decladed, U-shaped bending	1.33 ~ 1.35	~ 70 μm/RIU	3
Side-polished	MMF, part core polished	1.35 ~ 1.43	~ 3425 nm/RIU	4
D-type	SMF[b], half core polished	1.33 ~1.37	~ 2×10^{-6} RIU (phase)	5
Tapered tip	SMF, tapered tip	1.33 ~ 1.375	~ 4000 %/RIU (intensity)	6
Continuously tapered	SMF, tapering ratio	1.333 ~ 1.3424	~ 2400 nm/RIU	7
LPG	SMF, with cladding, multiplexing	1.329 ~ 1.34	~ 1100 nm/RIU	8
FBG	SMF, with cladding, tilted grating	1.42 ~ 1.45	~ 454 nm/RIU	43

[a]MMF = multimode fibre, [b]SMF = single mode fibre.

2.2.5.1 SPR sensors based on decladed optical fibres

The decladed optical fibres have been commonly used for the development of optical fibre SPR sensors. In general, the delcaded optical fibre SPR sensors are fabricated by partly removing the cladding of an optical fibre, and depositing a thin layer of metal film around the exposed fibre core. Fig. 2.7 (a) - (f) show the structures of three typical decladed optical fibre SPR sensors and their corresponding SPR spectra.

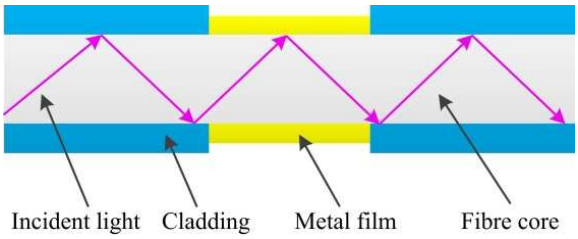

(a)

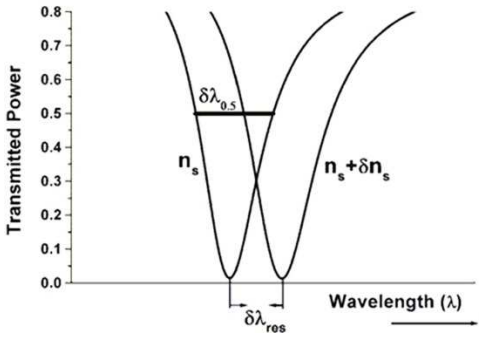

(b)

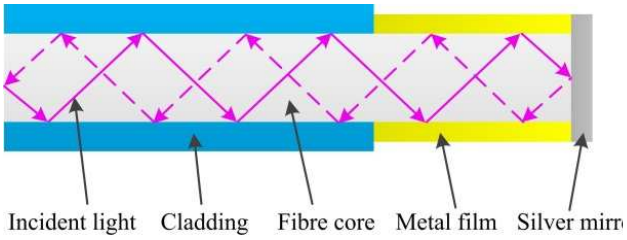

(c)

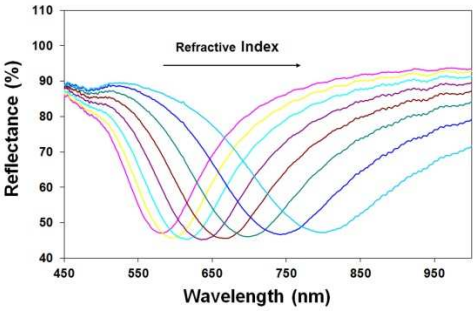

(d)

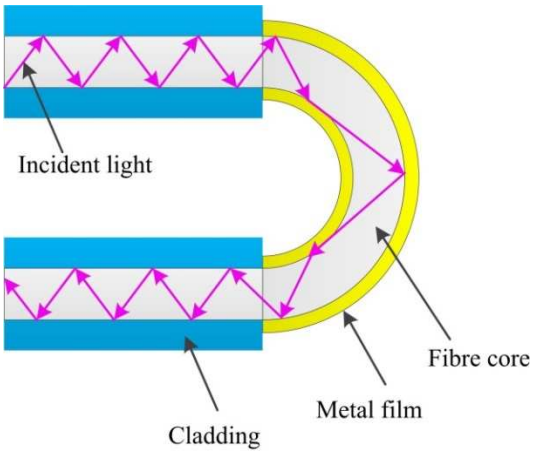

(e)

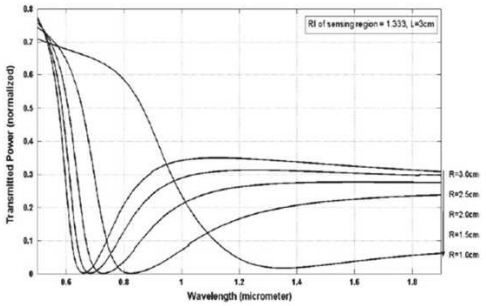

(f)

Fig. 2.7. (a) Optical fibre SPR sensor with transmission-based configuration and (b) it corresponding SPR spectrum [25], (c) optical fibre SPR sensor with reflection-based configuration and (d) its corresponding SPR spectrum [26], (e) optical fibre SPR sensor with U-shaped bending and (f) its corresponding SPR spectrum [27].

Transmission-based SPR sensor

In 1993, Jorgenson and Yee reported an optical fibre based SPR sensor with a transmission configuration for detecting the variations in the refractive index of solutions [16]. As illustrated in Fig. 2.7 (a), this sensor was fabricated by using a piece of conventional polymer cladded multimode optical fibre with about 10 mm cladding removed in the middle of the optical fibre. The exposed section of fibre core subsequently coated with a silver layer about 55 nm thick was then used as the sensing region. The incident light was coupled into the optical fibre from its end connected to a white light source and generated EW at the fibre core-metal interface. The EW further excited SPR at the metal-dielectric interface and the change of the incident light due to the variation in refractive index was detected by a spectrometer connected to the other end of the optical fibre. The wavelength interrogation technique was applied in their work, and the sensitivity of the SPR sensor created was reported to be comparable to that of a traditional prism based SPR sensor [16].

Reflection-based SPR sensor

Later, a terminated reflection-based fibre-optic SPR sensor system was also reported by Jorgenson and Yee [28]. The reflection-based optical fibre SPR sensor has the same sensing principle as the transmission-based optical fibre SPR sensor. However, as shown in Fig. 2.7 (c), in the reflection-based configuration the fibre cladding was removed at one end of the optical fibre rather than in the middle and a micro-fabricated mirror was also attached to the end of the fibre to reflect the light back. Therefore, the reflection-based sensor probe is constructed at the end of the optical fibre. Compared to the transmission-based optical fibre SPR sensor, the reflection-based optical fibre SPR sensor shows many potential advantages, suitable for practical sensing applications, including: elimination of a flow-cell needed for the transmission-based sensor, small volume of sample requirement, inexpensive disposable sensor probes, long distance remote sensing and miniaturized portable SPR sensor device.

U-shaped bending SPR sensor

Optical fibre sensors with a decladed U-shaped bending have been found to have higher absorbance sensitivity than that of a straight optical fibre sensor when they are used as absorbance based biochemical sensors. The enhancement in the absorbance sensitivity of optical fibre sensor with U-shaped bending is due to the reason that the penetration depth of evanescent field increases significantly in bending region [29]. Recently, Verma and Gupta proposed a SPR based fibre-optic sensor with a U-shaped probe [27]. As demonstrated in Fig. 2.7 (e), the decalded U-shaped bend used as the sensing region was coated with a thin metal film. The sensitivity of the sensor was analysed by using a bi-dimensional model. In

their study, they found that the bending radius of the sensor probe has an effect on the sensitivity and the sensitivity of the sensor increases with the decrease of the bending radius. However, when the bending radius decreases below a certain value, the sensitivity of the sensor starts to decrease dramatically due to the reason that the incident angle of light is less than the critical angle required for light to be guided in the bending region. Therefore, the maximum sensitivity of the U-shaped sensor can be obtained at an optimum value of the bending radius. The maximum sensitivity achieved in their work was reported to be several times higher than that of a SPR based optical fibre sensor with a tapered probe [27]. However, in terms of practical applications, despite higher sensitivity achieved, the optical fibre SPR sensor with U-shaped bending still remains to be disadvantageous as found in the transmission-based optical fibre SPR sensor.

2.2.5.2 SPR sensors based on side-polished optical fibres

The decladed optical fibre based SPR sensors introduced above were fabricated by using multimode fibres. Single mode fibres are not suitable for the same design, because the fibre core of single mode fibres is too small that it is very fragile and easy to break without the protection of cladding. Therefore, a side-polished technique was applied for developing SPR sensors based on the single mode optical fibres [30, 31]. A sketch of a typical side-polished single mode optical fibre SPR sensor is shown in Fig. 2.8 (a). At one side of the single mode optical fibre, the cladding of the fibre was removed by mechanical polish and a thin metal layer was deposited on the polished flat surface of the optical fibre working as the sensing surface. In this configuration, a fundamental mode propagating through the fibre couples with the SPW at metal-dielectric interface, which results in the excitation of SPR at the interface. It was reported that such side-polished single mode optical fibre SPR sensors have a higher sensitivity and better stability compared to the multimode optical fibre based SPR sensors [9].

Another type of side-polished single mode optical fibre SPR sensor called D-type optical fibre SPR sensor was also reported [32-34]. This sensor design is analogous to the traditional prism based SPR sensors. As demonstrated in Fig. 2.8 (c), apart from the cladding, half of the fibre core was also side-polished to form a flat surface which was covered by a thin metal film, so that the sensor probe has a ‘D’ shape when looking at its cross section. A similar sensor design but based on the multimode optical fibre was also reported [35]. The advantages of the D-type optical fibre SPR sensors are that they provide larger sensing area

and allow more biomolecules to be immobilized on their flat sensing surface when they are used as biosensors. However, for both the side-polished and D-type optical fibre sensors, the major drawback of these sensors is that their fabrication is much complicated and sophisticated in comparison to those using decladed multimode fibres. In addition, a reliable control of polarization state of optical wave propagating in the optical fibre is also required [31].

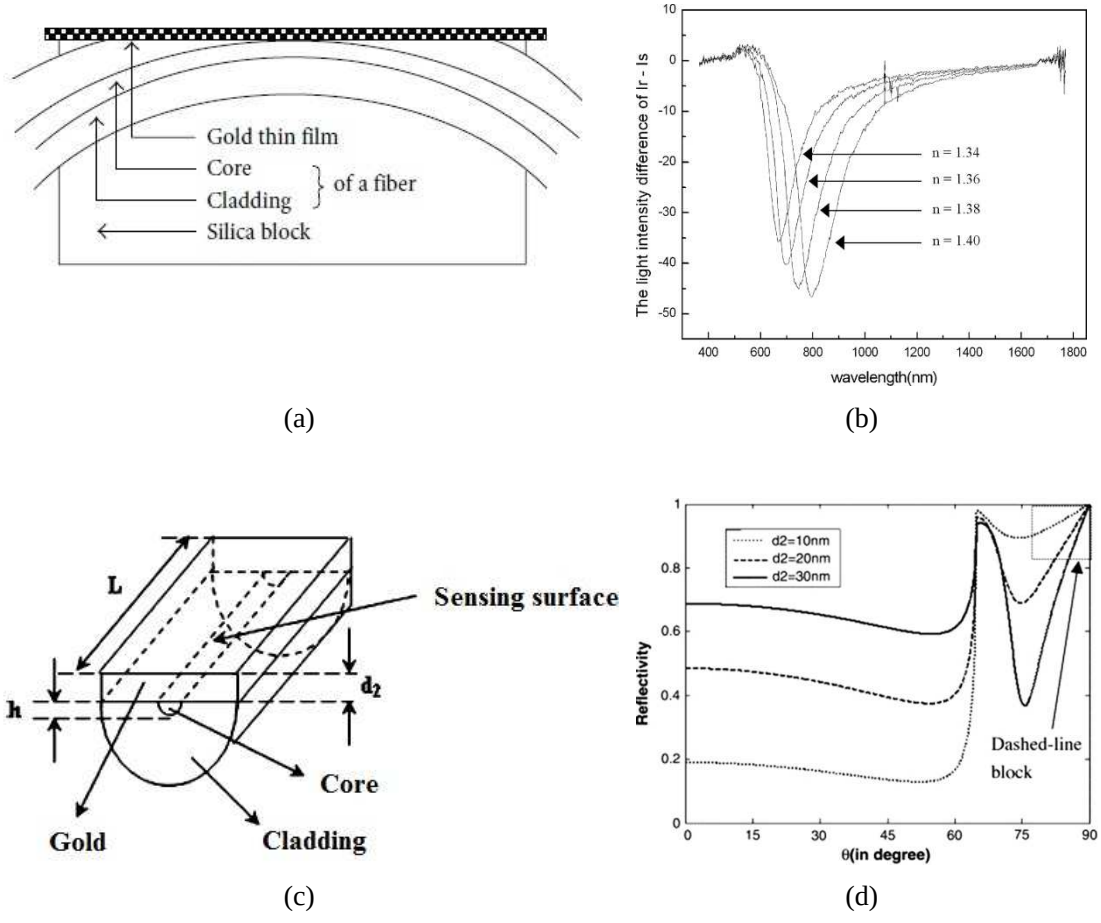

Fig. 2.8. SPR sensors based on side-polished optical fibres: (a) side-polished single mode optical fibre SPR sensor [36] and (b) it corresponding SPR spectrum [37], (c) D-type side-polished optical fibre SPR sensor [10] and (d) it corresponding SPR spectrum [38].

2.2.5.3 SPR sensors based on tapered optical fibres

It was also reported that the sensitivity of optical fibre sensors could be improved by changing the shape or geometry of the optical fibres. In addition to the U-shaped and the side-polished optical fibres introduced above, the tapered optical fibres have also shown the ability of enhancing the sensitivity of optical fibre sensors. In the comparison studies, researchers found that the tapered optical fibre sensors have higher sensitivity compared to the similar optical fibre sensors with uniform geometry when they were used as the evanescent field based sensors which uses the evanescent filed to directly interact with the analyte [39-41]. The increase of sensitivity of the tapered optical fibre sensors is due to the increase of evanescent filed magnitude and penetration depth in the tapered region [42]. The tapered optical fibre based SPR sensors have also shown higher sensitivities than the conventional non-tapered optical fibre SPR sensors [43,44].

Because of the great penetration depth of evanescent field, the tapered optical fibre SPR sensors can be fabricated by either removing the cladding and tapering the fibre core or tapering whole fibre without the removal of cladding. There are two types of geometries of tapered optical fibre commonly used in SPR sensors: tapered tip and continuously tapered fibre. As shown in Fig. 2.9 (a), the diameter of a tapered tip decreases gradually until the optical fibre becomes a sharp tip. The tapered tip at the end of an optical fibre is formed by chemically etching the fibre in strong acid solution [45]. The sharp tapered tip, subsequently covered by a thin metal film, is used as the sensing region. On the other hand, as demonstrated in Fig. 2.9 (c), the continuously tapered fibre normally contains three tapered regions with different diameters, which gradually decreases in region 1, keeps at a constant vale in sensing region, and finally gradually increases back to the original diameter in region 2. The continuously tapered fibre can be fabricated by softening the tapered region with flame heating and then stretching both sides of the optical fibre simultaneously during the heating [46]. To use a taper as a SPR sensor, a thin metal needs to be deposited on surface of the tapered fibre in the sensing region. It is because that the evanescent field is at its maximum in the region of the smallest diameter. It also has been found that the geometric parameters including diameter, length and taper ratio have influence on the sensitivity of the tapered optical fibre sensors [43, 44].

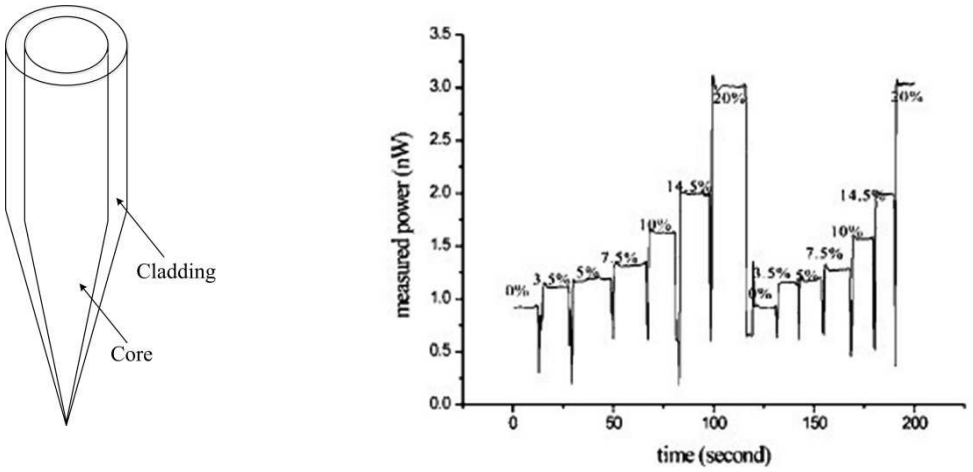

(a) (b)

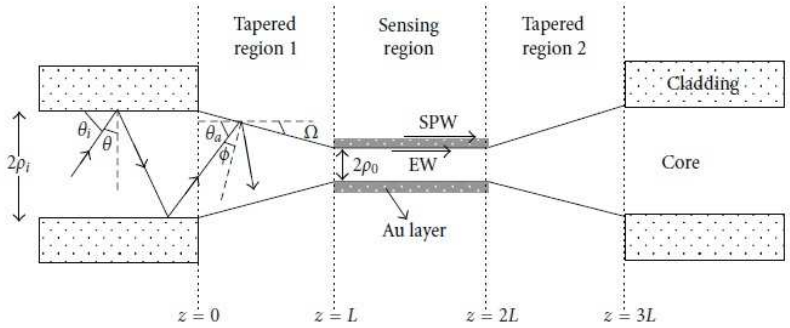

(c)

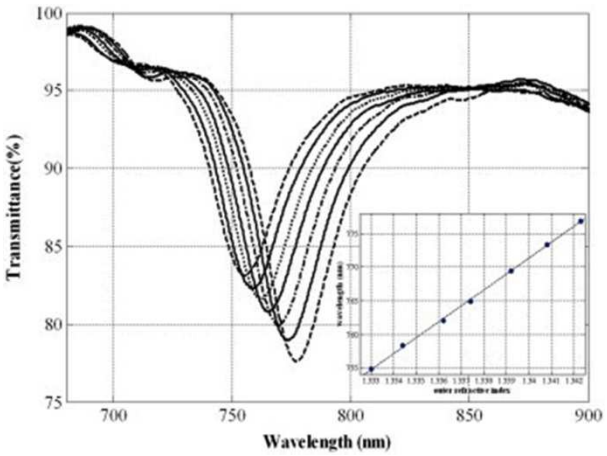

(d)

Fig. 2.9. SPR sensors based on tapered optical fibres: (a) optical fibre SPR sensor with a tapered tip and (b) its corresponding SPR spectrum [47], (c) optical fibre SPR sensor with continuously tapered regions [48] and (d) its corresponding SPR spectrum [49].

2.2.5.4 SPR sensors based on fibre gratings

Apart from the conventional single mode or multimode optical fibres based SPR sensors introduced above, single-mode optical fibre SPR sensors based on long period fibre grating (LPG) and fibre Bragg grating (FBG) have also been reported recently. The excitation of SPR for both LPG and FBG based SPR sensors is achieved by using LPG or FBG imprinted in the optical fibre to couple the light from core mode to cladding modes, and the EW generated at the cladding-metal interface further couples with the propagating SPW [50].

He *et al*. proposed an LPG based optical fibre SPR sensor for measuring the refractive index of analyte [51]. In their work, the sensor was fabricated by depositing a thin metal film on the cladding of an optical fibre with LPG written in the fibre (Fig. 2.10 (a)). The LPG with proper period was used to couple the core mode to the cladding mode. Such cladding mode then coupled with the co-propagating SPW, which results in the excitation of SPR at the metal-dielectric interface. The refractive index change of analyte was detected by measuring the core mode power at a fixed wavelength. In addition, FBGs have also applied for the excitation of SPR. However, since FBGs do not readily couple the core mode to the cladding modes, for the FBG based SPR sensors, a special sensor design is normally required in order to couple to SPW [52]. Nemova and Kashypa reported a theoretical study of an FBG based SPR sensor [53]. In their study, an FBG was inscribed in a specially designed single-mode fibre, which has a relatively large core (26 μm in diameter) and a thin cladding (2 μm in thickness) coated with thin gold film, in order to generate a nonzero core mode field amplitude at the cladding-gold interface. In this sensor design, the FBG is able to couple the fundamental core mode to the encountering SPW, thus exciting SPR at the gold-dielectric interface. Shevchenko and Albert experimentally demonstrated an optical fibre SPR sensor based on a tilted FBG [50]. As shown in Fig. 2.10 (c), the SPR sensor was fabricated by implanting a tilted FBG into a standard single-mode fibre with cladding covered by a thin gold film. The tilted FBG can couple the forward-propagating core mode out of the fibre core into the back-propagating cladding modes, which have nonzero evanescent fields extending into the gold film. The coupling of cladding mode and the SPW occurs when the axial component of the propagation constant of the cladding mode matches that of the SPW, resulting in the excitation of SPR. The transmission spectrum was used to monitor the resonance wavelength shift when the sensor was subjected to the exterior refractive index change surrounding the sensing area [50]. The advantage of the fibre gratings based SPR sensors is that, SPR can be excited by mode coupling without the need of bending, side polishing or tapering the fibre. In addition, with numbers of gratings written in the same

optical fibre, the fibre grating based SPR sensors are able to provide multiple sensing channels [51, 54].

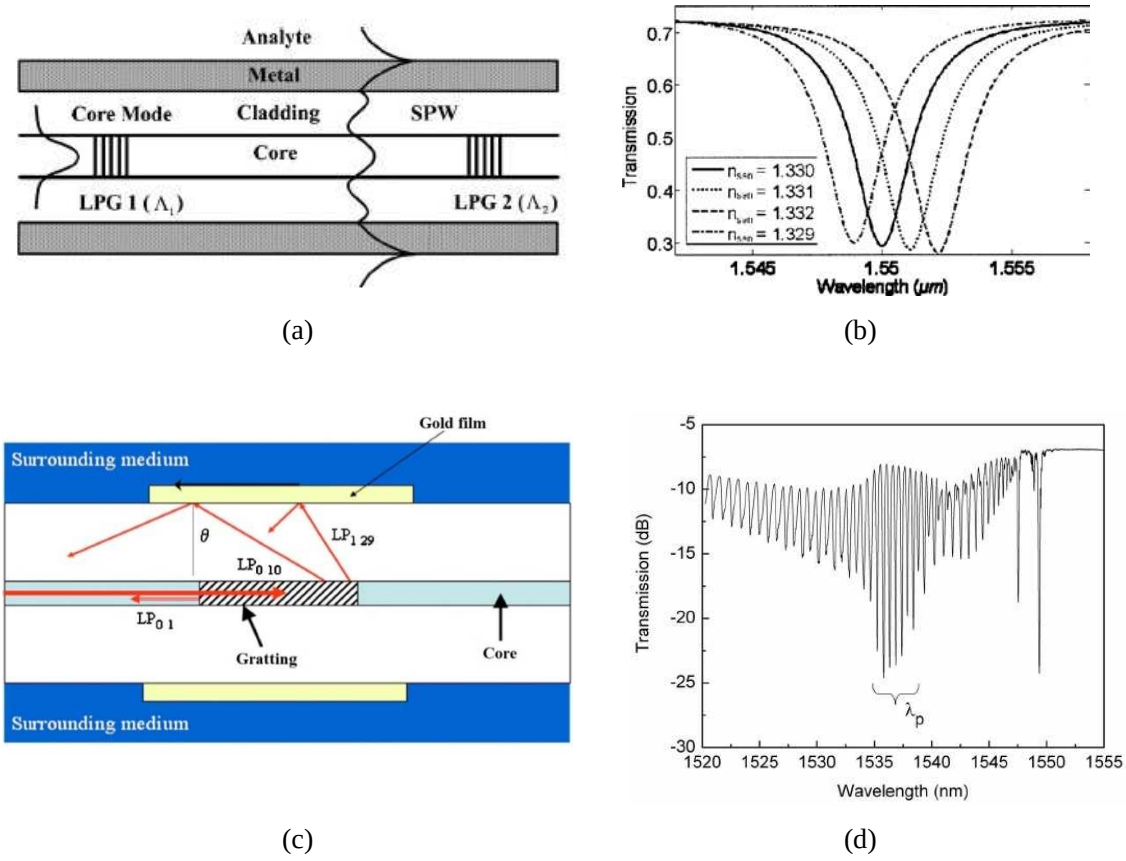

Fig. 2.10. (a) LPG based SPR sensor [41] and (b) it corresponding SPR spectrum [55], (c) Tilted FBG based SPR sensor and (d) its corresponding SPR spectrum [43].

2.2.6 Applications of SPR sensors

SPR sensors can be used for measuring physical quantities such as humidity [56] and temperature [57]. They also can be used as chemical sensors for either measuring the concentration of the analyte [58] or detecting the presence of target chemicals [59]. However, the major area where SPR sensors have been widely applied is biosensing applications. Rapid, sensitive, real-time and label-free detection, all of these desired characteristics make SPR biosensors an advanced and powerful tool for characterising and quantifying biological species. SPR biosensors have been applied in a number of important fields including biomedical analysis, food quality and safety, and environmental monitoring.

Therefore, in this section, we focus on reviewing some specific applications of SPR biosensors that have been reported.

2.2.6.1 Application in medical diagnostics

SPR biosensors, especially some commercial SPR biosensors, have been applied in medical diagnostics for detecting and analysing analytes of biomedical interest, such as biomarkers, antibodies, drugs and hormones.

Besselink *et al*. reported the detection of prostate-specific antigen (PSA), a biomarker for prostate cancer, in PBS buffer using the commercial SPR sensor Ibis II [60]. In their work, the monoclonal anti-PSA antibodies were first immobilized on the sensing surface via amine coupling to functionalize the sensor. Subsequently, the sample containing PSA was incubated on the sensing surface, which resulted in the specific binding between PSA and anti-PSA antibodies. To amplify the sensor response, rabbit anti-PSA polyclonal antibodies were further added to the sensing surface to bind the immobilized PSA, followed by the addition of goat anti-rabbit IgG-coated colloidal gold onto the sensing surface. The LOD of the SPR sensor after the amplification was found to be as low as 0.15 ng/mL. In a similar study, Huang *et al*. reported the detection of PSA using the commercial SPR sensor Biacore 2000 [61]. A direct detection format was first applied in their work by covalently immobilizing the PSA-receptor molecules consisting of a single-domain antigen-binding fragment on the sensing surface. The PSA molecules were then directly captured by the PSA-receptors and the LOD for PSA as low as 10 ng/mL was reported. The LOD was then further improved by applying a sandwiched assay using a biotinylated secondary antibody and streptavidin modified gold nanoparticles to bind the PSA previously captured by the PSA-receptors in order to amplify the sensor response. By this way, the improved LOD for PSA was found to be below 1 ng/mL. Chung *et al.* demonstrated the detection of antibodies against human hepatitis B virus (hHBV) in 5 % serum in PBS using the commercial SPR sensor Spreeta [62]. The hHBV antigens used as receptors were immobilized on the sensing surface via amine coupling chemistry. The LOD for antibodies against hHBV based on direct detection was about 9.2 nM. The sensor response was further enhanced by using a peroxidase-antiperoxidase method that 17-fold amplification was achieved and the LOD was reduced to be 0.64 nM. The detection of antibodies against human respiratory syncytial virus (RSV) in sera using commercial SPR sensor Biacore 2000 was reported by McGill *et al.* [63]. Monoclonal antibodies against the virus glycoproteins (F- and G-glycoproteins) were

covalently attached to the dextran matrix immobilized on sensing surface. The F- and G-glycoproteins, working as the receptors, were then bound to their corresponding antibodies respectively. Serum samples isolated from patients' respiratory tracts were diluted in HBS buffer (1:10) and filtered. The results showed that the SPR biosensor has the ability to recognize the antigenic differences between the two different genotypes of the virus. Dillon *et al*. reported the application of SPR biosensor for detecting morphine-3-glucuronide (M3G), the main metabolite of heroin and morphine [64]. The detection was based on the inhibition immunoassay and carried out by using the commercial SPR sensor Biacore 1000. A conjugate consisting of M3G and ovalbumin was produced and used for the generation and immobilization of antibodies against M3G. Two different polyclonal antibodies were generated and immobilized on the sensor. The binding-regeneration ability of the biosensor was about 60 cycles for one antibody and 50 cycles for second antibody. The detection of M3G was carried out in urine and the LOD for M3G was found to be less than 1 ng/mL for both antibodies. Chung *et al*. demonstrated the detection of pregnancyshuman chorionic gonadotropin (hCG) and human albumin (hA), both of which are related to the abortion and preterm delivery during early pregnancy, using commercial SPR sensor Spreeta [65]. Two types of antibodies against hCG and hA respectively were immobilized on the sensing surface as the receptors. A sequential analysis method was applied and the detection of hCG and hA was carried out in healthy human urine. In order to amplify the sensor response, another polyclonal anti-hCG and anti-hA antibodies were used after the capture of hCG and hA. The LODs for hCG and hA of 10-fold diluted samples were 46.4 mIU/ml and 2.5 µg/ml, respectively.

2.2.6.2 Application to enhance food quality and safety

The food quality and safety are vitally important to human being, as they are directly related to our health. Thus rapid, precise and reliable food analysis during every stage of food production is important and necessary to guarantee the quality and safety of food products. SPR biosensing technology has been considered as one of the techniques that can meet this requirement. More and more researches have begun to apply SPR biosensing technology to detect the target analytes which affect the food quality and safety.

Yu *et al*. reported the detection of domoic acid (DA), a neuroexcitatory toxin from marine diatoms and found in sea products, using SPR biosensor [66]. As DA has low molecular weight, the inhibition immunoassay was applied to amplify the sensor response in their

work. The detection of DA was based on a competitive principle. The DA molecules were first immobilized on the sensing surface via amine coupling chemistry. Anti-DA antibody solution with a fixed concentration was premixed with target DA solution with various concentrations. The mixed solution was then flowed in to the SPR cell and the unbound antibodies were captured by the DA molecules immobilized on the sensor surface. The SPR response decreased with the increase of target DA concentration. It was found that the LOD for DA was as low as 0.1 ng/mL. Tudos *et al*. demonstrated the application of SPR biosensor for detection of deoxynivalenol, a highly toxic fungal metabolite that may contaminate food and animal feed, based on a commercial SPR senor Biacore-Q [67]. The assay used in this work was also based on a competitive protocol. A conjugate of deoxynivalenol with the protein casein was first prepared and immobilized on the sensor surface via amine coupling chemistry. A monoclonal mouse anti-deoxynivalenol antibody solution with a certain concentration was mixed with the target deoxynivalenol solution. The mixed solution was then injected into the sensor system to start the binding competition for antibodies between the immobilized deoxynivalenol and free deoxynivalenol in the solution. The results showed the sensor could be regenerated for 500 cycles and LOD for deoxynivalenol was about 2.5 ng/mL. Folic acid is a widely used nutrient in infant formulae, athletic supplements and fruit drinks. Caselunghe *et al*. reported the detection of folic acid in food samples using a commercial SPR sensor Biacore Quant [68]. The detection was based on the inhibition immunoassay similar to the ones introduced above. Folic acid was first immobilized on the sensor surface, and the anti-folic acid antibodies solution with a fixed concentration was mixed with analyte samples with different concentrations. The folic acid immobilized on the sensor surface only captured the antibodies without binding to the free folic acid. The results showed that the method was of high accuracy and precision [68]. The detection of riboflavin (Vitamin B2) in milk samples was reported by Caelen *et al*. using the commercial SPR sensor system Biacore Q and inhibition immunoassay [69]. A riboflavin derivative was immobilized on the sensor surface via amine coupling chemistry. The riboflavin binding protein with a certain concentration was mixed with a sample containing riboflavin. The unbound riboflavin binding protein was measured by the SPR biosensor. The LOD for riboflavin was found to be 70 ng/mL. SPR sensor has also been used for the detection of food allergens. Mohammed *et al*. demonstrated the direct detection of peanut allergens using a miniature commercial SPR sensor Spreeta [70]. The peanut specific antibodies were immobilized on the sensor surface for capturing the peanut allergens. The LOD for the peanut allergen in buffer was established at 700 ng/mL.

2.2.6.3 Application in environmental monitoring

The development of modern technology greatly improved the quality of our lives, but meanwhile, as a trade-off it not only consumed the resources but also brought us some unwanted “by-products” which have negative impact on the environment. A great variety of toxic chemicals have been released from industrial pollution, domestic wastages, use of drugs and pesticides. In addition, military activities, terrorist attacks and biological weapons also caused the toxic pollution. Therefore, the development of biosensors for environmental monitoring is of significant importance. Many SPR based biosensors have been used for detecting a number of toxic chemicals.

Farre *et al*. reported the detection of atrazine in water using a portable SPR biosensor [71]. The detection was based on the inhibition immunoassay. An atrazine derivative was covalently immobilized on the alkanethiolate self-assembled monolayer (SAM) formed on the gold-coated sensor surface. The purified polyclonal antibodies were incubated sample containing analytes, and then the mixture was analyzed by the SPR sensor. A complete assay/regeneration was accomplished in 25 min. The LOD for atrazine was as low as 20 pg/mL. Miura et al. applied SPR technology to the detection of benzo[a]pyrene (BaP), which is a carcinogenic endocrine disrupting chemical and is a potential marker of environmental pollution [72]. An indirect inhibition assay was applied and BaP-BSA conjugate was synthesized and covalently immobilized on the sensor surface by physical adsorption. The anti-BaP-BSA antibody with a certain concentration was mixed with BaP solution, and the mixture was measured by the SPR sensor. The sensor chip was able to be reusable for more than 20 times and the LOD for BaP was determined as low as 10 ppt with a response time of approximately 15 min. Soh *et al*. developed a SPR biosensor for the detection of 2,4-dichlorophenol, a known dioxin precursor, using an indirect competitive immunoassay [73]. The SPR sensor was functionalized with monoclonal anti-(2,4-dichlorophenol) antibodies which was immobilized on the sensor surface via gold binding peptide and protein G. In order to improve the sensor response, 2,4-dichlorophenol-BSA conjugate was synthesized and mixed with analyte samples. The detection of 2,4-dichlorophenol was based on the competition between the analyte present in sample and the added 2,4-dichlorophenol-BSA conjugate. The LOD for 2,4-dichlorophenol was found to be 20 ng/mL. The detection of explosives and explosive related materials for preventing terrorist activities has received a great number of attentions. 2,4,6-trinitrotoluene (TNT) is one of the explosive molecules commonly existing in explosive weapons. Larsson et al. demonstrated the detection of TNT using a commercial SPR sensor Biacore 2000 and inhabitation immunoassay [74]. Two types

of thiols, OEG-alkylthiols terminated with a hydroxyl group and a TNT analogue (2,4-dinitrobenzene), were self-assembled on the gold-coated sensor surface. Three different TNT analogues and hydroxyl-terminated OEGthiols were mixed and the ratio was optimized to provide highly selective and sensitive biochips with minimum nonspecific binding. The LOD for TNT in buffer was found to be <10 pg/mL. Application of SPR technology for detecting heavy metal Cu^{2+} ion was reported by Ock et al. [75]. A thin polymer film containing squarylium dye (SQ-dye) was immobilized on the sensor surface as the sensing layer. The SQ-dye has a high selectivity to Cu^{2+} and the presence of Cu^{2+} was detected by the electro-static interaction between Cu^{2+} ion and SQ-dye, which resulted in the change of refractive index at the SPR sensor surface. The dynamic detection range of this sensor for detecting Cu^{2+} ion was from 1×10^{-12} to 1×10^{-4} M.

2.3 Background and development of LSPR sensor

2.3.1 Introduction to LSPR

The physical properties of noble metal change enormously from what we are usually familiar with to the size of the metals in the nanoscale, smaller than the wavelength of light [76, 77]. The colour of gold in nano world is no longer just golden. It can be as colourful as a rainbow. Such an example can be found in Fig. 2.11, where gold nanorods (GNRs) with various aspect ratios suspending in solutions display a range of different colours. The SPR phenomenon introduced in section 2.2 was also changed from surface plasmon resonance (SPR) to localized surface plasmon resonance (LSPR) when the bulk metal film was replaced by metallic nanoparticles (MNPs) to excite SPR. LSPR refers to the SPR phenomenon happened when light interacts with the MNPs, which results in a collective oscillation of conduction electrons of the MNPs at a resonant frequency [77]. The properties of LSPR are highly dependent on the MNPs' material, size and shape. Different from SPR that EW is the key to the success of the SPR excitation, LSPR can be excited when light interacts directly with the MNPs [78]. This gives great flexibility to the construction and fabrication of LSPR based sensors. For instance, the substrate of LSPR sensor platform can be either a prism or a piece of glass slide [79]; LSPR sensor can be based on either the MNPs immobilized on the substrate, or the metallic nanoparticle just suspending in solution [80]. In addition, as LSPR is highly localized in the each individual metallic nanoparticle, LSPR sensors can also be based on a bunch of nanoparticles or even single nanoparticles [81]. Because the properties of LSPR are highly dependent on the material, size and shape of the

MNPs, by manipulating these parameters, the LSPR wavelength can be conveniently tuned throughout the visible, near-infrared, and into the infrared region, thus the LSPR sensor could be constructed for particular applications where a specific wavelength is desired. Compared to SPR sensors, the sensors based on LSPR technology have also demonstrated a comparable sensitivity in biosensing applications as well as more flexibility and lower cost in terms of fabrication.

Fig. 2.11. GNRs solutions with different aspect ratios.

The advances in the fabrication of MNPs have led to a remarkable growth in the development of LSPR sensors in the past decade. At the early stage, most of the LSPR sensors were based on spherical gold nanoparticles due to their ease of synthesis. By now, quite a few of LSPR sensors based on noble nanoparticles with various shapes have been developed and have shown higher sensitivities and other advantages in comparison with gold nanospheres (GNSs) based LSPR sensors. Among these MNPs, GNRs have attracted a great deal of attentions due to their unique optical properties [82, 83]. More and more GNRs based LSPR sensors have been reported recently. Apart from the LSPR sensing applications, GNRs have also been applied in SERS sensing [84], chemical imaging [85] and even cancer therapy [86]. In this section, a review of the development of LSPR sensors, especially LSPR sensors based on GNRs, is given.

2.3.2 LSPR theory

MNPs have intriguing optical properties which are significantly different from those observed in bulk metal. When incident light interacts with MNPs, the electromagnetic field

of light induces a collective coherent oscillation of the surface conduction electrons of the MNPs in resonance with the frequency of light, and this phenomenon is known as LSPR [77, 78]. The electric field of light attracts the free electrons in nanoparticle leading to a charge separation between the free electrons and the ionic metal core, and in turn the Coulomb repulsion among the free electrons acting as a restoring force pushes the free electrons moving to the opposite direction, which results in the collective oscillation of electrons, or in another word, the excitation of LSPR. The occurrence of LSPR also results in a strong absorption of light. MNPs with different size, shape and material have different absorption bands and appear in different colours as shown in Fig. 2.11. Fig. 2.12 (a) illustrates the excitation of LSPR for a spherical nanoparticle. Only one absorption band can be observed in its absorbance spectrum as shown in Fig. 2.12 (b). For GNR, as demonstrated in Fig. 2.13 (b), two absorption bands can be found, namely longitudinal plasmon band and transverse plasmon band corresponding to the electron oscillation along the long axis and the short axis of GNR, respectively, as shown in Fig. 2.13 (a). The transverse plasmon band of GNRs is insensitive to the size of GNRs and the surrounding refractive index change, while the longitudinal plasmon band has been found to be red-shifted with the increase of aspect ratio and much more sensitive to the refractive index change than the transverse plasmon band [83, 87]. The LSPR condition is highly dependent on the nanoparticle size, shape, structure, the dielectric properties of the metal as well as the surrounding medium, as these factors affect the electron charge density on the particle surface [83, 88-90]. LSPR is also highly sensitive to the refractive index change in the local dielectric environment. Normally, the change of the peak wavelength or the peak absorbance in the absorption spectrum of MNPs is employed as an indicator of the LSPR sensor response [91, 92].

As demonstrated in Fig. 2.12 and Fig. 2.13, the excitation of LSPR results in a strong absorption of light. For spherical MNPs, the Mie solution to Maxwell's equations can be used to describe this light absorption caused by LSPR [93, 94]. According to the Mie theory, for the well separated spherical nanoparticles with radius *R*, which is much smaller than the wavelength of light λ (*R*/ λ < 0.1), the extinction cross-section *Cext*, can be expressed as:

$$C_{ext} = \frac{24\pi^2 R^3 {\varepsilon_m}^{3/2} N}{\lambda \ln(10)} \frac{\varepsilon_i}{(\varepsilon_r + 2\varepsilon_m)^2 + {\varepsilon_i}^2} \tag{2.7}$$

where ε_m is the dielectric constant of the surrounding medium, ε_r and ε_i are the real and imaginary part of the dielectric function of the MNPs, respectively, and *N* is the electron density. As indicated by Equation 2.6, the plasmon absorption band appears when $\varepsilon_r =$

$-2\varepsilon_m$. For gold and silver spherical nanoparticles, their plasmon absorption bands are located in the visible region, making these materials suitable for many applications.

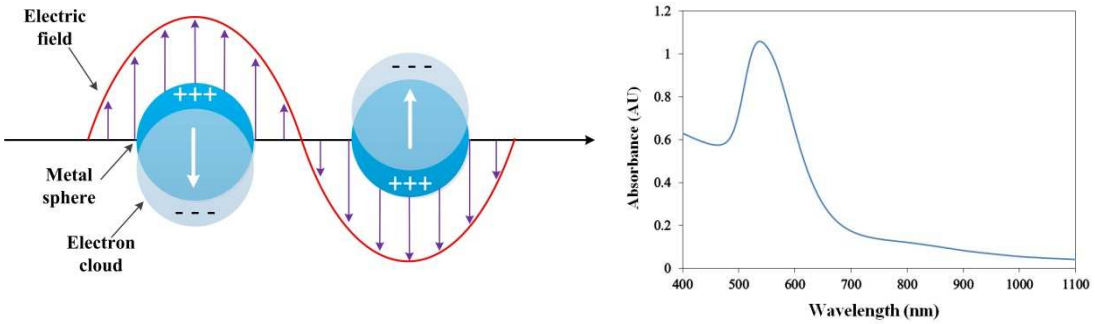

(a) (b)

Fig. 2.12. (a) Schematic illustration of LSPR excitation for GNSs; (b) A typical LSPR absorption band of GNSs.

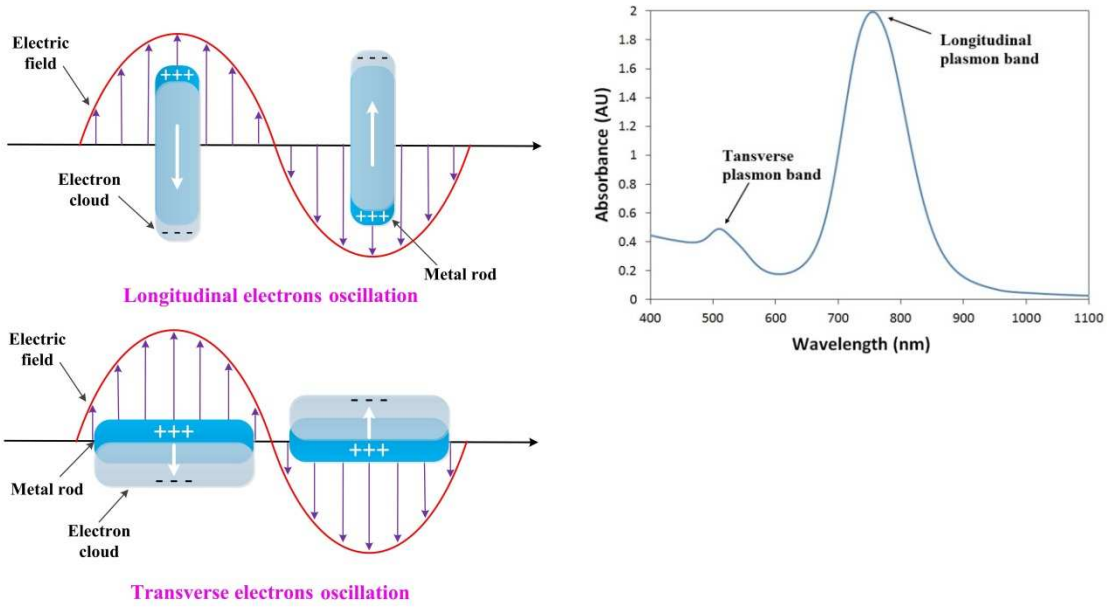

(a) (b)

Fig. 2.13. (a) Schematic illustration of LSPR excitation for GNRs; (b) LSPR absorption bands of GNRs: longitudinal and transverse plasmon bands corresponding to the electron oscillation along the long axis (Fig. 2.13 (a) top) and the short axis (Fig. 2.13 (a) below) of GNR respectively.

In the case of metallic nanorods, Gans predicted that for small ellipsoidal nanoparticles with dipole approximation, the surface plasmon mode would split into two distinct modes due to the surface curvature and geometry of the ellipsoidal nanoparticles [95]. The small rods have been commonly treated as ellipsoids when explaining the optical properties of these rod-shape particles [96, 97]. Therefore, Gans theory can be applied to describe the optical behaviour of metallic nanorods. According to Gans formula, the extinction cross-section C_{ext} for metallic nanorods can be calculated as follows [93, 98, 99]:

$$C_{ext} = \frac{2\pi V {\varepsilon_m}^{3/2}}{3\lambda} \sum_j \frac{\left(1/P_j^2\right)\varepsilon_i}{\left(\varepsilon_r + \frac{1-P_j}{P_j}\varepsilon_m\right)^2 + {\varepsilon_i}^2} \tag{2.8}$$

where V is volume of the particle and P_j is the depolarization factor. The depolarization factor for elongated particles is described as:

$$P_{length} = \frac{1-e^2}{e^2}\left[\frac{1}{2e}\ln\left(\frac{1+e}{1-e}\right) - 1\right] \tag{2.9}$$

$$P_{width} = \frac{1 - P_{length}}{2} \tag{2.10}$$

where e is ellipticity given by:

$$e^2 = 1 - \left(\frac{length}{width}\right)^{-2} \tag{2.11}$$

where *length/width* is the aspect ratio of rod. The LSPR occurs when $\varepsilon_r = -\left(\left(1 - P_j\right)/P_j\right)\varepsilon_m$, where $P_j = P_{length}$ for the longitudinal plasmon resonance and $P_j = P_{width}$ for the transverse plasmon resonance. Equation 2.7 also indicates that a small change in aspect ratio of nanorod will result in a significant change in plasmon band.

In addition, the LSPR wavelength is sensitive to the refractive index change. Thus, changes in the local medium surrounding the nanoparticles will result in a shift in the LSPR wavelength. This LSPR wavelength shift $\Delta\lambda$ in response to refractive index change is described by the following relationship [77, 100, 101]:

$$\Delta\lambda = m\Delta n\left[1 - exp\left(\frac{-2d}{l_d}\right)\right] \quad (2.12)$$

where m is the bulk refractive index response of the nanoparticles, also known as the sensitivity factor (in nm per refractive index unit, RIU), Δn is the change in refractive index (in RIU), d is the effective thickness of the adsorbed layer (in nm) and l_d is the characteristic electromagnetic field decay length (in nm). The expression given in Equation 2.11 forms the basis of the LSPR wavelength-shift based sensors, where the LSPR wavelength-shift is used to monitor the refractive index change at the surface of nanoparticle due to the adherence of biomolecule for instance.

2.3.3 Synthesis of gold nanorods (GNRs)

For SPR sensors, the thin metal film deposited on the substrate can be acquired by using a coating machine like sputter coater or evaporator. However, the same approach cannot be applied to the acquirement of MNPs for LSPR sensors. Several methods have been employed for synthesizing MNPs with various shapes and the commonly used approaches for the synthesis of GNRs are discussed in detail in this section.

2.3.3.1 Seed-mediated growth method

The seed-mediated growth method is the most popular method for the synthesis of colloidal GNRs due to its simple experimental procedure, high quality and yield of nanorods, ease of particle size controlling, and flexibility in structural modifications [82]. The history of seed-mediated growth of colloidal particles can date back to 1920s. But the application of this method for synthesizing colloidal GNRs was first demonstrated by Jana *et al*. in 2001 [102]. In their work, the seed solution was prepared by the reduction of gold salt (HAuCl4) with $NaBH_4$ in the presence of sodium citrate, which resulted in the formation of citrate-capped GNSs with a diameter about 3~4 nm used as the seed. Then the seed solution was added into a growth solution containing $HAuCl_4$, cetyl-trimethyl ammonium bromide (CTAB, as the template), ascorbic acid (as the reducing agent) and $AgNO_3$ (for shape induction) to allow the growth of GNRs. The GNRs with various aspect ratios ranging from 1 to 7 were acquired by adding different volumes of seed solution into the growth solution of different samples as shown in Fig. 2.14. Later, the same group modified the above method by introducing a three-step protocol in the absence of silver ions to grow GNRs with higher aspect ratio [103]. In

this method, the seed solution and the growth solution are prepared following a similar procedure for preparing the short GNRs but without the addition of $AgNO_3$. Then, at step one, the seed solution is added into the growth solution to form small GNRs, which are subsequently used as the seeds and added into growth solution to grow bigger GNRs at step two. The final step is adding the bigger GNRs into growth solution to grow GNRs with higher aspect ratio. However, the biggest drawback of these two methods is that, apart from the GNRs, a large amount of GNSs as well as particles with other shapes as the by-products are also produced, which alters significantly the overall shape of the plasmon absorption bands of the GNRs.

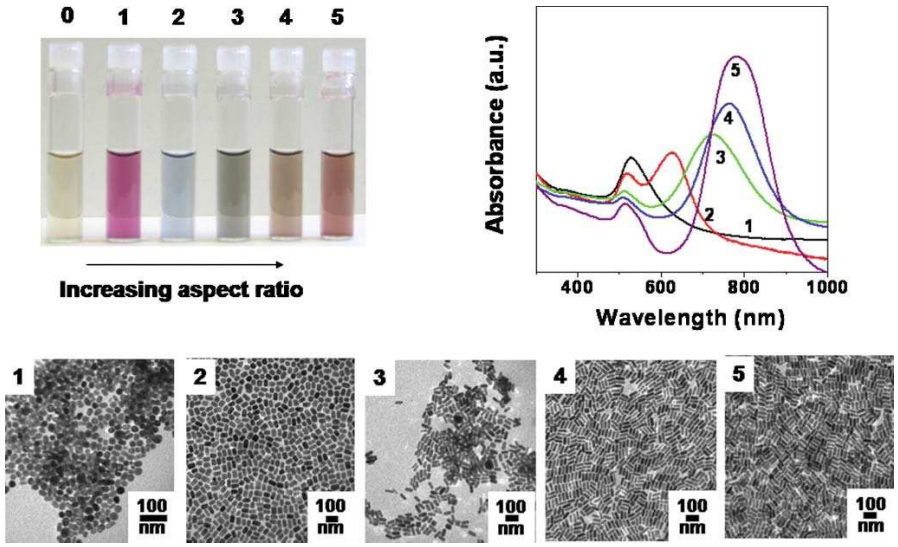

Fig. 2.14 GNRs with different aspect ratios were synthesized by the seed-mediated growth method. Top left, photograph of seed solution (vial 0) and GNRs solutions with increasing aspect ratio (vial 1-5) from 1 to 7; top right, absorbance spectra of GNRs in vial 1-5 and the corresponding TEM images (bottom) [85].

In 2003, Nikoobakht and El-Sayed made a significant improvement to the above method by introducing two important modifications to it: first, they replaced the originally used sodium citrate with CTAB, a stronger stabilizer, in the seed formation step; second, they adjusted the amount of silver ions in the growth solution to control the aspect ratio of GNRs [104]. In their work, the seed solution was prepared by reducing $HAuCl_4$ in the presence of CTAB surfactant with ice-cold $NaBH_4$. The growth solution was prepared by mixing $HAuCl_4$ and a certain volume of $AgNO_3$ solution in the presence of CTAB, followed by the addition of ascorbic acid. The GNRs start to grow directly after the addition of seed solution in the growth solution. Using this method, as high as 99% yield of GNRs with aspect ratios from

1.5 to 4.7 was achieved. To synthesize GNRs with higher aspect ratios, benzyldimethylhexadecylammonium chloride (BDAC) as a co-surfactant was introduced in the original growth solution. By adjusting the concentration of silver ions in the growth solution, GNRs with aspect ratios up to 10 had been synthesized [104]. Due to the high quality and yield of GNRs produced, the method reported by Nikoobakht and El-Sayed has been widely applied for synthesizing GNRs. However, the growth mechanism of GNRs produced by the seed-mediated method has still not been well understood so far.

2.3.3.2 Electrochemical method

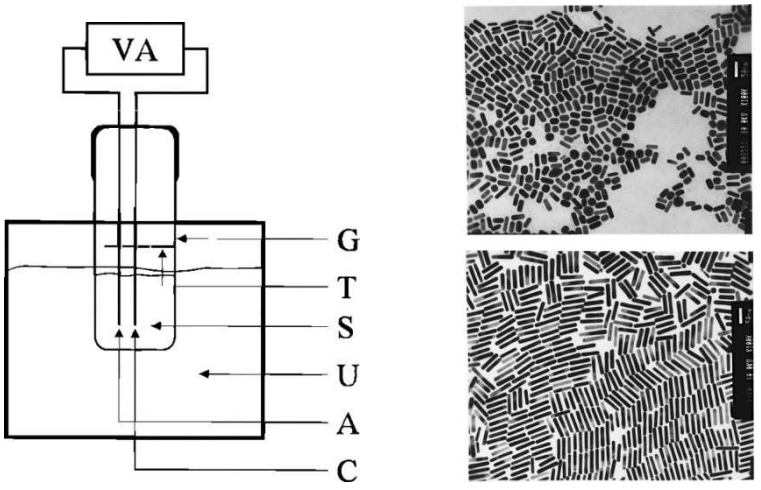

(a) (b)

Fig. 2.15. (a) Schematic diagram of the set-up for electrochemical synthesis of GNRs containing: VA, power supply; G, glassware electrochemical cell; T, Teflon spacer and the electrode holder; S, electrolytic solution; U, ultrasonic cleaner; A, anode (Au); C, cathode (Pt). (b) TEM images of Au nanorods with two different mean aspect ratios: 2.7 (top) and 6.1 (bottom) [106].

Despite the fact that the seed-mediated growth method has become a common approach for synthesizing GNRs, the preparation of high yield of GNRs was actually first demonstrated by using an electrochemical method, which was seen as the precursor of the seed-mediated growth method [105, 106]. In 1990s, Wang and co-workers first reported the formation of GNRs by extending their previous work on electrochemical synthesis of metal clusters in the reversed micelles in organic solvent. The synthesis of GNRs is conducted within a two-

electrode-type electrochemical cell as shown in Fig. 2.15 (a), where a gold metal plate used as the sacrificial anode and a platinum plate cathode are immersed into the electrolytic solution containing a rod-inducting cationic surfactant CTAB and a cationic co-surfactant Tetradodecylammonium bromide (TCAB). A small amount of acetone and cyclohexane are also added into the electrolytic solution before the electrolysis. Acetone is used for loosening the micellar framework and cyclohexane is necessary for enhancing the formation of elongated rod-like CTAB micelles [106]. During the electrolysis, the bulk gold metal anode is consumed to form $AuBr_4^-$, which then complexes with the cationic surfactants and migrate to the cathode where the reduction occurs. Ultrasonication is needed to dissipate the GNRs away from the cathode during the electrolysis. The aspect ratio of GNRs is controlled by gradually immersing a silver plate behind the platinum cathode. It has been found that the aspect ratio of the GNRs is influenced by the concentration and release rate of the silver ions produced from the redox reaction between the gold ions generated from the anode and the silver plate. However, the synthesis mechanism as well as the role of the silver ions is still unknown.

2.3.3.3 Template method

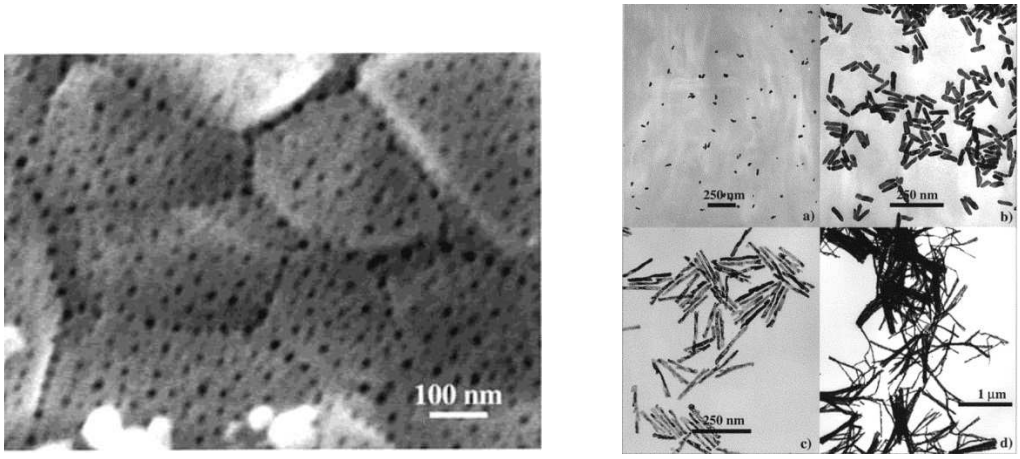

(a) (b)

Fig. 2.16. (a) FEG-SEM image of the alumina membrane template, (b) TEM images of GNRs obtained by the template method [111].

The template method is based on the electrochemical deposition of gold within the pores of nanoporous ion-track etched polycarbonate or alumina membrane template. This method was

initially used for the preparation of microscopic electrodes [107]. Martin and co-workers first employed the template method to synthesize GNRs [96, 108, 109]. The template was prepared by the anodization of aluminium in an acidic solution, which resulted in the formation of the uniform pores with diameters of 5-200 nm in the aluminium template. The pole length is dependent on the anodiazation time. The GNRs was formed through an electrochemical deposition of gold into the temple pores within an electrochemical cell, followed by the chemical etching of the aluminium template to release the synthesized GNRs. Fig. 2.16 (a) and (b) shows the alumina membrane template and the synthesized GNRs with different aspect ratios, respectively. The width of the rods created coincides with the diameter of the pores and the length of the rods can be controlled by varying the amount of the gold deposited within the pores of the template. The disadvantages of the template method include variance in length of GNRs due to the uneven deposition of gold and the low yield of GNRs [83, 110].

2.3.3.4 Electron beam lithography method

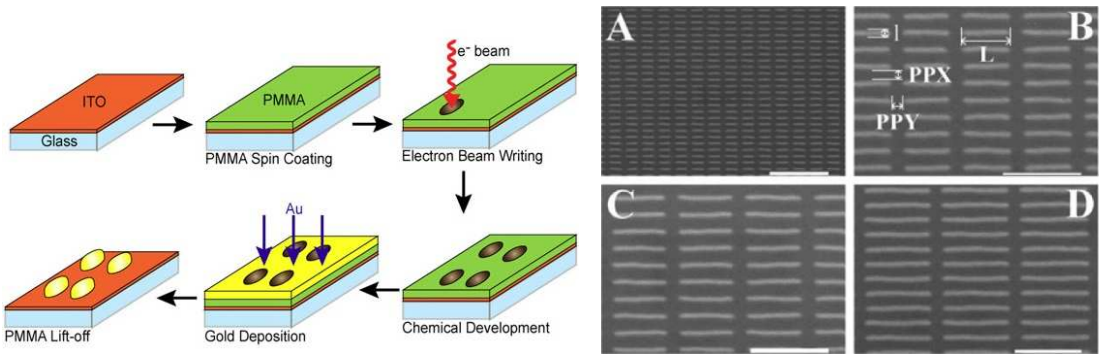

(a) (b)

Fig. 2.17. (a) Schematic diagram of the fabrication of gold nanoparticles using EBL [93], (b) SEM images of GNRs arrays produced by EBL. All of the rods have widths, *l*, of 60 nm, heights of 50 nm, and lengths, *L*, of A) 420 nm, B) 620 nm, C) 720 nm, and D) 1 µm [113].

Electron beam lithography (EBL) is a lithographic technique commonly used in the generation of metallic nanostructures. This technique allows for the precise control of size, shape and spatial distribution of nanoparticles [112]. Fig. 2.17 (a) illustrates the procedure of the fabrication of gold nanoparticles using EBL method. An electron-sensitive photoresist such as poly(methyl methacrylate), PMMA, is coated over a glass slide which is covered by

a conductive film such as indium tin oxide (ITO). The PMMA coated glass slide is then exposed to an electron beam to form a desired pattern on the PMMA film. A chemical developing agent is applied to selectively remove the electron beam exposed polymer segment, followed by the deposition of gold in the patterns by thermal evaporation. The unexposed PMMA film as well as the gold film deposited on it is finally removed by acetone that leaves the desired gold nanoparticle arrays on the glass slide as shown in Fig. 2.17 (b). Disadvantages of this technique involve time consuming and low yield of nanoparticles at one time due to the small producing region [93].

2.3.3.5 Other methods

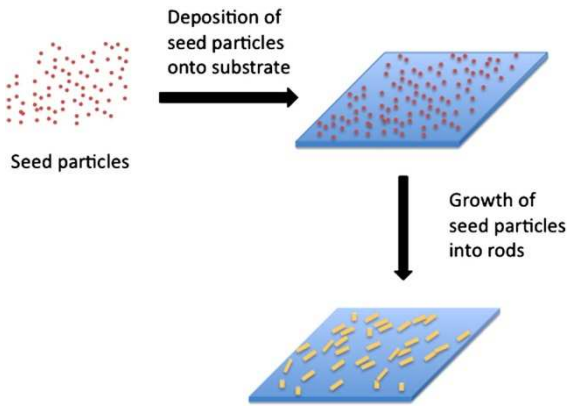

Fig. 2.18. Schematic diagram of the process of direct growth of GNRs on the substrate surface [121].

Yang and co-workers reported the synthesis of colloidal GNRs using a photochemical method [114]. In their work, the GNRs were formed by using a 254 nm UV light to irradiate a growth solution consisting of gold salt, CTAB and TCAB surfactants, silver nitrate, acetone and hexane, for more than 24 hours. The UV light works as a reducing agent, similar to the role of ascorbic acid in the seed-mediated growth method, to convert Au^{3+} to Au^{0}. The aspect ratio of the GNRs can be controlled by varying the concentration of silver ions in the growth solution, leading to the corresponding LSPR plasmon bands located at 600-800 nm. It is possible to extend the aspect ratio of GNRs by applying a 300 nm UV light instead, and synthesizing time can be shortened by increasing the light intensity [115]. Taub *et al*. developed a method that enables the GNRs to directly grow on the substrates [116], by adapting the seed-mediated growth method proposed by Jana and co-workers [103]. As demonstrated in Fig. 2.18, the spherical seed nanoparticles are first immobilized on the

surface of a mica, which is then immersed into the growth solution to allow the growth of GNRs. However, only 15 % of the seeds attached to the mica surface were found to grow as nanorods [116]. In addition, other less popular methods for the GNRs preparation have also been reported, such as proton beam irradiation [117], bioreduction [118], microwave reduction [119] and solvothermal reduction [120].

2.3.4 Surface modification of the CTAB-capped GNRs

For GNRs synthesized in the presence of CTAB surfactant using the wet-chemical methods, such as the seed-mediated growth method and electrochemical method, the surface of these GNRs is covered by a bilayer of positively charged CTAB molecules, as illustrated in Fig. 2.19. The CTAB surfactant is important to the synthesis of GNRs, because it not only works as a "structure-directing agent" to control the final particle shape, but also works as a stabilizer to protect the as-synthesized GNRs against aggregation [121, 122]. The CTAB-capped GNRs are stable when they are suspended in CTAB aqueous solution. However, the stability has been found to become poor under many conditions such as those with high salt content, low CTAB concentration and addition of organic solvents, thus limiting the further applications of GNRs [123, 124]. In addition, it also has been found in *in vitro* studies that the free CTAB molecules are cytotoxic to human cells, while the CTAB molecules bound to the GNRs surface are not toxic [125]. Despite the fact that most of the free CTAB can be removed by centrifugation, the complete removal of the free CTAB in solution as well as the CTAB attached to the GNRs will result in a serious aggregation and deposition of GNRs. Therefore, it is necessary to modify the surface condition of CTAB-capped GNRs in order to extend their applications, for example, for biosensing, biomedical imaging and drug delivery [82, 86]. Various approaches have been proposed for the surface modification of CTAB-capped GNRs. In general, there are two strategies applied for this purpose: surface covering and ligand exchange.

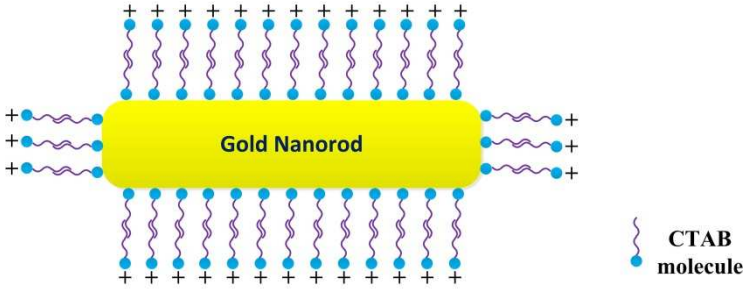

Fig. 2.19. A gold nanorod covered by a bilayer of positively charged CTAB molecules.

2.3.4.1 Surface covering

This approach aims to introduce additional coating to cover the entire surface of the CTAB-capped GNRs. An easy way of doing this is to coat the positively charged surface of the GNRs covered by CTAB molecules with the anionic polyelectrolytes via electrostatic absorption. Poly(sodium-4-styrenesulfonate) (PSS) has been applied to coat the GNRs. The anionic PSS not only switches the positive surface charge of GNRs to negative, but also enables antibodies to attach to the GNRs via hydrophobic interactions [86, 126]. Poly(acrylic acid) (PAA) is another anionic polyelectrolyte applied for the GNRs coating. The carboxylic group of PAA allows the proteins and amine-terminated biomolecules to be covalently bound to the PAA modified GNRs via EDC/NHS coupling reaction [127]. In addition, Gole and Murphy reported a layer-by-layer (LBL) technique which can be used to manipulate the surface condition of GNRs for different applications [128]. As shown in Fig. 2.20 (a), the anionic PSS and cationic poly(diallyldimethylammonium chloride) (PDADMAC) are alternately deposited onto the CTAB-capped GNRs, and multiplayers of coating can be obtained by repeating the cycle. This polyelectrolyte coating method is easy and fast, but the stability of the coating via electrostatic interaction is doubtful for long-term storage or for *in vivo* applications [82].

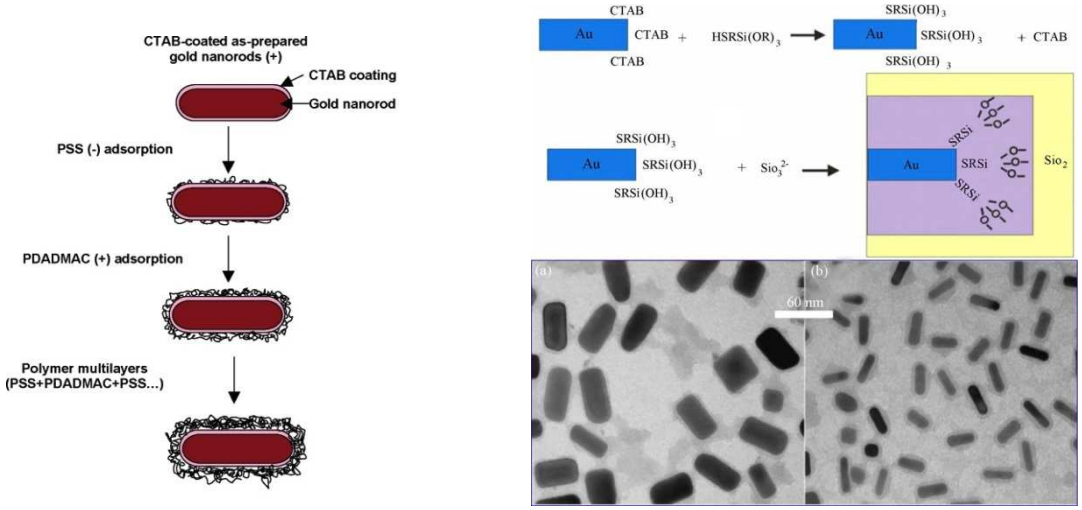

(a) (b)

Fig. 2.20. (a) Surface modification of CTAB-capped GNRs with polyelectrolytes using LBL technique [128], (b) Top: Scheme showing the steps required for silica coating of GNRs; Bottom: TEM images of silica coated GNRs with different aspect ratios (a: 1.94; b: 3.08) [99].

Surface modification of GNRs with a coating of hard inorganic materials, such as silver and silica, has also been achieved. Ah *et al*. reported the deposition of silver layer on to the surface of CTAB-capped GNRs by reducing silver chloride solution with hydroxylamine in the presence of GNRs [129]. The deposition of silver coating forms an Au/Ag core/shell structure of GNRs, and the thickness of the silver shell can be controlled by adjusting the concentrations of silver chloride and hydroxylamine. The silver shell can also be removed by using hydrochloric acid to restore the GNRs. Later, Liu and Guyot-Sionnest proposed a slightly different method for coating CTAB-capped GNRs with silver [130]. In their work, the deposition of silver coating was conducted by the reduction of silver nitrate with ascorbic acid in the presence of GNRs solution and stabilizing agent, either citrate or polyvinylpyrrolindone (PVP). It was also found that the pH of the coating solution has an impact on the deposition rate of silver that the higher the pH the higher the deposition rate [131]. The Au/Ag core/shell nanorods are more stable and show sharper, stronger and blue-shifted surface plasmon absorption bands than the original GNRs [129, 130].

Similar to the silver coating, a method, initially developed by Liz-Marzán *et al*. for the silica coating of citrate stabilized spherical gold nanoparticles [132], has been applied for the deposition of a silica coating onto the surface of CTAB-capped GNRs to form an Au/silica core/shell structure [133, 134]. As demonstrated in Fig. 2.20 (b), the silica coating is formed by simply adding sodium silicate solution into a premixed solution consisting of GNRs solution and 3-mercaptopropyl trimethoxysilane (MPTMS) or 3-mercaptopropyl triethoxysilane (MPTES) solution, and the formation of the silica shell results in a red-shift of the longitudinal plamson band of the GNRs due to the refractive index change at GNRs surface. Using another approach, the silica has also been successfully coated on the GNRs by the injection of tetraethoxysilane (TEOS) to the CTAB-capped GNRs solution in basic condition, which enables thin and highly porous silica shells covering the GNRs [135]. The silica coating allows the GNRs to be modified with silane coupling agents for further functionalization and transfer to organic solvents [82].

2.3.4.2 Ligand exchange

Another common strategy for the GNRs surface modification is to replace the attached CTAB bilayers with the thiol-terminated ligands which are then firmly bound to GNRs surface via the strong Au-S covalent bonds as illustrated in Fig. 2.21 (a). The advantages of this method include the reduction of the cytotoxicity of GNRs due to the removal of the CTAB molecules and the increase of the biocompatibility of GNRs when ligands with

functional groups are applied. However, as this method involves the removal of the CTAB molecule, the chance of GNRs aggregation will also increase due to the loss of protection of CTAB. Therefore, strict experimental conditions are sometimes required to prevent the GNRs from aggregating during the modification process. The thiol-terminated polyethyleneglycol (PEG) is one of the popular ligands commonly used for the GNRs surface modification [136-139]. One advantage of using thiolated PEG is that PEG is a water-soluble polymer so that the modification of GNRs can be conducted in an aqueous condition. The ligand exchange takes place after the addition of thiolated PEG solution into the centrifuged GNRs solution with the mixture being kept under constant stirring, followed by 3 days of dialysis or several rounds of centrifugation to remove the excess CTAB and PEG. Such PEG-modified GNRs are highly stable in aqueous and even in some organic solutions, and are useful in *in vivo* applications such as biomedical imaging and photothermal therapy [83, 140]. In addition, by employing the thiolated PEGs with biofunctional groups, it is also able to bind the biomolecules such as proteins and antibodies to the PEG-modified GNRs surface [123, 140]. However, the large size of the thiolated PEGs makes them difficult to reach the GNRs surface due to the dense CTAB bilayer, which will results in an incomplete removal of CTAB molecules. Besides, the large size of the thiolated PEGs also increases the distance between the analysts and the PEG-modified GNRs surface, which will reduce the sensitivity when they are used as LSPR biosensors [141]. Therefore, small thiol-terminated ligands such as 11-mercaptoundecaonic acid (MUA) and cysteamine are normally preferable for complete removal of CTAB [82].

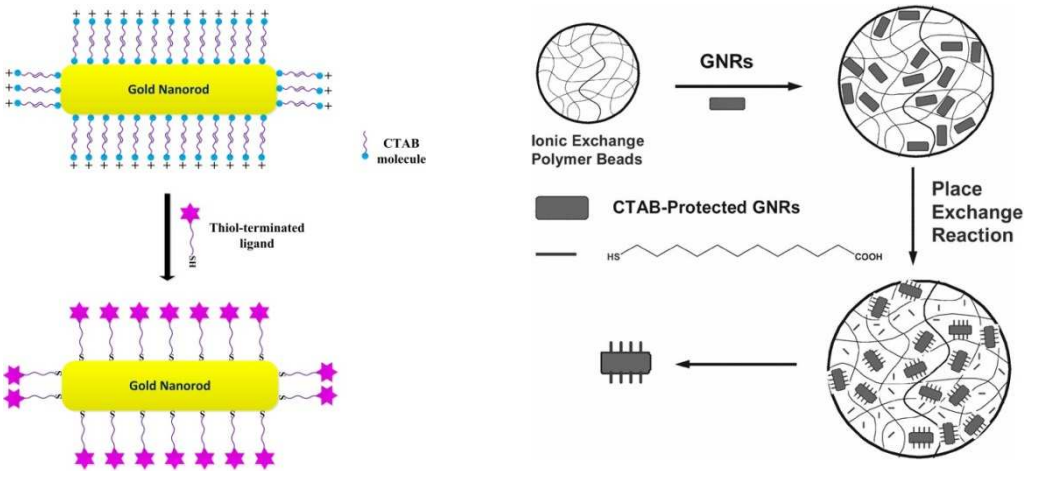

Fig. 2.21. (a) Schematic illustration of the surface modification of CTAB-capped GNRs with thiol-terminated ligands, (b) Schematic illustration of surface modification of GNRs using thiol place exchange reaction inside ionic exchange polymer beads [143].

The surface modification of GNRs with MUA has been reported in several studies [141-143]. MUA molecule has a carboxylic group which is desirable for the bioconjugation with amine-terminated biomolecules such as proteins and antibodies. Therefore, once the MUA molecules are bound to the GNRs surface, without further functionalization, biomolecules can be conveniently attached on to the GNRs via EDC/NHS coupling. However, like most thiol molecules, MUA is not water-soluble that it only dissolves in organic solvent such as ethanol and chloroform. The hydrophobic nature of MUA brings a big challenge to the surface modification of GNRs with MUA, because the CTAB-capped GNRs are very unstable in the presence of organic solvents, which will cause an irreversible aggregation of GNRs. Several approaches have been proposed in order to enable the MUA to be applied in the surfaced modification of GNRs. Yu *et al*. reported a method of complete removal of CTAB on GNRs with MUA [141]. The ligand exchange is conducted by adding a MUA-ethanol solution to a centrifuged GNRs solution under constant sonication to prevent the GNRs from aggregating. The temperature of the mixed solution is also elevated to 50 °C to release the CTAB molecules from the GNRs surface and then brought back to room temperature. The GNRs are finally purified with centrifugation. Although such MUA-modifed GNRs have been proven by the authors to be able to use as LSPR biosensor probes, significant aggregation of the GNRs was observed in our hands as well as by other researchers by following the same procedure reported, indicating that this method requires strict experimental conditions which makes it difficult for practical use. Thierry and co-workers later modified this method using a two steps strategy [142]. They first used the thiolated PEG to replace the majority of CTAB molecules on the GNRs surface in an aqueous condition. The PEG-modified GNRs have a neutral charge on the GNRs surface so that they do not aggregate in organic solvents as easily as the positively charged CTAB-capped GNRs. The second step involves the replacement of PEG with MUA following a similar procedure applied in the work of Yu *et al*. Although this approach may avoid the massive aggregation of GNRs as observed in in the work of Yu *et al.*, the thiolated PEG molecules are also bound to the GNRs via the strong Au-S bonds as MUA: whether MUA is able to effectively replace the PEG is still questionable for this route. In another study reported by Dai *et al*., to prevent the irreversible aggregation of GNRS, the surface modification with MUA was conducted inside an ionic exchange resin as shown in Fig. 2.21 (b) [143]. The CTAB-capped GNRs were first loaded into the polymer resin beads suspend in an aqueous solution to “trap” the GNRs in the resin beads. The ligand exchange took place after the addition of MUA chloroform solution to the resin beads suspension, and the MUA-modified GNRs diffused out of beads into the chloroform solution. The resin beads applied in this work can effectively prevent the GNRs from aggregating during the reaction. This

approach is smart and elegant. However, it also appears to be time consuming and complex to operate [142].

2.3.5 LSPR sensors with different configurations

As LSPR can be excited when light directly interacts with GNPs, the design of LSPR sensors is more flexible than that of SPR sensors. The LSPR sensors can be configured by either immobilizing GNPs onto a transparent substrate such as glass slide, or just simply leaving functionalized nanoparticles suspending in the solution in a cuvette, where the detection will take place after the addition of analytes. In general, there are three types of LSPR sensor configurations which are commonly used: chip-based, optical fibre-based and solution-phase-based LSPR sensors.

2.3.5.1 Chip-based LSPR sensor

The chip-based configuration is the most commonly used configuration of LSPR sensors [79, 92, 128, 144-146]. The chip-based LSPR sensor is normally fabricated by immobilizing GNPs on the surface of a flat transparent silica substrate such as glass slide and coverslip, without the need of bulk prism as used in the SPR sensors. For the GNPs synthesized by using the EBL technique or growing directly on the substrate, the sensor chip is simply obtained after the synthesis of the nanoparticles. For the nanoparticles suspending in solution, such as the GNRs synthesized by using the seed-mediated method, there are mainly two methods used for immobilizing GNPs. One method is using the electrostatic force [128]. A clean substrate is first immersed into a polyelectrolyte solution to make the substrate surface have a charge that is opposite to the surface charge of GNPs. Then, such charged substrate is dipped in the GNPs solution to coat the GNPs on its surface via the electrostatic force. However, the GNPs coating prepared by the electrostatic force method normally suffers from poor stability and poor uniformity. Another more commonly used method is based on the SAM technique [79, 144-147]. A clean substrate is first modified by immersing the substrate in an alkylsilane solution, such as 3-aminopropyltriethoxysilane (APTES) and MPTMS, to form an either amine-terminated or thiol- termined silane SAM on the substrate surface. Subsequently, the silanized substrate is incubated in a GNPs solution to form a monolayer of GNPs on the substrate surface via either electrostatic force or covalent bond. After the immobilization of GNPs, the GNPs surface can be further functionalized with various receptors, and then the sensor chip is ready for different applications. The UV-Vis

spectrophotometer is normally used for measuring the LSPR absorbance spectrum of GNPs based on the transmission mode as illustrated in Fig. 2.22.

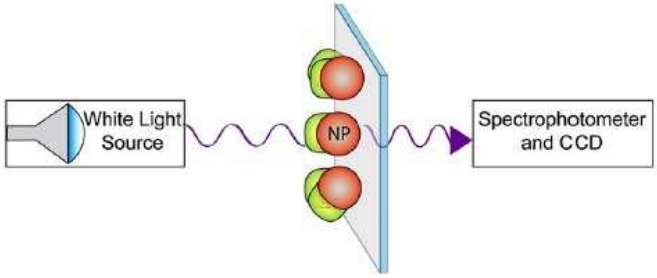

Fig. 2.22. Schematic diagram for instrumentation used in a chip-based LSPR sensor [93].

2.3.5.2 Optical fibre-based LSPR sensor

In 2003, Cheng and Chau first demonstrated the fabrication and application of an optical fibre-based LSPR sensor based on GNSs [148]. The sensor showed high sensitivity to the local refractive index change and capability of working as a biochemical sensor. Since then, a large number of optical fibre-based LSPR sensors have been developed for various applications [29, 91, 149-160]. The majority of the optical fibre-based LSPR sensors reported are fabricated by immobilizing GNPs on the unclad silica core of a multimode optical fibre with a structure similar to that of the decladed optical fibre-based SPR sensors introduced in Section 2.2.5.1. The transmission-based, reflection-based and U-shaped LSPR optical fibre sensors are illustrated in Fig. 2.23 (a), (b) and (c) respectively. The GNPs are coated onto the optical fibre by using the same coating approaches employed in the fabrication of the chip-based LSPR sensor. LSPR is excited at the core-GNPs boundary when light is transmitting in optical fibre. In addition, as LSPR can be excited by direct interaction of light with GNPs, it is also possible to coat GNPs on the distal end of the optical fibre to construct another type of reflection-based sensor probe as demonstrated in Fig. 2.23 (d). However, due to the low reflectivity of the GNPs coating, the intensity of the reflected light of such sensor may be not as high as that of the LSPR optical fibre sensor with a silver mirror coated at the fibre end as illustrated in Figure 2.23 (b). Apart from the multimode optical fibre based LSPR sensors, a few LSPR sensors using LPGs and tapered single-mode fibres have also been reported [46, 161, 162].

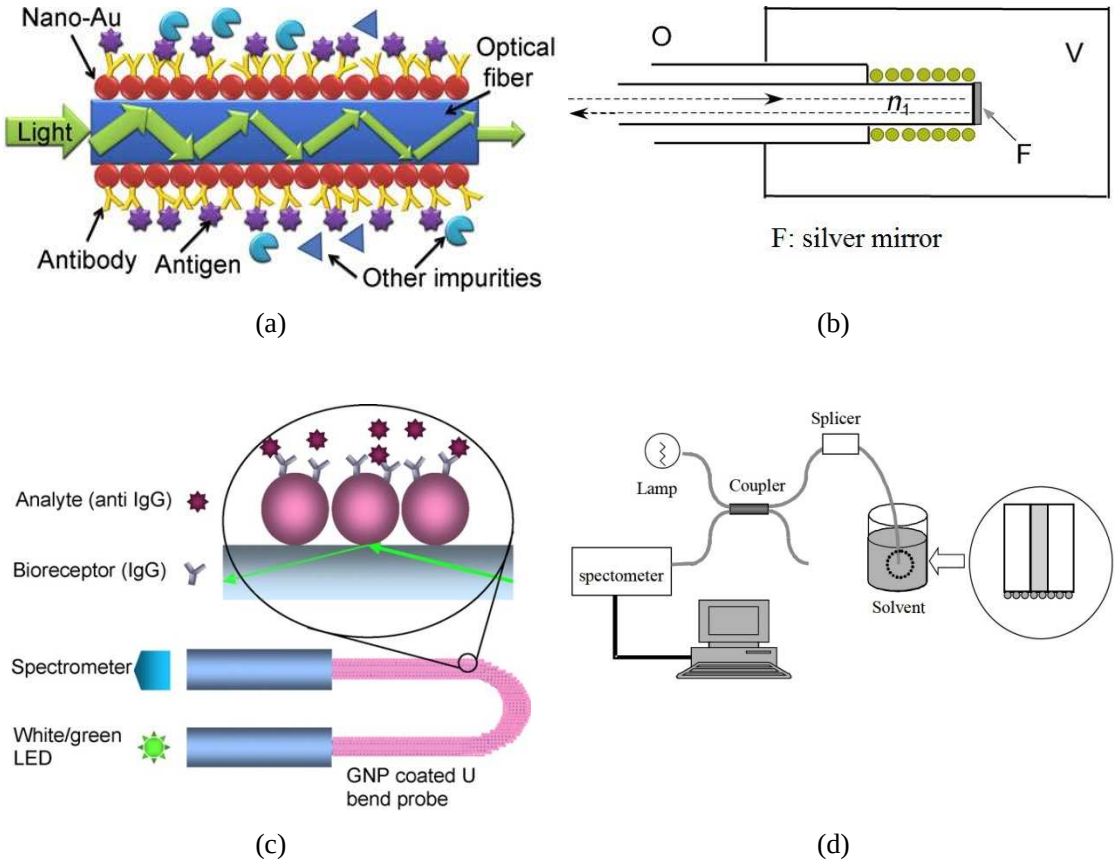

Fig. 2.23. Schematic illustration of optical fibre-based LSPR sensors with different configurations: (a) transmission-based LSPR optical fibre sensor [157], (b) reflection-based LSPR optical fibre sensor [150], (c) U-shaped LSPR optical fibre sensor [129], and (d) reflection-based LSPR optical fibre sensor with distal end coating [149].

2.3.5.3 Solution-phase-based LSPR sensor

The solution-phase-based LSPR sensors refer to the LSPR sensors with the GNPs suspending in the solution rather than immobilized on the substrates [80, 127, 137, 141, 163-166]. This sensor allows the surface modification and functionalization of GNPs as well as analytes detection to be carried out within the GNPs solution as shown in Fig. 2.24 (a). The fabrication of the solution-phase-based LSPR sensor often involves gentle vortexing to fully mix the functional molecules and GNPs, and multiple centrifugations to purify the functionalized GNPs. The analyte detection is normally conducted in a small container such as cuvette. A UV-Vis spectrophotometer used in the chip-based LSPR sensor is also applied for measuring the LSPR absorbance of the dispersed GNPs. For the solution-phase-based

LSPR sensors, there are two assays that are commonly employed for the analytes detection: LSPR sensing based on refractive index change and LSPR sensing based on nanoparticles aggregation. Which assay should be applied is normally dependent on the number of the binding sites of the target molecule. If the target molecule has only one binding site, it will be captured by only one functionalized GNP. The capture of target molecule will result in the refractive index change at the GNP surface and the corresponding LSPR absorbance change, such as a red-shift of the longitudinal plasmon band of the GNRs based LSPR sensor. However, if there are more than one binding sites on the surface for the target molecule, the same target molecule could be captured by GNPs as many as the amount of the binding sites theoretically.

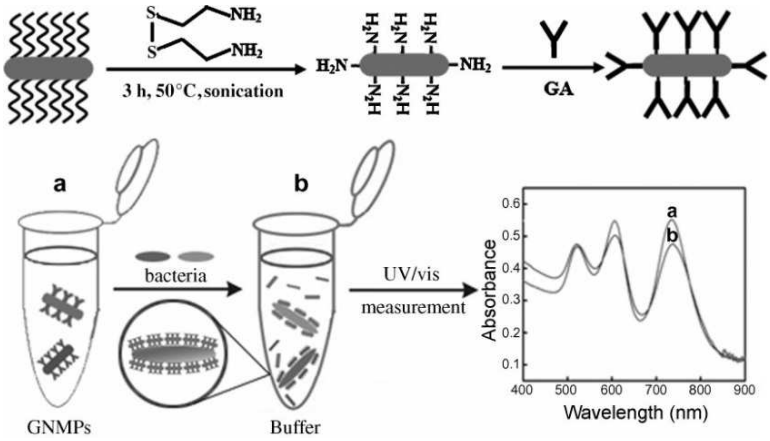

(a)

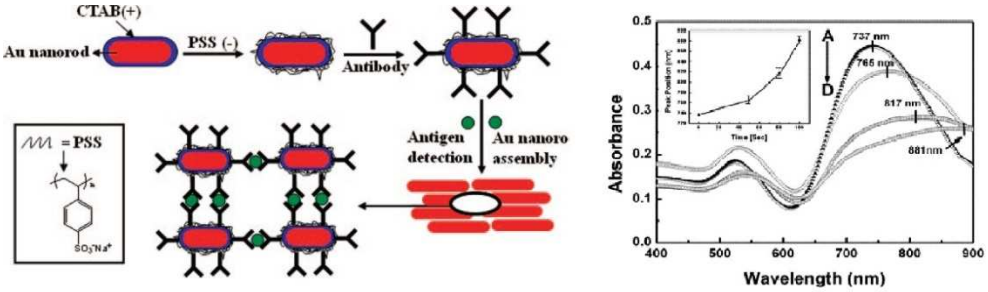

(b)

Fig. 2.24. (a) Schematic representation of the preparation of solution-phase-based LSPR sensor (top) and the detection of target molecules with many binding sites (bottom) [164], (b) schematic representation of the detection of target molecules with few binding sites through the assembly of GNPs (left) and the corresponding absorption spectra changing over a period of time from A to D (right) [165].

If the target molecule has many binding sites, a number of capturing nanoparticles would be bound to the same target molecule as demonstrated in Fig. 2.24 (a); if the target molecule only has few binding sites, it normally would induce the assembly of the capturing nanoparticles as illustrated in Fig. 2.24 (b). In either case, they all will result in the GNPs aggregation eventually. Correspondingly, the GNPs aggregation will not only cause a colour change in the GNPs solution that sometimes even can be identified by naked eye, but also result in a large shift the LSPR absorption spectra of GNPs. However, the aggregation also substantially distorts the original LSPR spectrum of dispersed GNPs, making the target molecules difficult to be accurately quantified. Compared to the substrate-based LSPR sensors, the preparation of the solution-phase-based LSPR sensors is easier. However, in terms of the long-term stability, the solution-phase-based LSPR sensors appear less stable than the substrate-based ones due to the aggregation and deposition of GNPs over a period of time.

2.3.6 Applications of LSPR sensors

Similar to SPR sensors, the majority of applications of LSPR sensors have been focused on the label-free biosensing. Compared to SPR biosensors, LSPR biosensor have shown advantages including competitive sensitivity, low-cost fabrication and flexible sensor design. Many SPR sensors employed in biosensing applications can be replaced by LSPR sensors. Therefore, the advantages of LSPR sensor have attracted more and more attentions and a significant amount of work has been done for the development of LSPR sensors for various biosensing applications in recent years. In this section, we briefly review the biosensing applications of LSPR sensors based on two widely used sensing strategies: refractive index change and MNPs aggregation. Some recent advances in LSPR biosensing are also included in this section.

2.3.6.1 LSPR biosensing based on refractive index change

Biosensing based on refractive index change is the basic sensing principle of LSPR biosensors. The refractive index change at the sensor surface, due to the target molecule binding, results in the variation of the parameters of the LSPR absorption spectrum, such as peak wavelength shift and absorbance change. Therefore, the analytes are able to be detected and quantified by monitoring these parameters. Numerous LSPR biosensing applications based on refractive index change have been reported. Nath and Chiltoki first reported a chip-

based LSPR label-free biosensor for the detection of streptavidin based on the well-known biotin- streptavidin interaction [167]. The sensor chip was fabricated by immobilizing a monolayer of spherical GNPs on the surface of an APTES modified glass coverslip. The surface of the immobilized GNPs was further functionalized with biotin which has extraordinary high affinity for streptavidin. The detection was performed by monitoring the absorbance change at a fixed wavelength using a commercial UV-Vis spectrophotometer in transmission mode. The LOD for streptavidin was found to be 16 nM. Later, the biosensor performance was significantly improved by optimizing the GNPs size and the LOD for streptavidin as low as 0.83 nM was achieved [145]. Base on the similar sensor configuration, the detection of streptavidin was also carried out by using a GNRs based LSPR biosensor developed by Chen *et al*. [168]. The sensor chip was fabricated by functionalizing the surface of GNRs previously immobilized on the MPTMS-modified glass slide surface with biotin molecules. This GNRs based sensor chip was found to have refractive index sensitivity nearly five times higher than that of GNSs based sensor chip reported by Nath and Chiltoki [168]. Instead of monitoring the absorbance change at a fixed wavelength, the peak wavelength shift of the longitudinal plasmon band of GNRs was employed for the detection of streptavidin, and the LOD was about 0.42 nM. Marinakos and co-workers also reported a similar GNRs based LSPR biosensor for detecting streptavidin, and the LOD of their sensor was found to be 94 pM and 19 nM corresponding to the detection carried out in PBS buffer and in serum, respectively [79]. Additionally, the detection of streptavidin using an optical fibre-based LSPR biosensor was also demonstrated [148]. The LOD of the spherical GNPs coated optical fibre LSPR sensor was determined to be 98 pM by using the intensity interrogation approach.

LSPR biosensors also have been widely applied for detecting the specific antibody-antigen recognition. A chip-based LSPR biosensor for detecting anti-human serum albumin (HSA) was reported by Fujiwara *et al*. [146]. In their work, GNSs with a mean diameter of 40 nm was synthesised and immobilized on the amine-modified glass slide. The surface of GNSs was further modified with MUA and functionalized with the capturing agent HSA. The LOD for the anti-HSA was found to be about 10 nM by monitoring the peak absorbance change due to the antigen-antibody specific binding. Mayer *et al.* developed a chip-based LSPR biosensor using GNRs for the detection of anti-rabbit IgG [91]. The GNRs were covalently immobilized on a glass slide and the GNRs surfaces were conjugated to rabbit IgG. The interaction between rabbit IgG and anti-rabbit IgG was monitored through the peak wavelength shift of the longitudinal plasmon band. The LOD for anti-rabbit IgG was as low as 1 nM. The detection of anti-human IgG using a U-shaped optical fibre LSPR biosensor

was demonstrated by Sai *et al* [29]. The sensor was fabricated by coating spherical GNPs on the decladed fibre core of a U-shaped multimode optical fibre followed by the functionalization of GNPs with human IgG molecules. The specific human IgG/anti-human IgG recognition was detected by measuring the absorbance change at a fixed wavelength. It was found that the LOD of the sensor for anti-human IgG was about 0.8 nM.

In addition to biotin-streptavidin and antigen-antibody interactions, LSPR biosensing based on refractive index change have also been applied to detect other bimolecular interactions, including deoxyribonucleic acid (DNA) hybridization [169], protein-carbohydrate [170], cytochrome-inhibitor [171] and aptamer-protein interactions [172].

2.3.6.2 LSPR biosensing based on MNPs aggregation

LSPR biosensors based on MNPs aggregation are suitable for fast detecting the presence of the target molecule with approximate quantification. The aggregation of the dispersed MNPs results in a visible colour change in MNPs solution and a large shift in the LSPR absorption spectrum of MNPs, which can be used for sensing purposes. Based on this principle, colorimetric LSPR biosensors based on GNPs aggregation for detecting DNA hybridization were developed [173-177]. In these assays, spherical GNPs were functionalized with thiolated non-complementary oligonucleotide. The addition of the target oligonucleotide, which is complementary to the immobilized oligonucleotide, leads to GNPs aggregation due to the DNA hybridization. The aggregation results in a colour change of GNPs solution from red to purple due to a red-shift in the LSPR absorption band of GNPs. The assembled nanoparticle can be separated by simply either changing the ionic strength of the solution or raising the temperature above the melting point of DNA, thus inducing a reversible DNA strands dehybridization. The colour changes in GNPs solution induced by GNPs aggregation allow a clear differentiation between complementary DNA strands and DNA strands with mismatches [175-177]. Colorimetric LSPR biosensors have also been used for the detection of adenosine and cocaine [178, 179]. In these detections, two bathes of spherical GNPs functionalized with two different DNA molecules were linked together by adenosine or cocaine aptamers via DNA hybridization, resulting in a colour change (from red to purple) in the GNPs solution due to the GNPs aggregation. In the presence of target molecules, adenosine or cocaine, the aptamer changed its structure to bind the target molecule, inducing the instability of the DNA hybridization. As a result, the assembled GNPs disassociated from each other, upon which the colour of the GNPs solution changed back from purple to red.

In addition to colorimetric biosensing, LSPR biosensors based on aggregation induced LSPR spectral change have also been developed for detecting antigen-antibody interaction. Thanh and Rosenzweig reported a generic aggregation-based LSPR immunoassay approach for the detection of anti-protein A [180]. Spherical GNPs were first functionalized with protein A molecules. Addition of anti-protein A induced the GNPs aggregation through the specific antigen-antibody interaction, which resulted in an absorbance change. The aggregation process was monitored at a fixed wavelength and the LOD for anti-protein A was found to be 1 μg/mL. GNRs were also employed for the aggregation-based LSPR biosensing applications. Wang et al. demonstrated the detection of human IgG through the assembly of GNRs driven by antibody-antigen recognition [165]. The surface of CTAB-capped GNRs were first modified by a negatively charged polyelectrolyte PSS to change the surface charge of GNRs. Such negatively charged were then functionalized with anti-human IgG via electrostatic interaction. The aggregation of anti-human IgG functionalized GNRs occurred after the addition of human IgG, which resulted in a red-shift in the longitudinal plasmon band of GNRs and broadening LSPR absorption spectra. The peak position of longitudinal plasmon band of GNRs was monitored during the aggregation process and the LOD for human IgG was about 60 ng/mL. The detection of a pervasive environmental toxin, microcystin-LR (MC-LR), using a LSPR biosensor based on the disassembly of GNRs was reported by Wang *et al*. [181]. Two batches of GNRs were functionalized with MC-LR antibodies and MC-LR analogues, which have affinity to MC-LR antibodies, respectively. The MC-LR antibodies and MC-LR analogues conjugated GNRs were then mixed together, forming assemblies of GNRs and resulting in a decrease in the LSPR absorbance. Addition of MC-LR led to a competition for the antibodies binding sites and a dissociation of assembled GNRs, thus gradually restoring the LSPR spectra of GNRs. By monitoring the peak absorbance change of longitudinal plasmon band during the disassembling process, the LOD for MC-LR was found to be 0.6 ng/mL for the side-by-side assemblies of GNRs and 0.03 ng/mL for the end-to-end assemblies.

Aggregation-based LSPR biosensors have also been used for the detection of other biomolecules, such as cysteine and glutathione amino acids [166], pathogens [164], concanavalin A [182] and streptavidin [183].

2.3.6.3 Advances in LSPR biosensing

Multiplex biosensing: As GNPs with different sizes and shapes possess different LSPR absorption bands, multiplex LSPR biosensing can be realized by employing different GNPs in the same assay. GNRs are often preferable to multiplex sensing for the reason that the longitudinal plasmon band of GNRs can be conveniently tuned by controlling the aspect ratio of GNRs. Yu and Irudayaraj demonstrated a multiplex biosensor for detecting multiple target molecules using GNRs with various aspect ratios. In their work, GNRs with three different aspect ratios were functionalized with three different antibodies, respectively, and mixed together to fabricate the solution-phased-based the multiplex biosensor. Three different longitudinal plasmon bands corresponding to the three aspect ratios appeared in the LSPR absorption spectra as shown in Fig. 2.25. The addition of one target molecules resulted in a significant red-shift in one of the longitudinal plasmon bands due to target specific binding and a small red-shift in the other two longitudinal plasmon bands due to non-specific binding (Fig. 2.25 (a)). This specific binding caused red-shift is large enough to be distinguished from the two small red-shifts induced by non-specific binding. Likewise, addition of two targets and three targets resulted in two and three clear red-shifts in longitudinal plasmon bands of the corresponding antibodies-conjugated GNRs, respectively (Fig. 2.25 (a) and (b)). Therefore, multiple targets can be detected at the same time by monitoring the wavelength shift in the corresponding longitudinal plasmon bands. Later, they applied this multiplex sensing technique to detect E. coli and salmonella for food safety applications [164]. Based on the same principle, Huang *et al*. developed a chip-based multiplex biosensor also using GNRs [92]. GNRs with various aspect ratios were immobilized on the separate glass slides, followed by functionalizing these GNRs with different antibodies respectively. These sensor chips were then assembled in a cuvette as the multiplex sensor. The multiplex sensing ability of the sensor was demonstrated by monitoring the peak absorbance change in each longitudinal plasmon band induced by the target specific binding.

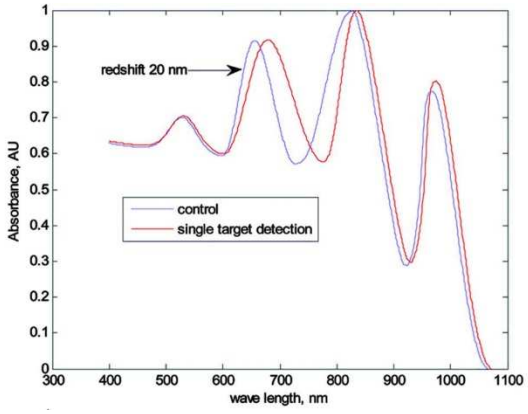

(a)

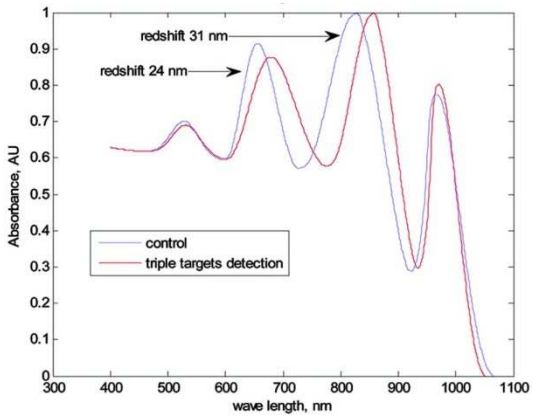

(b)

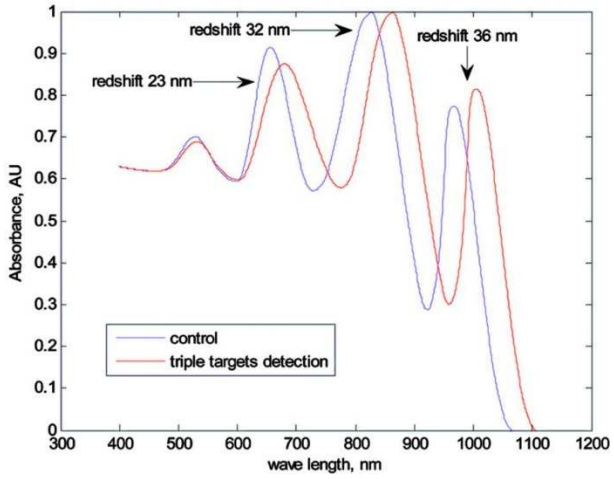

(c)

Fig. 2.25. Multiplexing detection of various targets using GNRs with different aspect ratios. (a) one target, (b) two targets and (c) three targets [163].

Single-nanoparticle based LSPR biosensing: most LSPR spectroscopy has been performed with ensembles of MNPs. However, each individual nanoparticle in the ensembles could serve as an independent LSPR sensor [81, 184]. Compared to the traditional nanoparticle array based LSPR sensors, single-nanoparticle based LSPR sensors have shown advantages such as higher sensitivity, lower detection limit and very small sample volumes requirement [77, 78]. Single-nanoparticle spectroscopy is normally performed by using a dark-filed microscopy system. Fig. 2.26 (a) shows an example of this in which a high-numerical aperture condenser brings white light to the sample and a low-numerical aperture microscope

objective collects the scattered light at low angles. The scattered light is then directed to a spectrometer and detector, such as a charge-coupled device camera, yielding an LSPR spectrum of the sample [77]. The sample is prepared by immobilizing MNPs on a transparent glass substrate. The label-free biosensing can be carried out by tracking the wavelength shift in the LSPR scattering spectrum of a single nanoparticle using the dark-filed microscopy as demonstrated in Fig. 2.26 (b). So far, MNPs with various nanostructures have been employed for developing single-nanoparticle based LSPR biosensors, such as silver nanoparticles [81], GNRs [184], GNSs [185], gold nanoholes [186] and gold nanorings [187]. Despite the advantages of these single-nanoparticle based LSPR sensors, the low single-to-noise ratio still remains as a big limitation for these sensors before they could be applied in practical applications in future [188, 189].

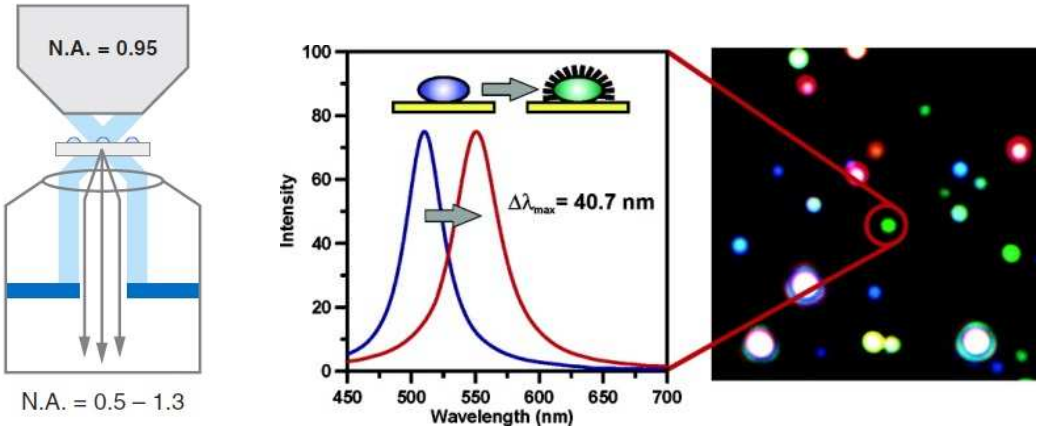

(a) (b)

Fig. 2.26. (a) Schematic representation of a dark-field microscopy system for measuring single-nanoparticle scattering spectra [77], (b) LSPR spectral shift induced by target molecules binding to a single silver nanoparticle (left), and the dark-field optical image of silver nanoparticles (right) [81].

2.4 Summary

As a powerful tool in biosensing area, a considerably significant amount of work on the development of both SPR and LSPR biosensors has been carried out so far. SPR sensing technique can be seen as the precursor to the LSPR technique. The two techniques have

some features in common, such as both are sensitive to refractive index change, but also have many differences between them. To better understand both the SPR and LSPR sensing techniques, it is necessary and important to have a good knowledge of their underpinning sensing mechanisms.

In this chapter, previous work reported in literature on the development of both SPR and LSPR sensors has been reviewed. The background, sensing principle and characteristics of both SPR and LSPR techniques have also been introduced, explained and compared. The fabrications of both SPR and LSPR sensors with various configurations have been described. The biosensing applications of both SPR and LSPR biosensors for detecting various target biomolecules have been thoroughly reviewed. Because GNRs have attracted more and more interests in recent years due to their unique optical properties, extensive research has been undertaken by the author on the development of GNRs based optical fibre LSPR biosensor and the use of a novel method for surface modification of GNRs. The details of the work are described and discussed in detail in the following chapters sequentially.

2.5 References

[1] R.W. Wood, On a remarkable case of uneven distribution of light in a diffraction grating spectrum, Philosophical Magazine, 4 (1902) 396-402.

[2] R.B.M. Schasfoort, A.J. Tudos, Handbook of surface plasmon resonance, RSC Publication, 2008.

[3] A. Otto, Exicitation of nonradiative surface plasma waves in silver by method of frustrated total reflection, Zeitschrift Fur Physik, 216 (1968) 398-410.

[4] E. Kretschm, H. Raether, Radiative decay of non radiative surface plasmons excited by light, Zeitschrift Fur Naturforschung Part A-astrophysik Physik Und Physikalische Chemie, 23 (1968) 2135-2136.

[5] I. Pockrand, J.D. Swalen, J.G. Gordon, M.R. Philpott, Surface-plasmon spectroscopy of organic monolayer assemblies, Surface Science, 74 (1978) 237-244.

[6] J.G. Gordon, S. Ernst, Surface-plasmons as a porbe of the electrochemical interface, Surface Science, 101 (1980) 499-506.

[7] B. Liedberg, C. Nylander, I. Lundstrom, Surface-plasmon resonance for gas-detection and biosensing, Sensors And Actuators, 4 (1983) 299-304.

[8] U. Jonsson, L. Fagerstam, B. Ivarsson, B. Johnsson, R. Karlsson, K. Lundh, S. Lofas, B. Persson, H. Roos, I. Ronnberg, S. Sjolander, E. Stenberg, R. Stahlberg, C. Urbaniczky, H. Ostlin, M. Malmqvist, Real-time biospecific interaction analysis using surface-plasmon resonance and a sensor chip technology, Biotechniques, 11 (1991) 620.

[9] J. Homola, S.S. Yee, G. Gauglitz, Surface plasmon resonance sensors: review, Sensors And Actuators B-Chemical, 54 (1999) 3-15.

[10] A.K. Sharma, R. Jha, B.D. Gupta, Fiber-optic sensors based on surface plasmon resonance: A comprehensive review, IEEE Sensensors Journal, 7 (2007) 1118-1129.

[11] K. Matsubara, S. Kawata, S. Minami, Optical chemical sensor based on surface-plasmon measurement, Applied Optics, 27 (1988) 1160-1163.

[12] B. Liedberg, I. Lundstrom, E. Stenberg, Principles of biosensing with an extended coupling matrix and surface-plasmon resonance, Sensors And Actuators B-Chemical, 11 (1993) 63-72.

[13] C. Nylander, B. Liedberg, T. Lind, Gas-detection by means of surface-plasmon resonance, Sensors And Actuators, 3 (1982) 79-88.

[14] M. Manuel, B. Vidal, R. Lopez, S. Alegret, J. Alonsochamarro, I. Garces, J. Mateo, Determination of probable alcohol yield in musts by means of an SPR optical sensor, Sensors And Actuators B-Chemical, 11 (1993) 455-459.

[15] L.M. Zhang, D. Uttamchandani, Optical chemical sensing employing surface-plasmon resonance, Electronics Letters, 24 (1988) 1469-1470.

[16] R.C. Jorgenson, S.S. Yee, A fiberoptic chemical sensor-based on surface-plasmon resonance, Sensors And Actuators B-Chemical, 12 (1993) 213-220.

[17] P.S. Vukusic, G.P. Bryanbrown, J.R. Sambles, Surface plasmon resonance on gratings as a novel means for gas sensing, Sensors And Actuators B-Chemical, 8 (1992) 155-160.

[18] J. Homola, Present and future of surface plasmon resonance biosensors, Analytical And Bioanalytical Chemistry, 377 (2003) 528-539.

[19] J. Homola, Surface plasmon resonance based sensors, Springer London, Limited, 2006.

[20] J. Homola, Surface plasmon resonance sensors for detection of chemical and biological species, Chemical Review, 108 (2008) 462-493.

[21] F. Villuendas, J. Pelayo, Optical fiber device for chemical sensing based on surface-plasmon excitation, Sensors And Actuators A-Physical, 23 (1990) 1142-1145.

[22] I. Garces, C. Aldea, J. Mateo, Four-layer chemical fiber optic plasmon-based sensor, Sensors And Actuators B-Chemical, 7 (1992) 771-774.

[23] L. Demaria, M. Martinelli, G. Vegetti, Fiber-optic sensor based on surface plasmon interrogation, Sensors And Actuators B-Chemical, 12 (1993) 221-223.

[24] R. Alonso, F. Villuendas, J. Tornos, J. Pelayo, New in-line optical-fiber sensor-based on surface plasmon excitation, Sensors And Actuators A-Physical, 37-8 (1993) 187-192.

[25] A.K. Sharma, B.D. Gupta, Comparison of performance parameters of conventional and nano-plasmonic fiber optic sensors, Plasmonics, 2 (2007) 51-54.

[26] J. Cao, E.K. Galbraith, T. Sun, K.T.V. Grattan, Cross-comparison of surface plasmon resonance-based optical fiber sensors with different coating structures, IEEE Sensors Journal, 12 (2012) 2355-2361.

[27] R.K. Verma, B.D. Gupta, Theoretical modelling of a bi-dimensional U-shaped surface plasmon resonance based fibre optic sensor for sensitivity enhancement, Journal Of Physics D-Applied Physics, 41 (2008).

[28] R.C. Jorgenson, S.S. Yee, Control of the dynamic-range and sensitivity of a surface-plasmon resonance based fiber optic sensor, Sensors And Actuators A-Physical, 43 (1994) 44-48.

[29] V.V.R. Sai, T. Kundu, S. Mukherji, Novel U-bent fiber optic probe for localized surface plasmon resonance based biosensor, Biosensors & Bioelectronics, 24 (2009) 2804-2809.

[30] J. Homola, R. Slavik, Fibre-optic sensor based on surface plasmon resonance, Electronics Letters, 32 (1996) 480-482.

[31] M. Piliarik, J. Homola, Z. Manikova, J. Ctyroky, Surface plasmon resonance sensor based on a single-mode polarization-maintaining optical fiber, Sensors And Actuators B-Chemical, 90 (2003) 236-242.

[32] M.H. Chiu, S.F. Wang, R.S. Chang, D-type fiber biosensor based on surface-plasmon resonance technology and heterodyne interferometry, Optics Letters, 30 (2005) 233-235.

[33] M.-H. Chiu, C.-H. Shih, Searching for optimal sensitivity of single-mode D-type optical fiber sensor in the phase measurement, Sensors And Actuators B-Chemical, 131 (2008) 596-601.

[34] M.-H. Chiu, C.-H. Shih, M.-H. Chi, Optimum sensitivity of single-mode D-type optical fiber sensor in the intensity measurement, Sensors And Actuators B-Chemical, 123 (2007) 1120-1124.

[35] H.-Y. Lin, W.-H. Tsai, Y.-C. Tsao, B.-C. Sheu, Side-polished multimode fiber biosensor based on surface plasmon resonance with halogen light, Applied Optics, 46 (2007) 800-806.

[36] B.D. Gupta, R.K. Verma, Surface plasmon resonance-based fiber optic sensors: principle, probe designs, and some applications, Journal Of Sensors, 2009 (2009).

[37] H.Y. Lin, W.H. Tsai, Y.C. Tsao, B.C. Sheu, Side-polished multimode fiber biosensor based on surface plasmon resonance with halogen light, Applied optics, 46 (2007) 800-806.

[38] S.F. Wang, M.H. Chiu, R.S. Chang, Numerical simulation of a D-type optical fiber sensor based on the Kretchmann's configuration and heterodyne interferometry, Sensors and Actuators B-Chemical, 114 (2006) 120-126.

[39] A.G. Mignani, R. Falciai, L. Ciaccheri, Evanescent wave absorption spectroscopy by means of bi-tapered multimode optical fibers, Applied Spectroscopy, 52 (1998) 546-551.

[40] J. Villatoro, D. Luna-Moreno, D. Monzon-Hernandez, Optical fiber hydrogen sensor for concentrations below the lower explosive limit, Sensors And Actuators B-Chemical, 110 (2005) 23-27.

[41] N. Diaz-Herrera, M.C. Navarrete, O. Esteban, A. Gonzalez-Cano, A fibre-optic temperature sensor based on the deposition of a thermochromic material on an adiabatic taper, Measurement And Science Technology, 15 (2004) 353-358.

[42] A. Leung, P.M. Shankar, R. Mutharasan, A review of fiber-optic biosensors, Sensors And Actuators B-Chemical, 125 (2007) 688-703.

[43] A.K. Sharma, B.D. Gupta, On the sensitivity and signal to noise ratio of a step-index fiber optic surface plasmon resonance sensor with bimetallic layers, Optics Communications, 245 (2005) 159-169.

[44] R.K. Verma, A.K. Sharma, B.D. Gupta, Surface plasmon resonance based tapered fiber optic sensor with different taper profiles, Optics Communicaitons, 281 (2008) 1486-1491.

[45] G.P. Anderson, J.P. Golden, F.S. Ligler, A fiber optic biosensor - combination tapered fibers designed for improved signal acquisition, Biosensors & Bioelectronics, 8 (1993) 249-256.

[46] H.Y. Lin, C.H. Huang, G.L. Cheng, N.K. Chen, H.C. Chui, Tapered optical fiber sensor based on localized surface plasmon resonance, Optics Express, 20 (2012) 21693-21701.

[47] Y.J. Chang, Y.C. Chen, H.L. Kuo, P.K. Wei, Nanofiber optic sensor based on the excitation of surface plasmon wave near fiber tip, Journal Of Biomedical Optics, 11 (2006).

[48] R.K. Verma, A.K. Sharma, B.D. Gupta, Modeling of tapered fiber-optic surface plasmon resonance sensor with enhanced sensitivity, IEEE Photonics Technology Letters, 19 (2007) 1786-1788.

[49] N. Diaz Herrera, O. Esteban, M.-C. Navarrete, A. Gonzalez-Cano, E. Benito-Pena, G. Orellana, Improved performance of SPR sensors by a chemical etching of tapered optical fibers, Optics And Lasers In Engeering, 49 (2011) 1065-1068.

[50] Y.Y. Shevchenko, J. Albert, Plasmon resonances in gold-coated tilted fiber Bragg gratings, Optics Letters, 32 (2007) 211-213.

[51] Y.J. He, Y.L. Lo, J.F. Huang, Optical-fiber surface-plasmon-resonance sensor employing long-period fiber gratings in multiplexing, Journal Of The Optical Society Of America B-Optical Physics, 23 (2006) 801-811.

[52] B. Lee, S. Roh, J. Park, Current status of micro- and nano-structured optical fiber sensors, Optical Fiber Technology, 15 (2009) 209-221.

[53] G. Nemova, R. Kashyap, Fiber-Bragg-grating-assisted surface plasmon-polariton sensor, Optics Letters, 31 (2006) 2118-2120.

[54] B. Spackova, M. Piliarik, P. Kvasnicka, C. Themistos, M. Rajarajan, J. Homola, Novel concept of multi-channel fiber optic surface plasmon resonance sensor, Sensors And Actuators B-Chemical, 139 (2009) 199-203.

[55] G. Nemova, R. Kashyap, Theoretical model of a planar integrated refractive index sensor based on surface plasmon-polariton excitation with a long period grating, Journal Of The Optical Society Of America B-Optical Physics, 24 (2007) 2696-2701.

[56] M.N. Weiss, R. Srivastava, H. Groger, Experimental investigation of a surface plasmon-based integrated-optic humidity sensor, Electronics Letters, 32 (1996) 842-843.

[57] A.K. Sharma, B.D. Gupta, Theoretical model of a fiber optic remote sensor based on surface plasmon resonance for temperature detection, Optical Fiber Technology, 12 (2006) 87-100.

[58] E.G. Ruiz, I. Garces, C. Aldea, M.A. Lopez, J. Mateo, J. Alonsochamarro, S. Alegret, Industrial-process sensor-based on surface-plasmon resonance (SPR) 1. Distillation process monitoring, Sensors And Actuators A-Physical, 37-8 (1993) 221-225.

[59] G.J. Ashwell, M.P.S. Roberts, Highly selective surface plasmon resonance sensor for NO2, Electronics Letters, 32 (1996) 2089-2091.

[60] G.A.J. Besselink, R.P.H. Kooyman, P. van Os, G.H.M. Engbers, R.B.M. Schasfoort, Signal amplification on planar and gel-type sensor surfaces in surface plasmon resonance-based detection of prostate-specific antigen, Analytical Biochemistry, 333 (2004) 165-173.

[61] L. Huang, G. Reekmans, D. Saerens, J.M. Friedt, F. Frederix, L. Francis, S. Muyldermans, A. Campitelli, C. Van Hoof, Prostate-specific antigen immunosensing based on mixed self-assembled monolayers, camel antibodies and colloidal gold enhanced sandwich assays, Biosensors & Bioelectronics, 21 (2005) 483-490.

[62] J.W. Chung, S.D. Kim, R. Bernhardt, J.C. Pyun, Application of SPR biosensor for medical diagnostics of human hepatitis B virus (hHBV), Sensors And Actuators B-Chemical, 111 (2005) 416-422.

[63] A. McGill, J. Greensill, R. Marsh, A.W. Craft, G.L. Toms, Detection of human respiratory syncytial virus genotype specific antibody responses in infants, Journal Of Medical Virology, 74 (2004) 492-498.

[64] P.P. Dillon, S.J. Daly, B.M. Manning, R. O'Kennedy, Immunoassay for the determination of morphine-3-glucuronide using a surface plasmon resonance-based biosensor, Biosensors & Bioelectronics, 18 (2003) 217-227.

[65] J.W. Chung, R. Bernhardt, J.C. Pyun, Sequential analysis of multiple analytes using a surface plasmon resonance (SPR) biosensor, Journal Of Immunological Methods, 311 (2006) 178-188.

[66] Q.M. Yu, S.F. Chen, A.D. Taylor, J. Homola, B. Hock, S.Y. Jiang, Detection of low-molecular-weight domoic acid using surface plasmon resonance sensor, Sensors And Actuators B-Chemical, 107 (2005) 193-201.

[67] A.J. Tudos, E.R. Lucas-van den Bos, E.C.A. Stigter, Rapid surface plasmon resonance-based inhibition assay of deoxynivalenol, Journal Of Agricultural And Food Chemistry, 51 (2003) 5843-5848.

[68] M.B. Caselunghe, J. Lindeberg, Biosensor-based determination of folic acid in fortified food, Food Chemistry, 70 (2000) 523-532.

[69] I. Caelen, A. Kalman, L. Wahlstrom, Biosensor-based determination of riboflavin in milk samples, Analytical chemistry, 76 (2004) 137-143.

[70] I. Mohammed, W.M. Mullett, E.P.C. Lai, J.M. Yeung, Is biosensor a viable method for food allergen detection?, Analytica Chimica Acta, 444 (2001) 97-102.

[71] M. Farre, E. Martinez, J. Ramon, A. Navarro, J. Radjenovic, E. Mauriz, L. Lechuga, M.P. Marco, D. Barcelo, Part per trillion determination of atrazine in natural water samples by a surface plasmon resonance immunosensor, Analytical And Bioanalytical Chemistry, 388 (2007) 207-214.

[72] N. Miura, M. Sasaki, K.V. Gobi, C. Kataoka, Y. Shoyama, Highly sensitive and selective surface plasmon resonance sensor for detection of sub-ppb levels of benzo a pyrene by indirect competitive immunoreaction method, Biosensors & Bioelectronics, 18 (2003) 953-959.

[73] N. Soh, T. Tokuda, T. Watanabe, K. Mishima, T. Imato, T. Masadome, Y. Asano, S. Okutani, O. Niwa, S. Brown, A surface plasmon resonance immunosensor for detecting a dioxin precursor using a gold binding polypeptide, Talanta, 60 (2003) 733-745.

[74] A. Larsson, J. Angbrant, J. Ekeroth, P. Mansson, B. Liedberg, A novel biochip technology for detection of explosives - TNT: Synthesis, characterisation and application, Sensors And Actuators B-Chemical, 113 (2006) 730-748.

[75] K. Ock, G. Jang, Y. Roh, S. Kim, J. Kim, K. Koh, Optical detection of Cu2+ ion using a SQ-dye containing polymeric thin-film on Au surface, Microchemical Journal, 70 (2001) 301-305.

[76] S. Eustis, M.A. El-Sayed, Why gold nanoparticles are more precious than pretty gold: Noble metal surface plasmon resonance and its enhancement of the radiative and nonradiative properties of nanocrystals of different shapes, Chemical Society Reviews, 35 (2006) 209-217.

[77] K.A. Willets, R.P. Van Duyne, Localized surface plasmon resonance spectroscopy and sensing, Annual Review Of Physical Chemistry, 58 (2007) 267-297.

[78] J.N. Anker, W.P. Hall, O. Lyandres, N.C. Shah, J. Zhao, R.P. Van Duyne, Biosensing with plasmonic nanosensors, Nature Materials, 7 (2008) 442-453.

[79] S.M. Marinakos, S. Chen, A. Chilkoti, Plasmonic detection of a model analyte in serum by a gold nanorod sensor, Analytical Chemistry, 79 (2007) 5278-5283.

[80] M. Potara, A.M. Gabudean, S. Astilean, Solution-phase, dual LSPR-SERS plasmonic sensors of high sensitivity and stability based on chitosan-coated anisotropic silver nanoparticles, Journal Of Materials Chemistry, 21 (2011) 3625-3633.

[81] A.D. McFarland, R.P. Van Duyne, Single silver nanoparticles as real-time optical sensors with zeptomole sensitivity, Nano Letters, 3 (2003) 1057-1062.

[82] X. Huang, S. Neretina, M.A. El-Sayed, Gold nanorods: from synthesis and properties to biological and biomedical applications, Advanced Materials, 21 (2009) 4880-4910.

[83] L. Vigderman, B.P. Khanal, E.R. Zubarev, Functional gold nanorods: synthesis, self-assembly, and sensing applications, Advanced Materials, 24 (2012) 4811-4841.

[84] Z.G. Xie, J. Tao, Y.H. Lu, K.Q. Lin, J. Yan, P. Wang, H. Ming, Polymer optical fiber SERS sensor with gold nanorods, Optics Communications, 282 (2009) 439-442.

[85] C.J. Murphy, A.M. Gole, S.E. Hunyadi, J.W. Stone, P.N. Sisco, A. Alkilany, B.E. Kinard, P. Hankins, Chemical sensing and imaging with metallic nanorods, Chemical Communications, (2008) 544-557.

[86] X. Huang, I.H. El-Sayed, W. Qian, M.A. El-Sayed, Cancer cell imaging and photothermal therapy in the near-infrared region by using gold nanorods, Journal Of The American Chemical Society, 128 (2006) 2115-2120.

[87] V. Sharma, K. Park, M. Srinivasarao, Colloidal dispersion of gold nanorods: Historical background, optical properties, seed-mediated synthesis, shape separation and self-assembly, Materials Science & Engineering R-Reports, 65 (2009) 1-38.

[88] E. Hutter, J.H. Fendler, Exploitation of localized surface plasmon resonance, Advanced Materials, 16 (2004) 1685-1706.

[89] S. Link, M.A. El-Sayed, Shape and size dependence of radiative, non-radiative and photothermal properties of gold nanocrystals, International Reviews In Physical Chemistry, 19 (2000) 409-453.

[90] S. Link, M.A. Ei-Sayed, Optical properties and ultrafast dynamics of metallic nanocrystals, Annual Review Of Physical Chemistry, 54 (2003) 331-366.

[91] K.M. Mayer, S. Lee, H. Liao, B.C. Rostro, A. Fuentes, P.T. Scully, C.L. Nehl, J.H. Hafner, A label-free immunoassay based upon localized surface plasmon resonance of gold nanorods, ACS Nano, 2 (2008) 687-692.

[92] H. Huang, C.C. He, Y.L. Zeng, X.D. Xia, X.Y. Yu, P.G. Yi, Z. Chen, A novel label-free multi-throughput optical biosensor based on localized surface plasmon resonance, Biosensors & Bioelectronics, 24 (2009) 2255-2259.

[93] E. Petryayeva, U.J. Krull, Localized surface plasmon resonance: Nanostructures, bioassays and biosensing-a review, Analytica Chimica Acta, 706 (2011) 8-24.

[94] K.M. Mayer, J.H. Hafner, Localized surface plasmon resonance sensors, Chemical Reviews, 111 (2011) 3828-3857.

[95] R. Gans, Über die form ultramikroskopischer goldteilchen, Annalen Der Physik, 342 (1912) 881-900.

[96] C.A. Foss, G.L. Hornyak, J.A. Stockert, C.R. Martin, Template-synthesized nanoscopic gold particles - optical-spectra and the effects of particle-size and shape, Journal Of Physical Chemistry, 98 (1994) 2963-2971.

[97] S. Link, M.B. Mohamed, M.A. El-Sayed, Simulation of the optical absorption spectra of gold nanorods as a function of their aspect ratio and the effect of the medium dielectric constant, Journal Of Physical Chemistry b, 103 (1999) 3073-3077.

[98] M. Hu, J. Chen, Z.-Y. Li, L. Au, G.V. Hartland, X. Li, M. Marquez, Y. Xia, Gold nanostructures: engineering their plasmonic properties for biomedical applications, Chemical Society Reviews, 35 (2006) 1084-1094.

[99] J. Perez-Juste, I. Pastoriza-Santos, L.M. Liz-Marzan, P. Mulvaney, Gold nanorods: Synthesis, characterization and applications, Coord. Chemical Reviews, 249 (2005) 1870-1901.

[100] L.S. Jung, C.T. Campbell, T.M. Chinowsky, M.N. Mar, S.S. Yee, Quantitative interpretation of the response of surface plasmon resonance sensors to adsorbed films, Langmuir : The ACS Journal Of Surfaces And Colloids, 14 (1998) 5636-5648.

[101] A.J. Haes, R.P. Van Duyne, A nanoscale optical blosensor: Sensitivity and selectivity of an approach based on the localized surface plasmon resonance spectroscopy of triangular silver nanoparticles, Journal Of The American Chemical Society, 124 (2002) 10596-10604.

[102] N.R. Jana, L. Gearheart, C.J. Murphy, Seed-mediated growth approach for shape-controlled synthesis of spheroidal and rod-like gold nanoparticles using a surfactant template, Advanced Materials, 13 (2001) 1389-1393.

[103] N.R. Jana, L. Gearheart, C.J. Murphy, Wet chemical synthesis of high aspect ratio cylindrical gold nanorods, Journal Of Physical Chemistry B, 105 (2001) 4065-4067.

[104] B. Nikoobakht, M.A. El-Sayed, Preparation and growth mechanism of gold nanorods (NRs) using seed-mediated growth method, Chemistry Of Materials, 15 (2003) 1957-1962.

[105] Y.Y. Yu, S.S. Chang, C.L. Lee, C.R.C. Wang, Gold nanorods: electrochemical synthesis and optical properties, Journal Of Physical Chemistry B, 101 (1997) 6661-6664.

[106] S.S. Chang, C.W. Shih, C.D. Chen, W.C. Lai, C.R.C. Wang, The shape transition of gold nanorods, Langmuir : The ACS Journal Of Surfaces And Colloids, 15 (1999) 701-709.

[107] R.M. Penner, C.R. Martin, Preparation and electrochemical characterization of ultramicroelectrode ensembles, Analytical Chemistry, 59 (1987) 2625-2630.

[108] C.R. Martin, Nanomaterials: a membrane-based synthetic approach, Science, 266 (1994) 1961-1966.

[109] C.R. Martin, Membrane-based synthesis of nanomaterials, Chemistry Of Materials, 8 (1996) 1739-1746.

[110] G.L. Hornyak, C.J. Patrissi, C.R. Martin, Fabrication, characterization, and optical properties of gold nanoparticle/porous alumina composites: The nonscattering Maxwell-Garnett limit, Journal Of Physical Chemistry B, 101 (1997) 1548-1555.

[111] B.M.I. van der Zande, M.R. Bohmer, L.G.J. Fokkink, C. Schonenberger, Colloidal dispersions of gold rods: synthesis and optical properties, Langmuir : The ACS Journal Of Surfaces And Colloids, 16 (2000) 451-458.

[112] A. Boltasseva, Plasmonic components fabrication via nanoimprint, Journal Of Optics A-Pure And Applied Optics, 11 (2009).

[113] L. Billot, M.L. de la Chapelle, A.S. Grimault, A. Vial, D. Barchiesi, J.L. Bijeon, P.M. Adam, P. Royer, Surface enhanced Raman scattering on gold nanowire arrays: Evidence of strong multipolar surface plasmon resonance enhancement, Chemical Physics Letters, 422 (2006) 303-307.

[114] F. Kim, J.H. Song, P.D. Yang, Photochemical synthesis of gold nanorods, Journal Of The American Chemical Society, 124 (2002) 14316-14317.

[115] O.R. Miranda, T.S. Ahmadi, Effects of intensity and energy of CWUV light on the growth of gold nanorods, Journal Of Physical Chemistry B, 109 (2005) 15724-15734.

[116] N. Taub, O. Krichevski, G. Markovich, Growth of gold nanorods on surfaces, Journal Of Physical Chemistry B, 107 (2003) 11579-11582.

[117] Y.J. Kim, G. Cho, J.H. Song, Synthesis of size and shape-selective Au nanocrystals via proton beam irradiation, Nuclear instruments & Methods In Physics Research Section B-Beam Interactions With Materials And Atoms, 246 (2006) 351-354.

[118] G. Canizal, J.A. Ascencio, J. Gardea-Torresday, M.J. Yacaman, Multiple twinned gold nanorods grown by bio-reduction techniques, Journal Of Nanoparticle Research, 3 (2001) 475-481.

[119] Y.J. Zhu, X.L. Hu, Microwave-polyol preparation of single-crystalline gold nanorods and nanowires, Chemistry Letters, 32 (2003) 1140-1141.

[120] J.M. Cao, X.J. Ma, M.B. Zheng, J.S. Liu, H.M. Ji, Solvothermal preparation of single-crystalline gold nanorods in novel nonaqueous microemulsions, Chemistry Letters, 34 (2005) 730-731.

[121] C.J. Murphy, L.B. Thompson, D.J. Chernak, J.A. Yang, S.T. Sivapalan, S.P. Boulos, J. Huang, A.M. Alkilany, P.N. Sisco, Gold nanorod crystal growth: From seed-mediated synthesis to nanoscale sculpting, Current Opinion In Colloid & Interface Science, 16 (2011) 128-134.

[122] B. Nikoobakht, M.A. El-Sayed, Evidence for bilayer assembly of cationic surfactants on the surface of gold nanorods, Langmuir : The ACS Journal Of Surfaces And Colloids, 17 (2001) 6368-6374.

[123] B.C. Rostro-Kohanloo, L.R. Bickford, C.M. Payne, E.S. Day, L.J.E. Anderson, M. Zhong, S. Lee, K.M. Mayer, T. Zal, L. Adam, C.P.N. Dinney, R.A. Drezek, J.L. West, J.H. Hafner, The stabilization and targeting of surfactant-synthesized gold nanorods, Nanotechnology, 20 (2009).

[124] A.P. Leonov, J. Zheng, J.D. Clogston, S.T. Stern, A.K. Patri, A. Wei, Detoxification of gold nanorods by treatment with polystyrenesulfonate, ACS Nano, 2 (2008) 2481-2488.

[125] E.E. Connor, J. Mwamuka, A. Gole, C.J. Murphy, M.D. Wyatt, Gold nanoparticles are taken up by human cells but do not cause acute cytotoxicity, Small, 1 (2005) 325-327.

[126] N.J. Durr, T. Larson, D.K. Smith, B.A. Korgel, K. Sokolov, A. Ben-Yakar, Two-photon luminescence imaging of cancer cells using molecularly targeted gold nanorods, Nano Letters, 7 (2007) 941-945.

[127] A. Gole, C.J. Murphy, Biotin-streptavidin-induced aggregation of gold nanorods: Tuning rod-rod orientation, Langmuir : The ACS Journal Of Surfaces And Colloids, 21 (2005) 10756-10762.

[128] A. Gole, C.J. Murphy, Polyelectrolyte-coated gold nanorods: Synthesis, characterization and immobilization, Chemistry Of Materials, 17 (2005) 1325-1330.

[129] C.S. Ah, S. Do Hong, D.J. Jang, Preparation of AucoreAgshell nanorods and characterization of their surface plasmon resonances, Journal Of Physical Chemistry B, 105 (2001) 7871-7873.

[130] M.Z. Liu, P. Guyot-Sionnest, Synthesis and optical characterization of Au/Ag core/shell nanorods, Journal Of Physical Chemistry B, 108 (2004) 5882-5888.

[131] C.C. Huang, Z.S. Yang, H.T. Chang, Synthesis of dumbbell-shaped Au-Ag core-shell nanorods by seed-mediated growth under alkaline conditions, Langmuir : The ACS Journal Of Surfaces And Colloids, 20 (2004) 6089-6092.

[132] L.M. Liz-Marzan, M. Giersig, P. Mulvaney, Synthesis of nanosized gold-silica core-shell particles, Langmuir : The ACS Journal Of Surfaces And Colloids, 12 (1996) 4329-4335.

[133] S.O. Obare, N.R. Jana, C.J. Murphy, Preparation of polystyrene- and silica-coated gold nanorods and their use as templates for the synthesis of hollow nanotubes, Nano Letters, 1 (2001) 601-603.

[134] J. Perez-Juste, M.A. Correa-Duarte, L.M. Liz-Marzan, Silica gels with tailored, gold nanorod-driven optical functionalities, Applied Surface Science, 226 (2004) 137-143.

[135] I. Gorelikov, N. Matsuura, Single-step coating of mesoporous silica on cetyltrimethyl ammonium bromide-capped nanoparticles, Nano Letters, 8 (2008) 369-373.

[136] S. Pierrat, I. Zins, A. Breivogel, C. Sonnichsen, Self-assembly of small gold colloids with functionalized gold nanorods, Nano Letters, 7 (2007) 259-263.

[137] H.W. Liao, J.H. Hafner, Gold nanorod bioconjugates, Chemistry Of Materials, 17 (2005) 4636-4641.

[138] T. Niidome, Y. Akiyama, K. Shimoda, T. Kawano, T. Mori, Y. Katayama, Y. Niidome, In vivo monitoring of intravenously injected gold nanorods using near-infrared light, Small, 4 (2008) 1001-1007.

[139] T. Niidome, M. Yamagata, Y. Okamoto, Y. Akiyama, H. Takahashi, T. Kawano, Y. Katayama, Y. Niidome, PEG-modified gold nanorods with a stealth character for in vivo applications, Journal Of Controlled Release, 114 (2006) 343-347.

[140] D. Bartczak, A.G. Kanaras, Preparation of peptide-functionalized gold nanoparticles using one pot EDC/Sulfo-NHS coupling, Langmuir : The ACS Journal Of Surfaces And Colloids, 27 (2011) 10119-10123.

[141] C. Yu, L. Varghese, J. Irudayaraj, Surface modification of cetyltrimethylammonium bromide-capped gold nanorods to make molecular probes, Langmuir : The ACS Journal Of Surfaces And Colloids, 23 (2007) 9114-9119.

[142] B. Thierry, J. Ng, T. Krieg, H.J. Griesser, A robust procedure for the functionalization of gold nanorods and noble metal nanoparticles, Chemical Communications, (2009) 1724-1726.

[143] Q. Dai, J. Coutts, J. Zou, Q. Huo, Surface modification of gold nanorods through a place exchange reaction inside an ionic exchange resin, Chemical Communications, (2008) 2858-2860.

[144] H.W. Huang, C.R. Tang, Y.L. Zeng, X.Y. Yu, B. Liao, X.D. Xia, P.G. Yi, P.K. Chu, Label-free optical biosensor based on localized surface plasmon resonance of immobilized gold nanorods, Colloid And Surface B-Biointerfaces, 71 (2009) 96-101.

[145] N. Nath, A. Chilkoti, Label-free biosensing by surface plasmon resonance of nanoparticles on glass: optimization of nanoparticle size, Analytical Chemistry, 76 (2004) 5370-5378.

[146] K. Fujiwara, H. Watarai, H. Itoh, E. Nakahama, N. Ogawa, Measurement of antibody binding to protein immobilized on gold nanoparticles by localized surface plasmon spectroscopy, Analytical And Bioanalytical Chemistry, 386 (2006) 639-644.

[147] K.C. Grabar, R.G. Freeman, M.B. Hommer, M.J. Natan, Preparation and characterization of au colloid monolayers, Analytical Chemistry, 67 (1995) 735-743.

[148] S.F. Cheng, L.K. Chau, Colloidal gold-modified optical fiber for chemical and biochemical sensing, Analytical Chemistry, 75 (2003) 16-21.

[149] K. Kajikawa, K. Mitsui, Optical fiber biosensor based on localized surface plasmon resonance in gold nanoparticles, Nanosensing: Materials And Devices, (2004) 494-501.

[150] T.J. Lin, C.T. Lou, Reflection-based localized surface plasmon resonance fiber-optic probe for chemical and biochemical sensing at high-pressure conditions, Journal Of Supercritical Fluids, 41 (2007) 317-325.

[151] T.J. Lin, M.F. Chung, Detection of cadmium by a fiber-optic biosensor based on localized surface plasmon resonance, Biosensors & Bioelectronics, 24 (2009) 1213-1218.

[152] W.H. Ni, H.J. Chen, X.S. Kou, M.H. Yeung, J.F. Wang, Optical fiber-excited surface plasmon resonance spectroscopy of single and ensemble gold nanorods, Journal Of Physical Chemsitry C, 112 (2008) 8105-8109.

[153] K. Mitsui, Y. Handa, K. Kajikawa, Optical fiber affinity biosensor based on localized surface plasmon resonance, Applied Physics Letters, 85 (2004) 4231-4233.

[154] S.K. Srivastava, V. Arora, S. Sapra, B.D. Gupta, Localized surface plasmon resonance-based fiber optic U-shaped biosensor for the detection of blood glucose, Plasmonics, 7 (2012) 261-268.

[155] Y.B. Lin, Y. Zou, R.G. Lindquist, A reflection-based localized surface plasmon resonance fiber-optic probe for biochemical sensing, Biomedical Optics Express, 2 (2011) 478-484.

[156] R. Dutta, R. Bharadwaj, S. Mukherji, T. Kundu, Study of localized surface-plasmon-resonance-based optical fiber sensor, Applied Optics, 50 (2011) E138-E144.

[157] C.H. Chen, T.C. Tsao, W.Y. Li, W.C. Shen, C.W. Cheng, J.L. Tang, C.P. Jen, L.K. Chau, W.T. Wu, Novel U-shape gold nanoparticles-modified optical fiber for localized plasmon resonance chemical sensing, Microsystem Technologies, 16 (2010) 1207-1214.

[158] T.J. Lin, M.F. Chung, Using monoclonal antibody to determine lead ions with a localized surface plasmon resonance fiber-optic biosensor, Sensors, 8 (2008) 582-593.

[159] B.Y. Hsieh, Y.F. Chang, M.Y. Ng, W.C. Liu, C.H. Lin, H.T. Wu, C. Chou, Localized surface plasmon coupled fluorescence fiber-optic biosensor with gold nanoparticles, Analytical Chemistry, 79 (2007) 3487-3493.

[160] L.K. Chau, Y.F. Lin, S.F. Cheng, T.J. Lin, Fiber-optic chemical and biochemical probes based on localized surface plasmon resonance, Sensors And Actuators B-Chemical, 113 (2006) 100-105.

[161] J.L. Tang, S.F. Cheng, W.T. Hsu, T.Y. Chiang, L.K. Chau, Fiber-optic biochemical sensing with a colloidal gold-modified long period fiber grating, Sensors And Actuators B-Chemical, 119 (2006) 105-109.

[162] J.L. Tang, J.N. Wang, Chemical sensing sensitivity of long-period grating sensor enhanced by colloidal gold nanoparticles, Sensors, 8 (2008) 171-184.

[163] C. Yu, J. Irudayaraj, Multiplex biosensor using gold nanorods, Analytical Chemistry, 79 (2007) 572-579.

[164] C. Wang, J. Irudayaraj, Gold nanorod probes for the detection of multiple pathogens, Small, 4 (2008) 2204-2208.

[165] C.G. Wang, Y. Chen, T.T. Wang, Z.F. Ma, Z.M. Su, Biorecognition-driven self-assembly of gold nanorods: A rapid and sensitive approach toward antibody sensing, Chemistry Of Materials, 19 (2007) 5809-5811.

[166] P.K. Sudeep, S.T.S. Joseph, K.G. Thomas, Selective detection of cysteine and glutathione using gold nanorods, Journal Of The American Chemical Society, 127 (2005) 6516-6517.

[167] N. Nath, A. Chilkoti, A colorimetric gold nanoparticle sensor to interrogate biomolecular interactions in real time on a surface, Analytical Chemistry, 74 (2002) 504-509.

[168] C.D. Chen, S.F. Cheng, L.K. Chau, C.R.C. Wang, Sensing capability of the localized surface plasmon resonance of gold nanorods, Biosensors & Bioelectronics, 22 (2007) 926-932.

[169] S.Y. Yoo, D.K. Kim, T.J. Park, E.K. Kim, E. Tamiya, S.Y. Lee, Detection of the most common corneal dystrophies caused by BIGH3 gene point mutations using a multispot gold-capped nanoparticle array chip, Analytical Chemistry, 82 (2010) 1349-1357.

[170] S. Morokoshi, K. Ohhori, K. Mizukami, H. Kitano, Sensing capabilities of colloidal gold modified with a self-assembled monolayer of a glucose-carrying polymer chain on a glass substrate, Langmuir : The ACS Journal Of Surfaces And Colloids, 20 (2004) 8897-8902.

[171] A.J. Haes, S.L. Zou, J. Zhao, G.C. Schatz, R.P. Van Duyne, Localized surface plasmon resonance spectroscopy near molecular resonances, Journal Of The American Chemical Society, 128 (2006) 10905-10914.

[172] T.J. Lin, K.T. Huang, C.Y. Liu, Determination of organophosphorous pesticides by a novel biosensor based on localized surface plasmon resonance, Biosensors & Bioelectronics, 22 (2006) 513-518.

[173] C.A. Mirkin, R.L. Letsinger, R.C. Mucic, J.J. Storhoff, A DNA-based method for rationally assembling nanoparticles into macroscopic materials, Nature, 382 (1996) 607-609.

[174] R.A. Reynolds, C.A. Mirkin, R.L. Letsinger, Homogeneous, nanoparticle-based quantitative colorimetric detection of oligonucleotides, Journal Of The American Chemical Society, 122 (2000) 3795-3796.

[175] R. Elghanian, J.J. Storhoff, R.C. Mucic, R.L. Letsinger, C.A. Mirkin, Selective colorimetric detection of polynucleotides based on the distance-dependent optical properties of gold nanoparticles, Science, 277 (1997) 1078-1081.

[176] J.J. Storhoff, R. Elghanian, R.C. Mucic, C.A. Mirkin, R.L. Letsinger, One-pot colorimetric differentiation of polynucleotides with single base imperfections using gold nanoparticle probes, Journal Of The American Chemical Society, 120 (1998) 1959-1964.

[177] J.J. Storhoff, A.A. Lazarides, R.C. Mucic, C.A. Mirkin, R.L. Letsinger, G.C. Schatz, What controls the optical properties of DNA-linked gold nanoparticle assemblies?, Journal Of The American Chemical Society, 122 (2000) 4640-4650.

[178] J.W. Liu, Y. Lu, Fast colorimetric sensing of adenosine and cocaine based on a general sensor design involving aptamers and nanoparticles, Angewandte Chemie International Edition, 45 (2006) 90-94.

[179] J. Zhang, L.H. Wang, D. Pan, S.P. Song, F.Y.C. Boey, H. Zhang, C.H. Fan, Visual cocaine detection with gold nanoparticles and rationally engineered aptamer structures, Small, 4 (2008) 1196-1200.

[180] N.T.K. Thanh, Z. Rosenzweig, Development of an aggregation-based immunoassay for anti-protein A using gold nanoparticles, Analytical Chemistry, 74 (2002) 1624-1628.

[181] L.B. Wang, Y.Y. Zhu, L.G. Xu, W. Chen, H. Kuang, L.Q. Liu, A. Agarwal, C.L. Xu, N.A. Kotov, Side-by-side and end-to-end gold nanorod assemblies for environmental toxin sensing, Angewandte Chemie International Edition, 49 (2010) 5472-5475.

[182] D.C. Hone, A.H. Haines, D.A. Russell, Rapid, quantitative colorimetric detection of a lectin using mannose-stabilized gold nanoparticles, Langmuir : The ACS Journal Of Surfaces And Colloids, 19 (2003) 7141-7144.

[183] S. Connolly, D. Fitzmaurice, Programmed assembly of gold nanocrystals in aqueous solution, Advanced Materials, 11 (1999) 1202-1205.

[184] G.J. Nusz, S.M. Marinakos, A.C. Curry, A. Dahlin, F. Hook, A. Wax, A. Chilkoti, Label-free plasmonic detection of biomolecular binding by a single gold nanorod, Analytical Chemistry, 80 (2008) 984-989.

[185] G. Raschke, S. Kowarik, T. Franzl, C. Sonnichsen, T.A. Klar, J. Feldmann, A. Nichtl, K. Kurzinger, Biomolecular recognition based on single gold nanoparticle light scattering, Nano Letters, 3 (2003) 935-938.

[186] T. Rindzevicius, Y. Alaverdyan, A. Dahlin, F. Hook, D.S. Sutherland, M. Kall, Plasmonic sensing characteristics of single nanometric holes, Nano Letters, 5 (2005) 2335-2339.

[187] E.M. Larsson, J. Alegret, M. Kall, D.S. Sutherland, Sensing characteristics of NIR localized surface plasmon resonances in gold nanorings for application as ultrasensitive biosensors, Nano Letters, 7 (2007) 1256-1263.

[188] B. Sepulveda, P.C. Angelome, L.M. Lechuga, L.M. Liz-Marzan, LSPR-based nanobiosensors, Nano Today, 4 (2009) 244-251.

[189] A.B. Dahlin, S. Chen, M.P. Jonsson, L. Gunnarsson, M. Kall, F. Hook, High-resolution microspectroscopy of plasmonic nanostructures for miniaturized biosensing, Analytical Chemistry, 81 (2009) 6572-6580.

Chapter 3

Fabrication and characterization of novel GNR-based LSPR optical fibre sensors

3.1 Introduction

Compared to other types of LSPR sensors, optical fibre-based LSPR sensors have shown many advantages including small sample volume requirement, simplified optical design, remote sensing capability and resistance to electromagnetic interference [1, 2]. In light of such advantages, extensive research has been undertaken to develop a number of interesting and promising optical fibre-based LSPR sensors in recent years. Most of these sensors were fabricated by employing the commonly used spherical GNPs [3-9]. GNRs, however, have been found to possess higher refractive index sensitivity than that of spherical GNPs [10, 11], due to their unique optical properties. Thus, the employment of GNRs is expected to improve the performance of optical fibre-based LSPR sensors. However, no research had been reported on the development of GNR-based LSPR optical fibre sensor before this work started.

This chapter introduces the fabrication of novel GNR-based LSPR optical fibre sensors, including the synthesis of GNRs with various aspect ratios, the preparation of optical fibres as sensor probes, and the immobilization of GNRs on the optical fibres. The experimental set-up consisting of different instruments has also been demonstrated. In addition, the performance of the as-prepared LSPR optical fibre sensors in response to the surrounding refractive index change has been evaluated, and the effect of the aspect ratio of GNRs on the refractive index sensitivity has also been studied and discussed in this chapter.

3.2 Synthesis of GNRs with various aspect ratios

3.2.1 Materials

Gold (III) chloride trihydrate ($HAuCl_4 \cdot 3H_2O$), ascorbic acid, silver nitrate ($AgNO_3$), cetyltrimethylammonium bromide (CTAB), 3-Mercaptopropyltrimethoxysilane (MPTMS), sodium borohydride ($NaBH_4$), potassium hydroxide (KOH), tin (II) chloride dehydrate and dextrose were purchased from Sigma Aldrich. De-ionized (DI) water purchased from Fisher Scientific was used to prepare all solutions. All reagents were of analytical grade and used as received. All procedures were conducted at room temperature unless specified otherwise.

3.2.2 Procedure of seed-mediated synthesis of GNRs

Despite the fact that there are several GNRs synthesis methods have been proposed, such as electrochemical method [12], template method [13] and electron beam lithography method [14], so far, the seed-mediated growth method is still considered as the most popular one due to the ease of preparation and high yield of GNRs. Therefore, the seed-mediated growth method was chosen for the preparation of GNRs in this work. In detail, GNRs were synthesized by following the method reported by Nikoobakht and EI-Sayed [15] with slight modification. Firstly, seed solution was prepared by mixing 5 mL of 0.2 M CTAB solution with 5 mL of 0.5 mM $HAuCl_4 \cdot 3H_2O$ solution with vigorous stirring, followed by the addition of 600 µL of 0.01 M ice-cold $NaBH_4$ to the stirred solution, resulting in the formation of a brownish solution. After additional 2 min vigorous stirring, the seed solution was aged at room temperature (25 °C) without being disturbed for 3 h before use.

The growth solutions for growing GNRs with different aspect ratios were prepared by adding 120, 180, 240 and 330 µL of 0.02 M $AgNO_3$ solutions to four identical 30 mL of 0.2 M CTAB solutions with stirring, respectively, followed by adding 30 mL of 0.001 M $HAuCl_4 \cdot 3H_2O$ solution to each stirred solution. To each mixed solution, 420 µL of 0.0788 M ascorbic acid solution, which works as a mild reducing agent, was added with stirring. This step was seen to change the colour of growth solutions from dark yellow to colourless. To grow GNRs, 100 µL of seed solution was added into each growth solution at about 30 °C. The colours of the mixtures were gradually changed within 20 min due to the growth of GNRs. It has been observed that the colour of GNRs with low aspect ratio changes quicker

than that of GNRs with high aspect ratio. The mixtures were then kept in an oil bath at 30 °C without being disturbed for 24 h to allow GNRs to grow fully.

Prior to the immobilization of GNRs on the surface of an optical fibre, excess CTAB in the as-synthesized GNRs solutions was removed by two rounds of centrifugations at 8000 rpm for 20 min for each round. The supernatant was carefully decanted and the GNRs deposited at the bottom of the centrifuge tube were finally re-suspended and dispersed in an equal amount of DI water.

3.2.3 Characterization of as-synthesized GNRs

The absorption spectra of the GNRs solutions were measured by using a LAMBDA 35 UV/VIS spectrophotometer (Perkin Elmer Inc.), over the wavelength range from 400 nm to 1100 nm. The mean aspect ratios of GNRs were determined by using a JEOL 1010 transmission electron microscope (TEM). The TEM samples were prepared by placing 2 µL of diluted GNRs solution on a 3 mm 400-mesh Formvar coated copper grid (purchased from Agar Scientific) and evaporating the solution at room temperature.

Fig. 3.1 (a) shows the different colours of the four GNRs solutions synthesized using the seed-mediated method, and Fig. 3.1 (b) shows the corresponding normalized absorption spectra of the as-synthesized GNRs with four aspect ratios of 2.6 ± 0.2, 3.1 ± 0.3, 3.7 ± 0.3 and 4.3 ± 0.4, respectively. The normalized spectra as well as the value of peak wavelength of LPB were acquired by the built-in functions of the software installed in the commercial spectrophotometer (LAMBDA 35) used in this work. The resolution of the spectrophotometer is 0.01 nm. As illustrated in Fig. 3.1 (b), two plasmon resonance bands can be observed in the absorption spectra of the GNRs with different aspect ratio, with one being the transverse plasmon band (TPB) and the other the longitudinal plasmon band (LPB), corresponding to the electron oscillations along the short and long axes of the rod, respectively. It is noticed that, for all the GNRs with various aspect ratios, their TPBs are all located at about 510 nm without any significant shift. However, with the increase of the aspect ratio, a red-shift in the LPBs clearly can be observed, indicating that the position of LPB of GNRs can be tuned by adjusting the aspect ratio. It also has been found that the dispersion of the aspect ratio has an influence on the absorption spectra of GNRs that it either results in a slight red or blue shift of the peak wavelength of LPB, but no peak wavelength shift of TPB was observed. Fig. 3.2 demonstrates the corresponding TEM

images of the as-synthesized GNRs, confirming their different aspect ratios. It is obvious to see from the TEM images that the length of GNRs increases with the increase of aspect ratio. The mean aspect ratio of the GNRs was calculated by measuring about 100 GNRs per TEM grid.

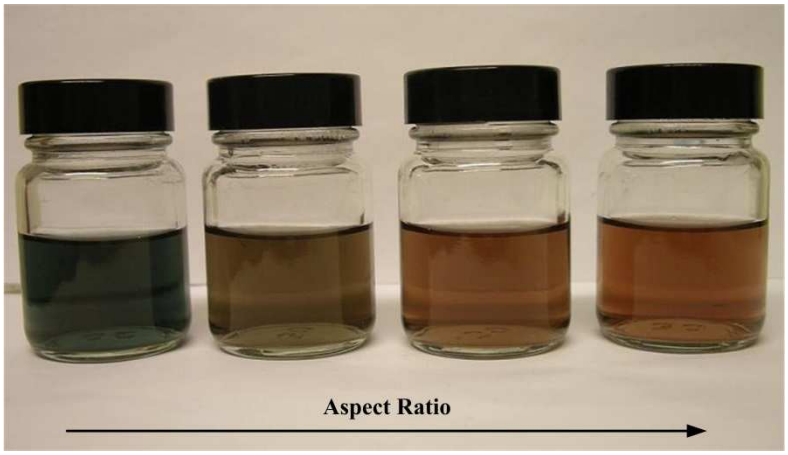

(a)

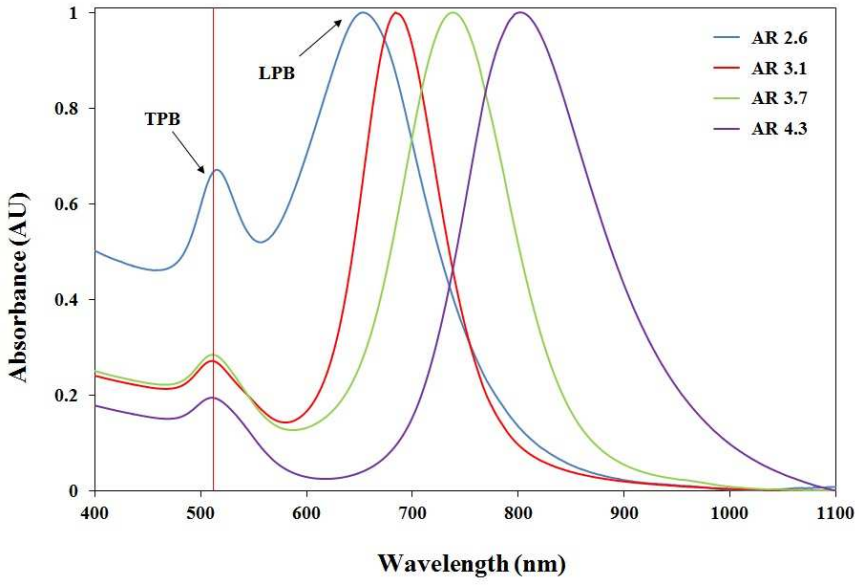

(b)

Fig. 3.1. (a) Illustration of seed-mediated synthesized GNRs solutions with aspect ratio of 2.6 ± 0.2, 3.1 ± 0.3, 3.7 ± 0.3 and 4.3 ± 0.4 (from left to right), and (b) their corresponding normalized absorption spectra.

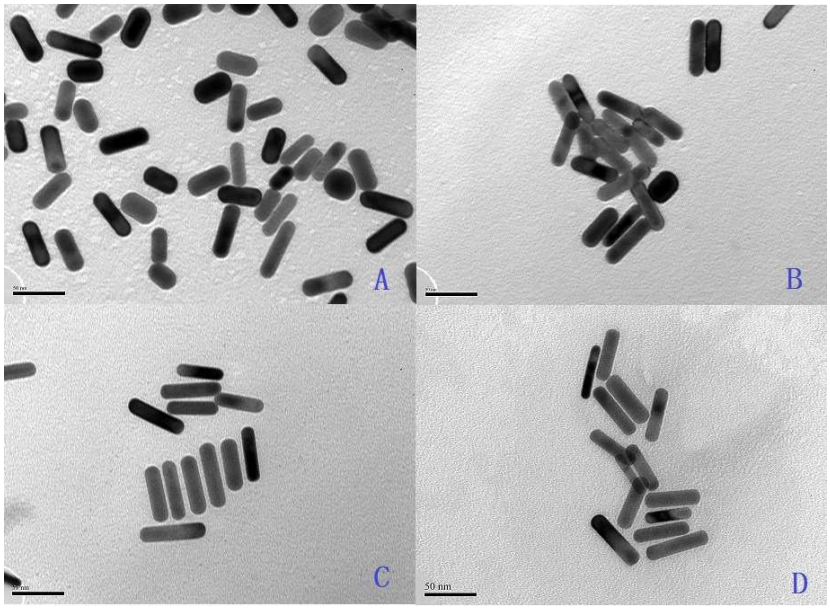

Fig. 3.2. TEM images of GNRs with four aspect ratios: A-2.6, B-3.1, C-3.7 and D-4.3. All scale bars are 50 nm.

3.2.4 Discussions

The advantage of using the seed-mediated growth method is that the aspect ratio of GNRs can be easily controlled by adding different amounts of silver ions into the growth solutions. However, according to the author's experience, the seed-mediated synthesis of GNRs appears to be a delicate experiment that several factors may affect the quality and even the success of the GNRs synthesis, thus, special attentions should be paid to these issues.

First and foremost, for the seed-meditated growth method, both the seed and growth solutions need to be prepared in the presence of high-concentration CTAB solution. CTAB plays a very important role in the synthesis of GNRs that, it not only works as a structure directing agent assisting in the formation of the rod shape nanoparticles, but also works as a stabilizer attaching to the GNRs surface to prevent GNRs from aggregation during and after the synthesis [16]. The CTAB molecules have very low solubility in water at room temperature (about 27 °C), therefore, the CTAB solution must be prepared at an elevated temperature (normally around 60 °C) to allow the CTAB molecules to be totally dissolved in the water. The temperature of GNRs solution needs to be brought down to room temperature before it can be used. However, the dissolved CTAB molecules in aqueous solution are every easy to crystallize at the temperature even a bit lower than the room temperature. Once

the crystallization of CTAB is formed in the seed and growth solutions after their preparations, such crystallized solutions are not able to be used. Even the crystallization of CTAB can be decrystallized by heating, however, two situations normally would happen after using the decrystallized seed or growth or both solutions: no GNRs can be synthesized; the majority of the synthesized nanoparticles have non-rod shapes. So far, the reason of why the crystallization of CTAB will cause the failure of the GNRs synthesis is still unknown, and no explanations have been reported by other researchers either. However, in order to successfully synthesize GNRs, it is vitally important to make sure no crystallization is formed in the seed and growth solutions before the use of them.

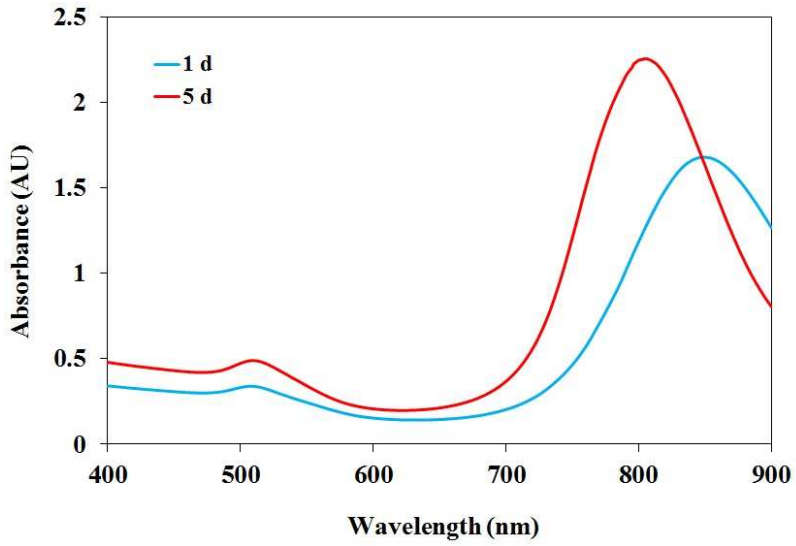

Fig. 3.3. Absorption spectra of GNRs solution after being aged for 1 day (blue) and 5 days (red) respectively.

In addition, the ageing time of both seed solution and GNRs growth has an effect on the synthesis of GNRs. On one hand, the seed solution containing spherical gold particles plays an important role in determining the physical characteristics of the GNRs. Gole and Murry reported that the length, thickness and aspect ratio of GNRs can be affected by the size and nature of the gold seed [17]. The gold seed, after its preparation, normally needs to be aged in the seed solution for at least 2 h in order to grow to a certain size (~ 4 nm) before adding it to the growth solution. If the gold seed is being aged for less than 2 h, no nanorod could be formed in the growth solution due to the small size of the gold seed. If the gold seed is being aged for days, the majority of the GNRs yielded will be distorted as reported by Jiang and Pileni [18]. On the other hand, as the gold seeds start to grow GNRs after the addition of

seed solution to the growth solution, if the ageing time for the GNRs growth is too short, such as only a few hours, the GNRs are not able to fully grow to the desired size. However, if the GNRs are kept growing over a certain period of time, rather than growing longitudinally along the long axis, the GNRs start to grow along the short axis. A blue shift of LPB in the absorption spectrum of the GNRs solution after being aged for 5 days was observed as shown in Fig. 3.3. This blue shift is due to the decrease of the aspect ratio of GNRs. Therefore, in this work, based on the results obtained from numerous experiments, the optimum ageing time for the seed solution and GNRs growth were set to 3 h and 24 h, respectively, which resulted in a high yield of GNRs (~ 90%, judging from the TEM images) achieved.

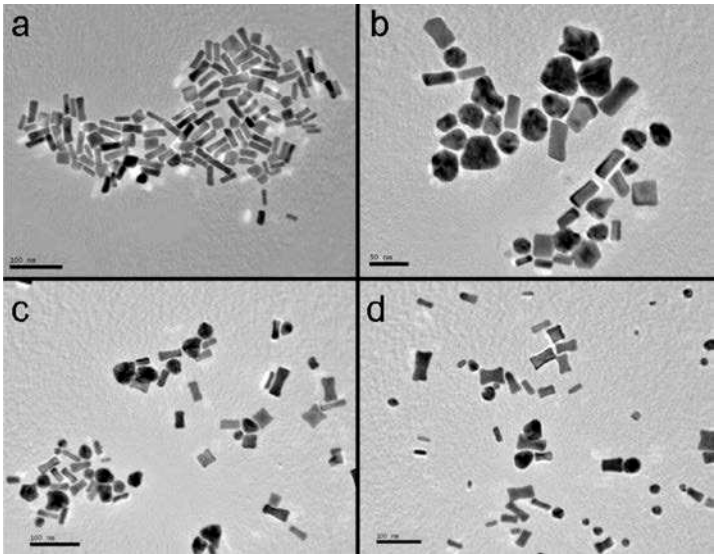

Fig. 3.4. TEM images of four samples prepared at: (a) 25 °C, (b) 55 °C, (c) 80 °C and (d) 95 °C. The scale bar is 100 nm for images a, c and d, and 50 nm for image b [19].

Moreover, it is worth noting that the variation of the temperature can also affect the growth of the GNRs [19]. GNRs synthesized at different temperatures could show different aspect ratios and significantly different shapes. For example, when GNRs grow at high temperature, the growing speed is increased accordingly. The increase of growing speed, however, has a negative impact on the formation of GNRs. As demonstrated in Fig. 3.4, the growth of GNRs at high temperature resulted in the distortion of the GNRs, for instance, forming the “dog-bone” shape of nanoparticles. However, when GNRs grow at a low temperature, the crystallization of CTAB in GNRs solution will be induced. It is also worth noting that, in the original method, the temperature of the growth solution was kept at 27~30 °C [15]. However, we found that the high yield of GNRs only could be obtained at 30 °C. Fig. 3.5 illustrates the

yield of GNRs as a function of temperature. Herein, the peak absorbance of LPB was employed to represent the yield of GNRs, due to the simple reason that the more GNRs synthesized, the more incident light will be absorbed. As can be observed in Fig. 3.5, for all of the three aspect ratios of GNRs, the yield of GNRs is proportional to the absorption of light, indicating that more GNRs can be acquired at a higher temperature in the range of 27~30 °C. Therefore, in this work, we slightly modified the original approach by maintaining the temperature of growth solution at 30 °C in order to obtain high yield of GNRs. The GNRs growth solutions were kept in an oil bath placed on a hot plate and the temperature was monitored by using a thermometer to maintain the temperature at the set value through the growth process. In addition, a larger volume of growth solution (10 mL in the original work, 60 mL in this work) was also applied in order to grow more GNRs at a time.

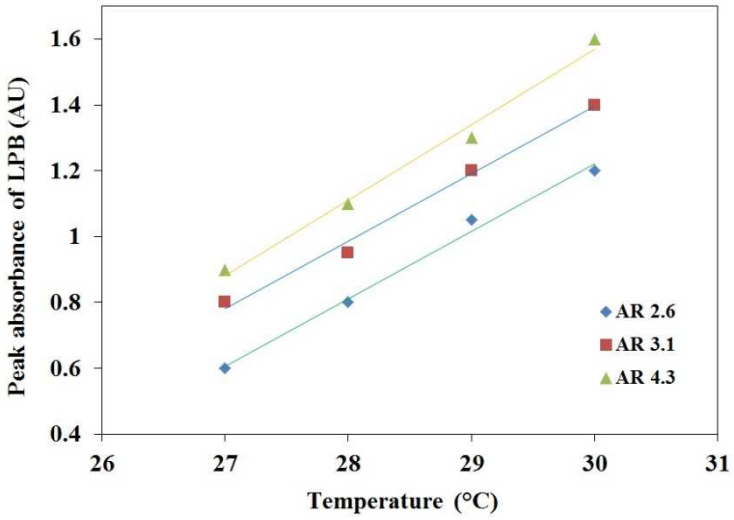

Fig. 3.5. The yield of GNRs with aspect ratios of 2.6, 3.1, 4.3, respectively, as function of temperature.

Last but not least, the seed-mediated growth method reported by Nikoobakht and EI-Sayed can produce GNRs with aspect ratios ranging from 1.5 to 4.5 [15]. In order to synthesize GNRs with aspect ratios higher than 4.5, the same group also introduced a slightly different approach involving the use of another surfactant — BDAC [15]. However, it has been found that more by-products of nanoparticle with other shapes rather than rod are produced by applying this method. Therefore, due to this limitation, in this work, we only prepared GNRs with aspect ratios ranging from 1.5 to 4.5.

3.3 Preparation of novel GNR-based LSPR optical fibre sensor probes

3.3.1 Materials

Ethanol and sulphuric acid (H_2SO_4) were purchased from Fisher Scientific, hydrogen peroxide (H_2O_2), 3-Mercaptopropyltrimethoxysilane (MPTMS), potassium hydroxide (KOH), ammonia (NH_3), silver nitrate ($AgNO_3$), tin (II) chloride dehydrate and dextrose were purchased from Sigma Aldrich. Multimode optical fibre of diameter 600 µm and NA=0.37 with polymer cladding were purchased from Thorlabs.

3.3.2 Procedure of preparation of LSPR sensor probes

Fig. 3.6 demonstrates the procedure of preparation of a GNR-based LSPR optical fibre sensor. In detail, a piece of polymer-clad silica multimode optical fibre with a core diameter of 600 µm was cut into several 10 cm long sections to be used as sensor substrates. Subsequently each fibre section was carefully and manually polished at both distal end surfaces by using polishing films with 5, 3, 1 and 0.3 µm roughness in sequential order. A 1 cm unclad portion at one distal end of the fibre was used as the sensing area after the polymer cladding having been removed with acetone [20]. The sensing area of the fibre was then cleaned by use of piranha solution (H_2O_2: H_2SO_4; 30%:70%) for 30 minutes (It should be noted that this solution is extremely aggressive and thus required handling with extreme care). After a thorough rinse with DI water, the optical fibres were then placed inside an oven, set at 100°C, for 1 hour. This cleaning procedure resulted in the formation of hydroxyl groups on the unclad fibre core as shown in Fig 3.6. Subsequently, the clean surface of the unclad optical fibres was modified with MPTMS by immersing the fibres into 5 % (V/V) MPTMS-ethanol solution overnight. The methoxyl groups of MPTMS interacts with the hydroxyl groups on the unclad fibre thus forming a covalent Si-O-Si bond, which results in a self-assembled film of MPTMS with terminal mercapto groups generated on the unclad fibre surface [21]. The excess and unbound MPTMS molecules were removed from the fibres by washing the fibres in ethanol under sonication for a few minutes, followed by thoroughly rinsing the fibres with ethanol and DI water alternately. The N_2 blow-dried MPTMS modified fibres were then incubated in the GNRs solutions synthesized above for 6 h to enable the immobilization of GNRs onto the unclad fibres surfaces. Finally, a self-assembled

monolayer of GNRs was formed on the fibre surface via the covalent Au-S bond as illustrated in Fig. 3.6.

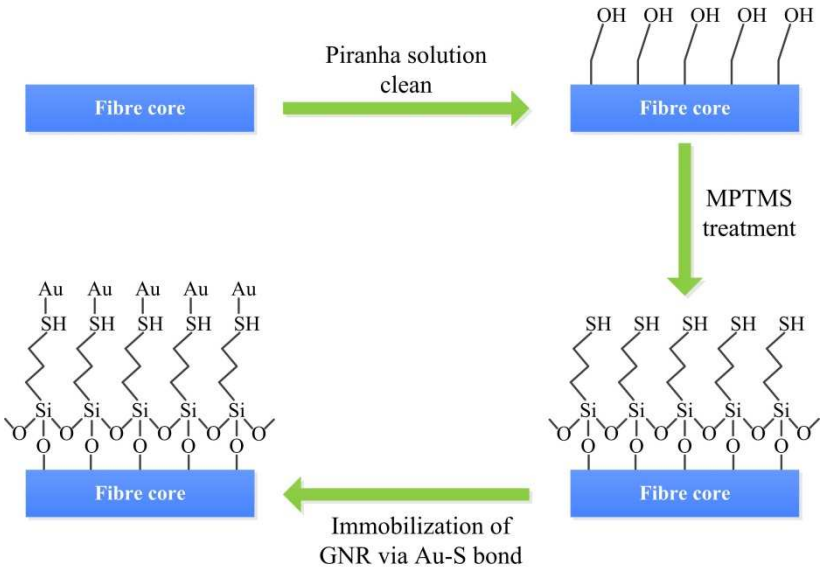

Fig. 3.6. Schematic diagram of self-assembly of GNRs on MPTMS modified optical fibre.

The LSPR sensors used in this experiment were fabricated as the reflective sensor probes, because the reflective sensor is easier for probing any form of samples and potentially could be used as the disposable sensor probe. In order to make the SPR probe operate as a reflective sensor, a thin silver mirror was also coated onto the end surface of the fibre to allow the reflection of the incident light, as illustrated in Fig. 3.7 (a). The silver mirror coating was realized by using a chemical technique with the use of Tollen's reagent [22]. Tollen's reagent was synthesized by dropwise adding NH_3 solution to 2 mL of 0.1 M $AgNO_3$ solution. After the brown precipitate totally dissolved, 1.4 mL of 0.8 M KOH was added, by which the colour of the mixed solution was changed from colourless to black. After additional NH_3 was added dropwise until the black precipitated dissolved, the Tollen's reagent was acquired. Before coating the silver mirror onto the fibre end surface, the fibre was first rinsed in 0.2% tin (II) chloride dehydrate solution to sensitize the coating area and subsequently rinsed with water. After dipping the fibre into the Tollen's reagent, 0.4 mL of dextrose (0.25M) was added, and then the fibre was kept in the reagent for a period of 2 min to allow the formation of the silver mirror at the fibre tip. After 2 min, the fibre was removed from the coating solution and rinsed with water and blow dried by N_2. Fig. 3.7 (b) shows the photo of a real LSPR optical fibre sensor probe prepared in this work.

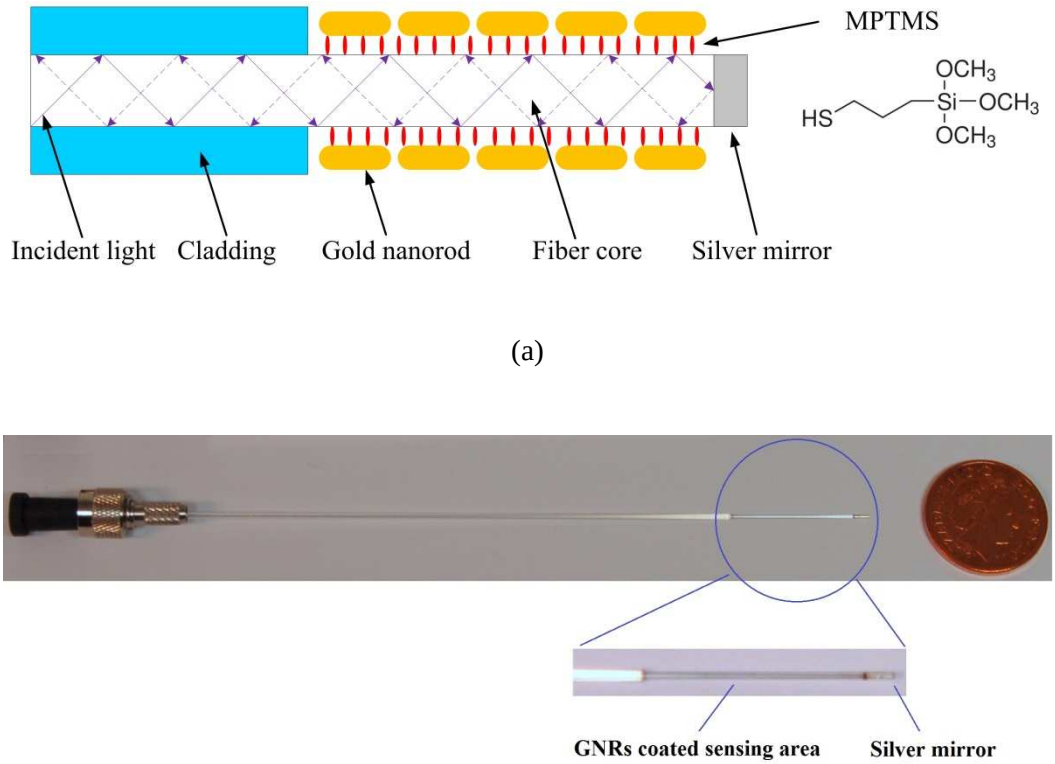

(a)

(b)

Fig. 3.7. (a) Schematic diagram of the structure of a GNR-coated LSPR optical fibre sensor; (b) photograph of the as-prepared LSPR optical fibre sensor probe.

3.3.3 Discussions

The immobilization of GNRs on the unclad fibre core is the key step in the fabrication of the GNR-based LSPR optical fibre sensor. In this work, multimode optical fibre with a hard polymer cladding was chosen specifically due to ease of cladding removal with the help of acetone. Prior to the GNRs immobilization, the surface of the unclad portion needs to be cleaned properly, followed by modifying the unclad surface with cross-linkers. APTES with positively charged amino groups has been commonly used for linking the citrate-reduced GNPs for the reason that Au has strong affinity with amino groups [21, 23]. Via electrostatic adherence, the negatively charged GNPs can be immobilized on the positively charged surface of substrate modified with APTES. However, as the GNRs surface is covered by the bilayer of positively charged CTAB molecules, it is not able to coat the GNRs on the ATPES modified substrate due to the repulsive force between the CTAB molecules and amino groups. This point has also been confirmed through our experiments that, by immersing two

APTES modified substrates in the citrate-reduced GNPs and CTAB covered GNRs solutions, respectively, only GNPs could be coated on the substrate while no GNRs were found to be coated on. Although the negatively charged polyelectrolyte could be used for linking the GNRs, as both the adherence of polyelectrolyte to the substrate and the binding of GNRs are via electrostatic force, the robustness of such polyelectrolyte modified substrate is questionable. In this work, an alternative to APTES, MPTMS, was chosen as the linker for immobilizing GNRs. Both the surface modification with MPTMS and the immobilization of GNRs are via the strong Si-O-Si and Au-S covalent bonds, respectively, ensuring the robustness of the sensor probe. It is worth to note that, the unbound MPTMS molecules must be completely removed from the fibre surface before dipping the fibre into the GNRs solution, because the unbound MPTMS molecules in the GNRs solution will induce an irreversible aggregation and deposition of GNRs, thus, resulting in a poor quality of GNRs coating or even failure of GNRs immobilization.

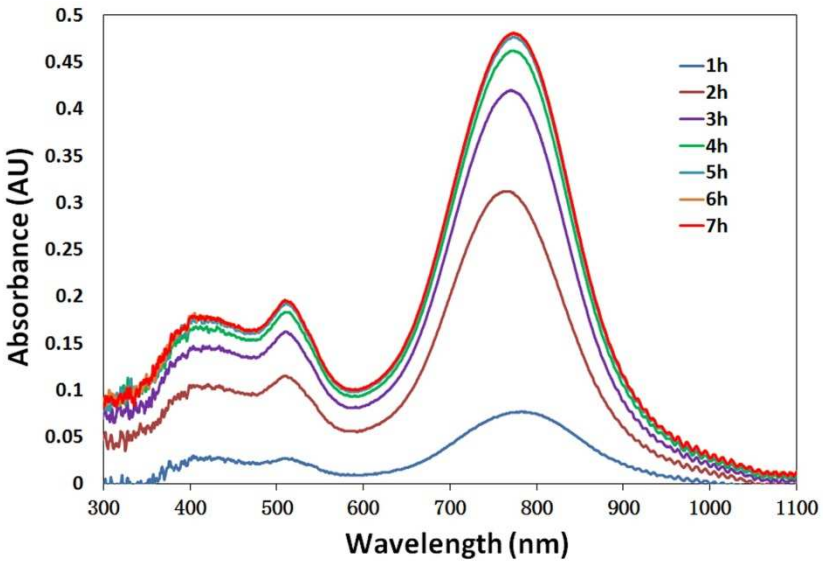

Fig. 3.8. Absorbance of the GNRs (aspect ratio = 3.6) based LSPR sensor as a function of GNR-coating time under continuous monitoring.

In addition, in order to obtain an optimum GNRs coating, the coating process was continuously monitored and the results acquired are shown in Fig. 3.8. As shown in Fig. 3.8, after the immersion of the MPTMS modified fibre into the GNRs solution, the LSPR absorption of GNRs occurs and the absorbance increases gradually with time due to the GNRs binding to the fibre surface. After a period of 6 h, no significant absorbance increase can be observed, indicating the saturation of the GNRs coating that no more GNRs can be

coated on the fibres. Therefore, in this work, 6 h coating time is specifically chosen as the optimum coating time for preparing the LSPR optical fibre sensors.

3.4 Evaluation of GNR-based LSPR optical fibre sensor performance

3.4.1 Experimental set-up

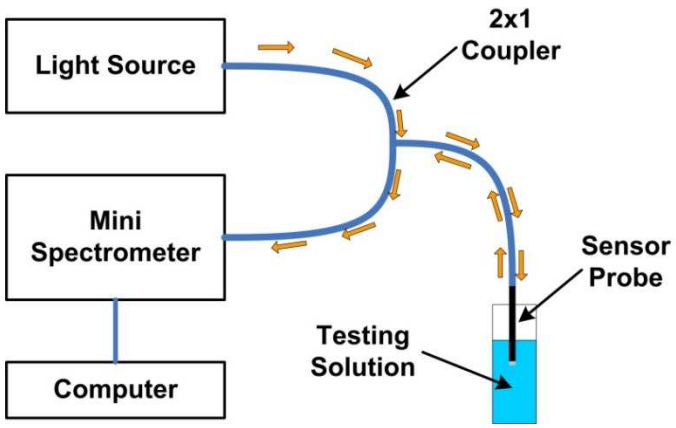

(a)

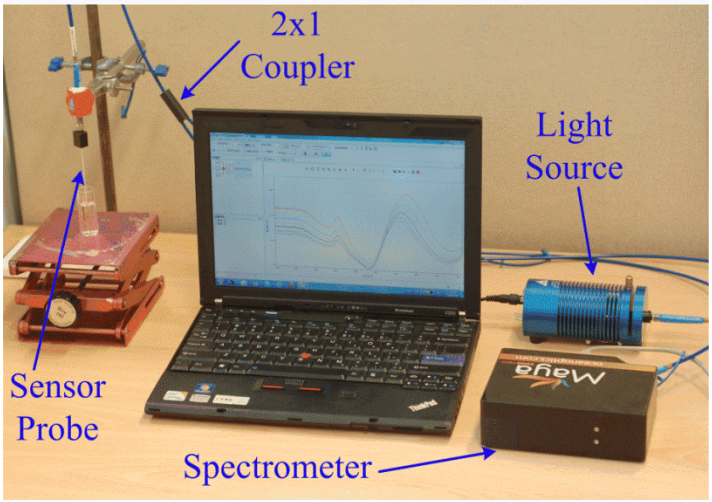

(b)

Fig. 3.9. (a) Schematic diagram of the sensor system. (b) Photograph of the experimental set-up used.

The experimental set-up for evaluating the performance of the GNR-based LSPR optical fibre sensors fabricated in this work is shown in Fig. 3.9. As illustrated in Fig. 3.9 (a), the sensor probe is connected to one end of a 2x1 fibre coupler and it is illuminated by light from a white light source connected to the other end of the coupler. In order to evaluate the LSPR sensor performance, the sensor probe is dipped into a testing solution with a known refractive index. The incident light interacts with the GNRs immobilized on the sensor surface and the reflected signal is captured by a mini-spectrometer (Ocean Optics Maya 2000pro) with resolution of 0.01 nm, which is connected to the other end of the coupler. Thus the signals obtained can be displayed and monitored by a computer connected to the mini-spectrometer. The signal was interrogated every 10 microseconds and the data were acquired and recorded by using Spectrasuite software. The real experimental set-up employed in this work is shown in Fig. 3.9 (b).

3.4.2 Refractive index sensitivity test

The evaluation of the refractive index sensitivities of the as-prepared LSPR optical fibre sensors to the surrounding refractive index change were conducted by immersing the sensor probes into testing solutions with various refractive index, ranging from 1.34 to 1.41. The testing solutions were prepared by mixing solvents of methanol, ethanol and toluene at different ratios, and their refractive indices were measured using a refractometer (purchased from Fisher Scientific).

3.4.3 Results and discussions

3.4.3.1 Sensitivity to surrounding refractive index change

Fig. 3.10 (a)-(d) shows clearly the absorption spectra of the LSPR optical fibre sensors based on GNRs with various aspect ratios, when the sensors were exposed to testing solutions with different refractive indexes. It has been observed that, for all the as-prepared LSPR sensors, when the sensor probe was dipped into a testing solution, immediately the absorption spectrum of the sensor occurred and then quickly stabilized at a specific position, which is corresponding to the refractive index of the testing solution. When changing the testing solution to a one with a different refractive index, the absorption spectrum of the sensor rapidly changed and stabilized at a different position accordingly. These phenomena indicate

that the as-prepared GNR-based LSPR optical fibre sensors have fast response to the surrounding refractive index change.

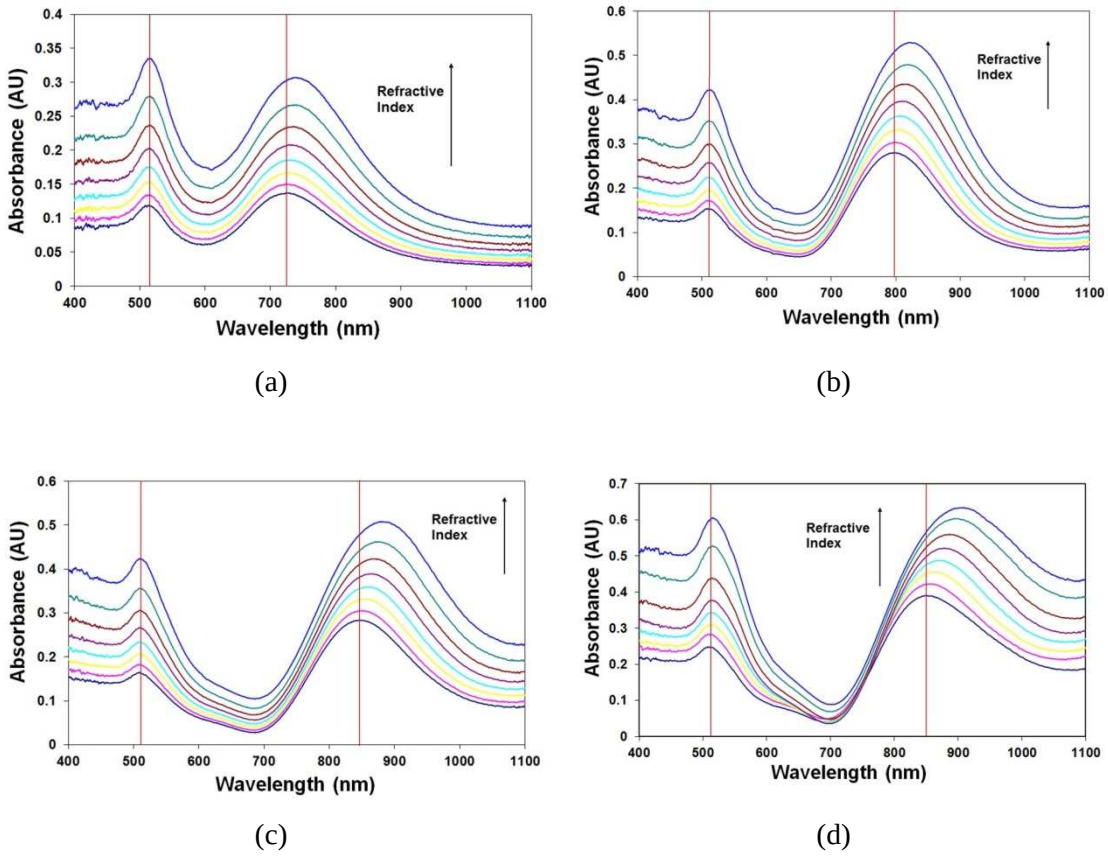

Fig. 3.10. Overlapping absorption spectra of LSPR optical fibre sensors based on GNRs with aspect ratios of (a) 2.6, (b) 3.1, (c) 3.7 and (d) 4.3, with increase of refractive index from 1.34 to 1.41.

As shown in Fig. 3.10 (a)-(d), two plasmon resonance bands can be observed from the absorption spectra of the as-prepared GNR-based LSPR sensors, with one being the TPB and (shorter peak wavelength) and the other the LPB (longer peak wavelength), demonstrating a similar spectral profile of GNRs solutions as shown in Fig. 3.1 (b). It is noticeable that, when the GNR-based LSPR sensors with different aspect ratios were immersed into the testing solution with the same refractive index, the TPBs in the absorption spectra of these sensors were almost located at the same wavelength about 510 nm, while the LPBs were red-shifted with the increase of the aspect ratio of GNRs as demonstrated in Fig. 3.10 (a)-(d). With the increase of the solution refractive index, no significant wavelength shift but only an increase of the absorbance in the TPBs was observed. However, for the LPBs, not only did the absorbance increase, but also the peak wavelength of LPB showed a red-shift with the

increase of refractive index in the range from 700 nm to 1000 nm. This observation indicates that the LPB is much more sensitive to the refractive index change than the TPB. Therefore, the peak wavelength of LPB in the absorption spectrum was chosen as an indicator for evaluating the refractive index sensitivities of the GNR-based LSPR sensors. It was also found in Fig. 3.1 (b) and Fig. 3.10 (a)-(d) that, the position of LPB peak wavelength of GNRs suspending in solution is slightly different from that of GNRs immobilized on the optical fibre. Compared to the spectra of GNRs suspending in solution, a red shift of LPB peak wavelength was observed after the GNRs were coated on fibre. This could be caused by the refractive index difference between the GNRs solution and optical fibre, because the LPB peak wavelength of GNRs are highly sensitive to the refractive index change and the refractive index of an optical fibre is a higher than that of GNRs solution. When the refractive index varies from 1.34 to 1.41, a total peak wavelength shift of 18, 27, 35 and 54 nm were observed for the LSPR sensors with the GNR aspect ratio ranging from 2.6 to 4.3 respectively, indicating that the higher the GNR aspect ratio, the more sensitive to the refractive index change the GNR-based LSPR sensor will be. It was also observed that when the GNR sensors with different aspect ratios, such as 3.1 and 4.3 as indicated in Fig. 3.10 (b) and (d) respectively, are subjected in the solution with the same refractive index, the peak of LPBs of the sensors appears at different wavelengths. This indicates that multiplex LSPR sensing for detecting multiple targets could be realized in future when the construction of a LSPR sensor probe involves the employment of GNRs with different aspect ratios. However, as demonstrated in Fig. 3.10 (a)-(d), it was also noted that the LPB becomes slight broader with the increase of aspect ratio of GNRs. This could be due to the reason that, since multimode optical fibres were employed in this work, more modes of incident light in the optical fibre are able to couple with GNRs with higher aspect ratio to excite LSPR, which results in the broadening of absorption spectrum.

The refractive index sensitivity is defined as the peak wavelength shift relative to the corresponding refractive index change and has as a unit of nm/RIU (where RIU = refractive index unit). Fig. 3.11 (a) summarises the results obtained from the refractive index sensitivity tests of the GNR-based LSPR sensors with different aspect ratios, showing the peak wavelength shift of LPB of the LSPR sensors as a function of refractive index variation of the surrounding medium ranging from 1.34 to 1.41. The refractive index sensitivities of the as-prepared GNR-based LSPR sensors with aspect ratios from 2.6 to 4.3 are about 269, 401, 506 and 766 nm/RIU, respectively, calculated by a linear fit as shown in Fig. 3.10, thus, indicating that the GNR-based LSPR optical fibre sensors with higher aspect ratio possess higher refractive index sensitivity. In addition, as can be seen in Fig. 3.11 (a), all the GNR-

based LSPR sensors created have also demonstrated a good linearity of their sensitivities to the refractive index change. These results obtained are in good agreement with those previously published results acquired from either chip-based [24] or solution-phase-based [10] LSPR sensors using GNRs.

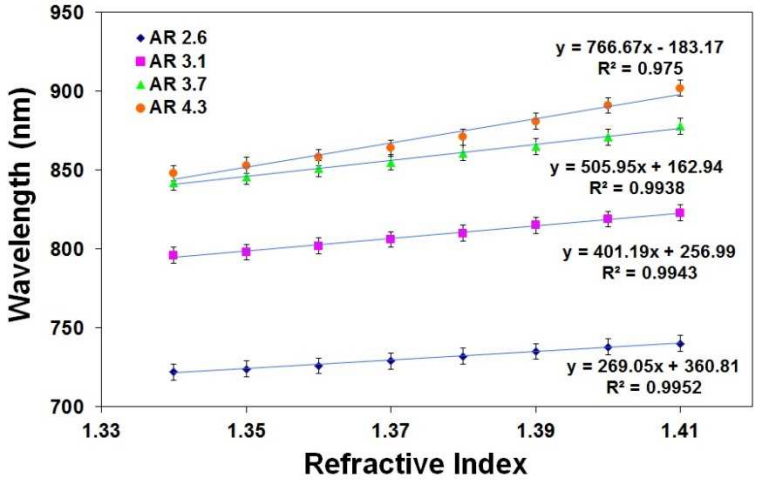

(a)

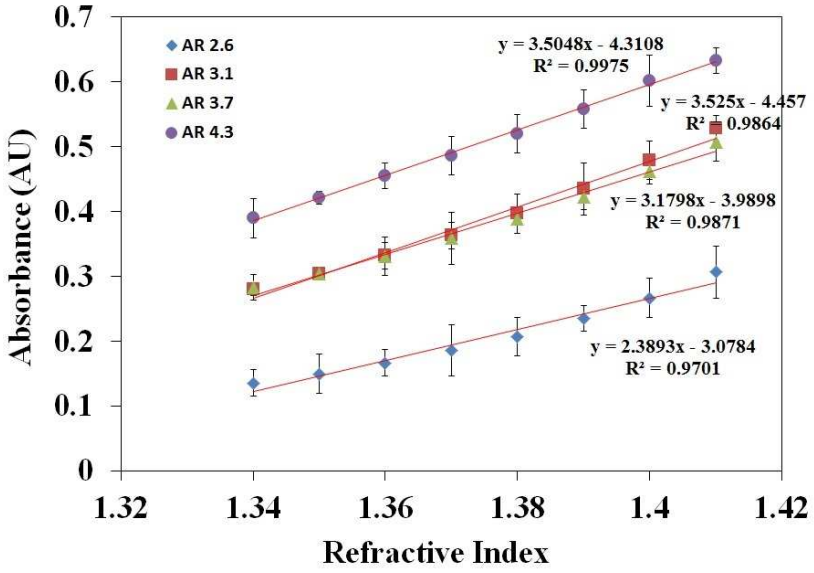

(b)

Fig. 3.11. (a) Peak wavelength shift of LPB of GNRs with four aspect ratios as a function of refractive index change, (b) peak absorbance shift of LPB of GNRs with four aspect ratios as a function of refractive index change (AR = aspect ratio).

In comparison with the results obtained from a similar LSPR optical fibre sensor but based on spherical GNPs [25], despite an increasing sensitivity with the increase of particles size as reported, both the lowest and highest refractive index sensitivities (154 and 571 nm/RIU) corresponding to the LSPR sensors using the smallest and largest particles (13 and 60 nm), respectively, reported in that work are much lower than those of the GNR-based LSPR sensors with the lowest and highest aspect ratios (269 and 766 nm/RIU corresponding to aspect ratios of 2.6 and 4.3, respectively). Moreover, judging from the R-squared value shown in Fig. 3.11 (a), the linearity of the refractive index sensitivity of the GNR-based LSPR optical fibres sensors creased in the work is much better than those of the LSPR sensors based on spherical GNPs [25]. These advantages make the GNR-based LSPR sensors more suitable for LSPR sensing applications than the LSPR sensors based on the conventionally used spherical GNPs. In addition, the peak absorbance shift of LPB of as a function of refractive index change was also shown in Fig. 3.11 (b).

3.4.3.2 Stability of the sensor probe

In order to verify the stability of the as-prepared LSPR sensor probes, the peak wavelength of LPB in absorption spectrum of one freshly prepared GNR-based LSPR sensor probe with aspect ratio of 3.7 was monitored and recorded every two days over a period of two weeks when the same sensor probe was subjected to testing solutions with refractive index of 1.34, 1.36 and 1.38. After each round of test, the sensor probe was preserved in the DI water at room temperature. The peak wavelength and peak absorbance of LPB, being recorded over a two week period, is shown in Fig. 3.12. As illustrated in Fig. 3.12 (a), the peak wavelength of LPB for the GNR-based LSPR sensor was shown to be rather constant over the test period. Only very small variation in the peak wavelength (by less than 0.05 nm) were found, indicating that GNR-based LSPR sensors prepared in this work have a high stability for at least two weeks. However, as can be observed in Fig. 3.12 (b), the peak absorbance of LPB irregularly shifted during the testing period, which could be due to either the variation in intensity of light source or changes in alignment of sensor probe and coupler for each test. The stability difference between the peak wavelength and peak absorbance also indicates that the wavelength based measurement applied in this work is more reliable than the intensity/absorbance based measurement. Moreover, when the as-prepared LSPR sensor probes were stored in DI water in dark environment at 4 °C, the performance of the sensors preserved in such way was found to be stable for more than 6 months before any form of degradation was observed.

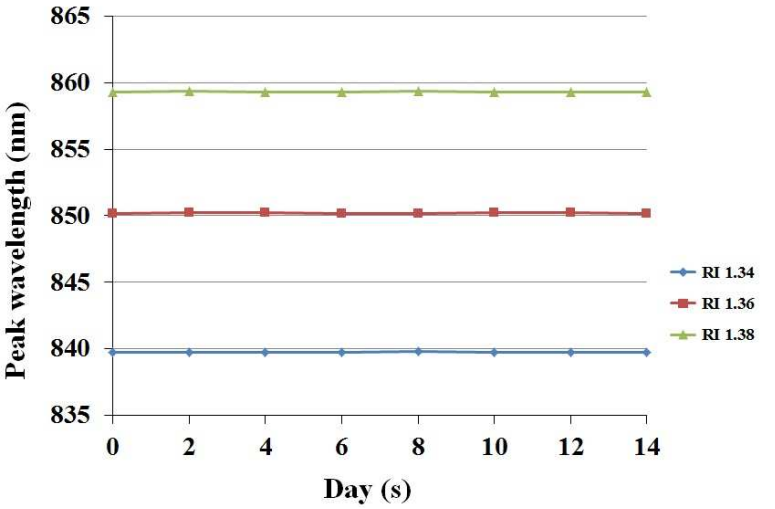

(a)

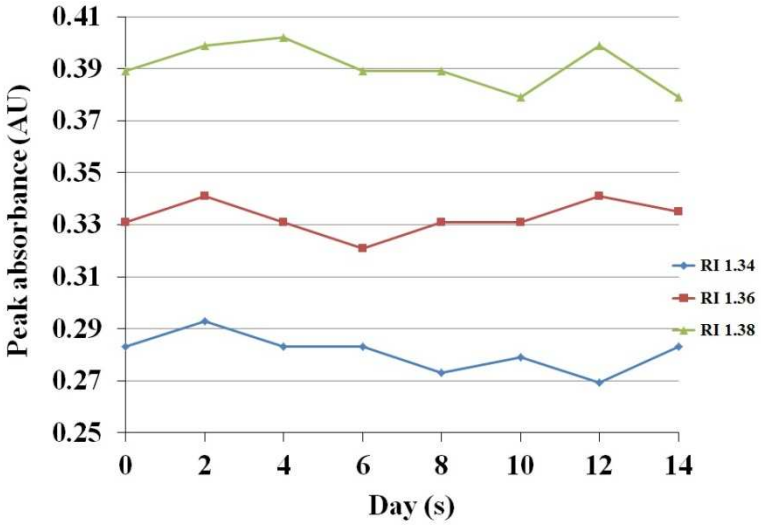

(b)

Fig. 3.12. (a) Peak wavelength and (b) peak absorbance monitoring of the GNR-based LSPR sensor subjected in testing solutions with different refractive indexes for a period of two weeks.

3.5 Summary

In this chapter, the development of GNR-based LSPR optical fibre sensors, designed with different aspect ratios, has been described, and the performances of the sensors created have been evaluated and cross-compared. The procedure of the synthesis of GNRs with various aspect ratios using seed-mediated method has been introduced in detail, the characteristics of

the as-synthesized GNRs have been studied, and the issues which may affect the quality of the GNRs have been pointed out and discussed. Additionally, the preparation of the GNR-based LSPR optical fibre sensor probe including the surface modification of the optical fibre and the immobilization of GNRs onto the unclad optical fibre has been described. Finally, refractive index sensitivities of the as-prepared LSPR sensors were evaluated when they were subjected to the testing solutions with different refractive indexes. The results show that the GNR-based LSPR sensors fabricated in this work have refractive index sensitivities of 269, 401, 506 and 766 nm/RIU, corresponding to the aspect ratios of 2.6, 3.1, 3.7 and 4.3 respectively, indicating that the sensitivity of the LSPR sensor increases with the increase of the aspect ratio of GNRs. In comparison with the LSPR optical fibre sensors based on the commonly used spherical GNPs, the GNR-based LSPR optical fibre sensors fabricated in this work not only showed higher refractive index sensitivities, but also demonstrated a better linearity in their performance. In addition, the GNR-based LSPR sensors have proved to be highly stable for up to months. The promising results obtained show that the GNR-based LSPR sensors created in this work have the ability to work as a sensitive label-free biosensor for biosensing applications. The development of GNR-based label-free LSPR biosensor and its biosensing ability will be demonstrated in the next chapter.

3.6 References

[1] J. Cao, E.K. Galbraith, T. Sun, K.T.V. Grattan, Cross-comparison of surface plasmon resonance-based optical fiber sensors with different coating structures, IEEE Sensors Journal, 12 (2012) 2355-2361.

[2] J. Cao, M.H. Tu, T. Sun, K.T.V. Grattan, Wavelength-based localized surface plasmon resonance optical fiber biosensor, Sensors And Actuators B-Chemical, 181 (2013) 611-619.

[3] S.F. Cheng, L.K. Chau, Colloidal gold-modified optical fiber for chemical and biochemical sensing, Analytical Chemistry, 75 (2003) 16-21.

[4] K. Kajikawa, K. Mitsui, Optical fiber biosensor based on localized surface plasmon resonance in gold nanoparticles, Nanosensing: Materials And Devices, Bellingham, 5593 (2004) 494-501.

[5] L.K. Chau, Y.F. Lin, S.F. Cheng, T.J. Lin, Fiber-optic chemical and biochemical probes based on localized surface plasmon resonance, Sensors And Actuators B-Chemical, 113 (2006) 100-105.

[6] J.L. Tang, S.F. Cheng, W.T. Hsu, T.Y. Chiang, L.K. Chau, Fiber-optic biochemical sensing with a colloidal gold-modified long period fiber grating, Sensors And Actuators B-Chemical, 119 (2006) 105-109.

[7] T.J. Lin, C.T. Lou, Reflection-based localized surface plasmon resonance fiber-optic probe for chemical and biochemical sensing at high-pressure conditions, Journal Of Supercritical Fluids, 41 (2007) 317-325.

[8] T.J. Lin, M.F. Chung, Detection of cadmium by a fiber-optic biosensor based on localized surface plasmon resonance, Biosensors & Bioelectronics, 24 (2009) 1213-1218.

[9] V.V.R. Sai, T. Kundu, S. Mukherji, Novel U-bent fiber optic probe for localized surface plasmon resonance based biosensor, Biosensors & Bioelectronics, 24 (2009) 2804-2809.

[10] H.J. Chen, X.S. Kou, Z. Yang, W.H. Ni, J.F. Wang, Shape- and size-dependent refractive index sensitivity of gold nanoparticles, Langmuir : The ACS Journal Of Surfaces And Colloids, 24 (2008) 5233-5237.

[11] T.K. Sau, A.L. Rogach, F. Jackel, T.A. Klar, J. Feldmann, Properties and applications of colloidal nonspherical noble metal nanoparticles, Advanced Materials, 22 (2010) 1805-1825.

[12] Y.Y. Yu, S.S. Chang, C.L. Lee, C.R.C. Wang, Gold nanorods: Electrochemical synthesis and optical properties, Journal Of Physical Chemistry B, 101 (1997) 6661-6664.

[13] C.A. Foss, G.L. Hornyak, J.A. Stockert, C.R. Martin, Template-synthesized nanoscopic gold particles - optical-spectra and the effects of particle-size and shape, Journal Of Physical Chemistry, 98 (1994) 2963-2971.

[14] A. Boltasseva, Plasmonic components fabrication via nanoimprint, Journal of Optics A-Pure And Applied Optics, 11 (2009).

[15] B. Nikoobakht, M.A. El-Sayed, Preparation and growth mechanism of gold nanorods (NRs) using seed-mediated growth method, Chemistry Of Materials, 15 (2003) 1957-1962.

[16] C.J. Murphy, L.B. Thompson, D.J. Chernak, J.A. Yang, S.T. Sivapalan, S.P. Boulos, J. Huang, A.M. Alkilany, P.N. Sisco, Gold nanorod crystal growth: From seed-mediated synthesis to nanoscale sculpting, Current Opinion In Colloid & Interface Science, 16 (2011) 128-134.

[17] A. Gole, C.J. Murphy, Seed-mediated synthesis of gold nanorods: Role of the size and nature of the seed, Chemistry Of Materials,16 (2004) 3633-3640.

[18] X.C. Jiang, M.P. Pileni, Gold nanorods: Influence of various parameters as seeds, solvent, surfactant on shape control, Colloids And Surfaces A-Physicochemical And Engineering Aspects, 295 (2007) 228-232.

[19] R. Becker, B. Liedberg, P.-O. Kall, CTAB promoted synthesis of Au nanorods - temperature effects and stability considerations, Journal Of Colloid And Interface Science, 343 (2010) 25-30.

[20] D.F. Merchant, P.J. Scully, N.F. Schmitt, Chemical tapering of polymer optical fibre, Sensors And Actuators A-Physical, 76 (1999) 365-371.

[21] Q. Zhang, C.Y. Xue, Y.L. Yuan, J. Lee, D. Sun, J.J. Xiong, Fiber surface modification technology for fiber-optic localized surface plasmon resonance biosensors, Sensors, 12 (2012) 2729-2741.

[22] D.W. Kim, Y. Zhang, K.L. Cooper, A.B. Wang, In-fiber reflection mode interferometer based on a long-period grating for external refractive-index measurement, Applied Optics, 44 (2005) 5368-5373.

[23] N. Nath, A. Chilkoti, Label-free biosensing by surface plasmon resonance of nanoparticles on glass: optimization of nanoparticle size, Analytical Chemistry, 76 (2004) 5370-5378.

[24] P.K. Jain, S. Eustis, M.A. El-Sayed, Plasmon coupling in nanorod assemblies: Optical absorption, discrete dipole approximation simulation, and exciton-coupling model, Journal Of Physical Chemistry B, 110 (2006) 18243-18253.

[25] M.H. Tu, T. Sun, K.T.V. Grattan, Optimization of gold-nanoparticle-based optical fibre surface plasmon resonance (SPR)-based sensors, Sensors And Actuators B-Chemical, 164 (2012) 43-53.

Chapter 4

Development of novel GNR-based LSPR optical fibre biosensor

4.1 Introduction

Similar to SPR sensors, label-free biosensing could be the most important application of LSPR sensors. Despite the fact that the sensitivity of SPR sensors to bulk refractive index change is much higher than that of LSPR sensors [1-3], it has been proved that LSPR biosensors can offer a comparable sensitivity to the small variation in refractive index caused by the biomolecular interaction at sensing surface for instance [3, 4]. In addition, LSPR sensors not only retain many advantages of SPR sensors, such as high refractive index sensitivity, fast, real-time and label-free detection, but also show other advantages including better flexibility and simpler sensor design and cost-effectiveness in sensor fabrication, making the LSPR sensors more attractive to biosensing applications. A number of promising optical fibre based LSPR biosensors have been developed so far [5-13]. Most of these previously reported LSPR optical fibre sensors have shown good refractive index sensitivities with their resonance peak wavelength shifts being observed when the sensors were subjected to the bulk refractive index change. However, when these sensors were used as a biosensor, absorbance or intensity measurement is widely considered rather than the peak wavelength shift [8-13]. This is because that the resonance wavelength of these sensors has not demonstrated a sensitivity significant enough to detect the small refractive index change caused by the biomolecular interaction, although this wavelength-based technique is preferable due to its insensitivity to the interference arising from the surrounding environment, compared to absorbance and intensity-based techniques.

This chapter introduces the development of a novel GNR-based LSPR optical fibre biosensor and its biosensing performance. The fabrication of the LSPR sensor probe is based on the work introduced in Chapter 3, with the aspect ratio of GNRs and sensing length of the optical fibre being chosen in particular to enhance the sensitivity of LSPR sensor. The sensor probe is further functionalized with bioreceptors, which have the specific bioaffinity for the target biomolecule, to make the LSPR sensor work as a label-free biosensor. The evaluation of the biosensing ability of the LSPR biosensor created is performed by using the antigen-antibody recognition model, which has been widely used in the study of biosensor development [6, 14-19], based on a wavelength-based interrogation method rather than the conventional absorbance or intensity-based technique to improve the quality of the measurement.

4.2 Preparation of GNR-based LSPR sensor probe

4.2.1 Materials

Gold (III) chloride trihydrate ($HAuCl_4 \cdot 3H_2O$), ascorbic acid, silver nitrate ($AgNO_3$), cetyltrimethylammonium bromide (CTAB), 3-Mercaptopropyltrimethoxysilane (MPTMS), sodium borohydride ($NaBH_4$), hydrogen peroxide (H_2O_2), ammonia (NH_3), potassium hydroxide (KOH), tin (II) chloride dehydrate and dextrose were purchased from Sigma Aldrich. Ethanol, sulphuric acid (H_2SO_4) and de-ionized (DI) water purchased from Fisher Scientific was used to prepare all solutions. All reagents were of analytical grade and used as received. All procedures were conducted at room temperature unless specified otherwise. Multimode optical fibres of diameter 600 µm and NA=0.37 with polymer cladding were purchased from Thorlabs.

4.2.2 Fabrication and characterization of LSPR sensor probe

In this experiment, the GNR-based LSPR optical fibre sensor probes were prepared by following the same fabrication procedure described in Chapter 3. Based on the previous findings that the higher the aspect ratio, the higher the refractive index sensitivity, GNRs with slightly high aspect ratio were synthesized particularly in this experiment, in order to enhance the sensitivity of the LSPR sensor. Briefly, the seed solution was prepared following the procedure exactly the same as the one applied in the Chapter 3. Because the aspect ratio

of GNRs is controlled by the amount of silver ions in the seed-mediated growth method, to synthesize GNRs with high aspect ratio, 310 µL of 0.02 M $AgNO_3$ solution was added into the growth solution. Except the $AgNO_3$ solution, the volumes as well as the concentrations of other chemicals applied in this experiment are consistent with those of chemicals used in the previous experiment described in Chapter 3. Fig. 4.1 (a)-(c) demonstrates the colour, the TEM image and the absorption spectrum of the as-synthesized GNRs solution, respectively. The mean aspect ratio of the GNRs is about 4.1 $\pm$ 0.3 determined by the TEM analysis.

(a)

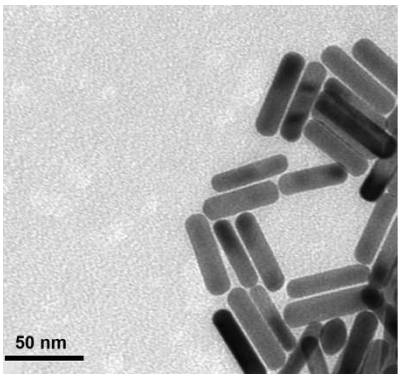

(b)

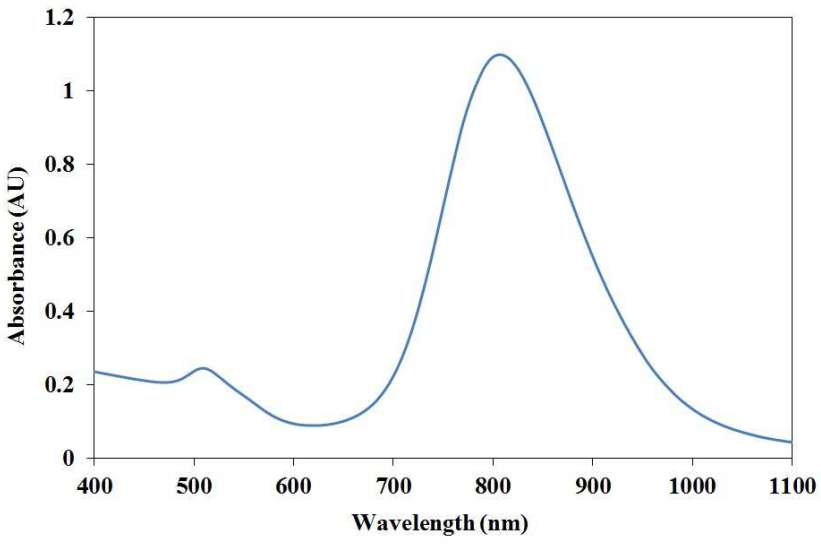

(c)

Fig. 4.1. The photograph (a), TEM image (b), and absorption spectrum (c) of the GNRs solution with aspect ratio of 4.1 synthesized using the seed-mediated growth method.

The preparation of the optical fibre sensor probe and the immobilization of GNRs on the fibre were conducted by following the same procedures introduced previously in Chapter 3. In addition, the LSPR sensor probes can be easily reproduced by removing the GNRs immobilized on the sensor surface with a piece of tissue and ethanol, and repeating the cleaning and coating procedures introduced in Chapter 3. In order to investigate the influence of the sensing length on the refractive index sensitivity, a series of GNR-based LSPR sensor probes, with sensing lengths of 0.5 cm, 1 cm and 2 cm were prepared and tested respectively. The performance of these sensors was also evaluated by dipping the sensor probes in the testing solutions with various refractive indexes ranging from 1.34 to 1.41 and monitoring the change in their absorption spectra. Fig. 4.2 (a) shows the overlapping absorption spectra of a LSPR sensor probe with 2 cm sensing length. Again, a red-shift in the LPB with the increase of refractive index can be observed. For each length, the peak wavelength shift of LPB as a function of the refractive index of the surrounding medium, acquired from seven batches of different sensor probes, was fitted to a linear function to determine the refractive index sensitivity. As shown in Fig. 4.2 (b), the refractive index sensitivity of the GNR-based LSPR sensor increases with the increase of sensing length. For each sensing length, the results shown in Fig. 4.2 (b) were obtained from three different sensor probes in order to calculate the standard deviations and averages. The sensor with a sensing length of 2 cm demonstrates the highest refractive index sensitivity of ~ 601 nm/RIU, showing a considerable promise of working as an effective biosensor to detect the small refractive index changes caused by the interaction between biomolecules. Compared to the results shown in Fig. 3.11 (a), the refractive index sensitivity of sensor probe with a 2 cm sensing length shown in Fig. 4.2 (b) is much higher than those of sensor probes with a 1 cm sensing length and with GNRs aspect ratios lower than 4.1, but still lower than that of sensor probe with GNRs aspect ratio of 4.3. This indicates that the refractive index sensitivity of GNR-based optical fibre sensor not only depends on the sensing length, but also depends on the aspect ratio of GNRs. In addition, Zayats's group has found that when GNRs are vertically immobilized on a substrate, the refractive index sensitivity of such LSPR sensor can be significantly improved and a refractive index sensitivity as high as 30,000 nm/ RIU has been reported [20]. Considering the fact that, in this work, the GNRs were randomly immobilized on the surface of optical fibre (because it is difficult to control the orientation of the GNRs by using the dip coating method), thus, increasing the sensing length could also increase the chance that more GNRs can be vertically immobilized on the surface of fibre, which results in the increase in sensitivity. Therefore, for the GNR-based optical fibre sensors with the same aspect ratio of GNRs but different sensing length, the rise in sensitivity could be attributed to two reasons: first, a greater level of nanoparticle-incident

light interaction at the longer sensing lengths; second, more GNRs vertically immobilized on the surface of optical fibres with longer sensing lengths. However, for the LSPR sensors with sensing lengths of greater than 2 cm, due to the loss of protection from cladding and jacket, the sensing area is more prone to damage, both during the sensor preparation and in practical applications, which makes such sensors more difficult to handle. Therefore, in order to enhance the sensor performance, a sensing length of 2 cm was chosen for further biosensing applications.

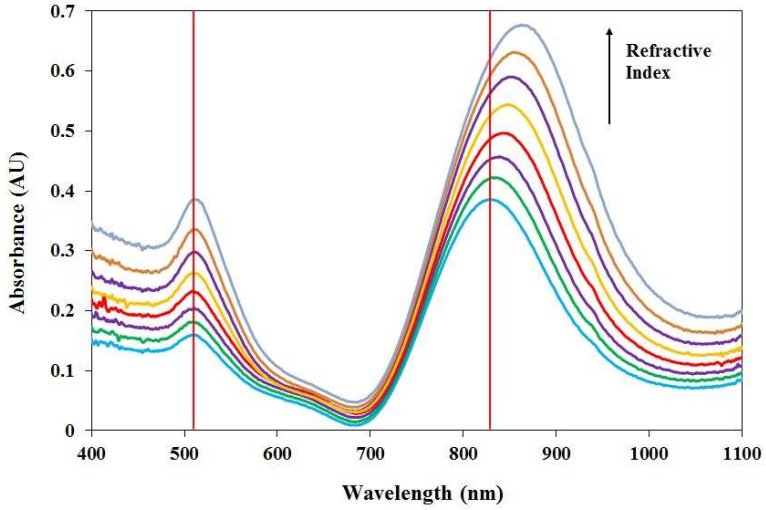

(a)

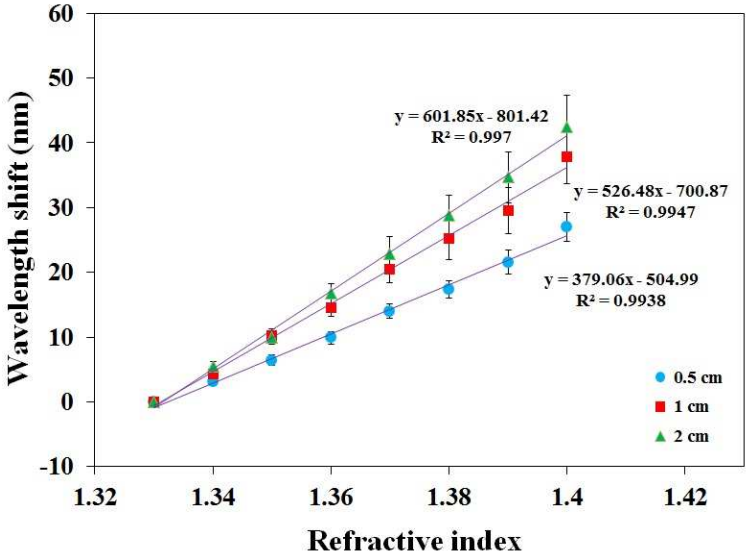

(b)

Fig. 4.2. (a) Overlapping absorption spectra of the GNRs-based LSPR sensor with a sensing length of 2 cm, with increase of the refractive index, (b) refractive index sensitivities of GNR-based LSPR sensors with different sensing length of 0.5, 1 and 2 cm.

4.3 Functionalization of LSPR sensor probe

4.3.1 Materials

Human IgG (purified immunoglobulin, reagent grade), anti-humanIgG (whole molecule, produced in goat), 11-Mercaptoundecanoic acid (MUA), bovine serum albumin (BSA), N-(3-Dimethylaminopropyl)-N′-ethylcarbodiimide hydrochloride (EDC) and *N*-hydroxysulfosuccinimide (Sulfo-NHS) were purchased from Sigma Aldrich. Ultrapure de-ionized (DI) water (18 MΩ) was used to prepare all solutions.

4.3.2 Procedure of functionalizing GNRs to create LSPR sensor probe

In order to evaluate the biosensing performance of the GNR-based LSPR optical fibre sensor probes prepared above when working as a label-free biosensor, the sensor probes were further functionalized with human IgG to detect anti-human IgG through the specific recognition between them using a EDC/NHS coupling method, which has been commonly applied for the proteins immobilization and conjugation [19, 21-23]. Fig. 4.3 illustrates the functionalization process, and the detailed procedure is described below.

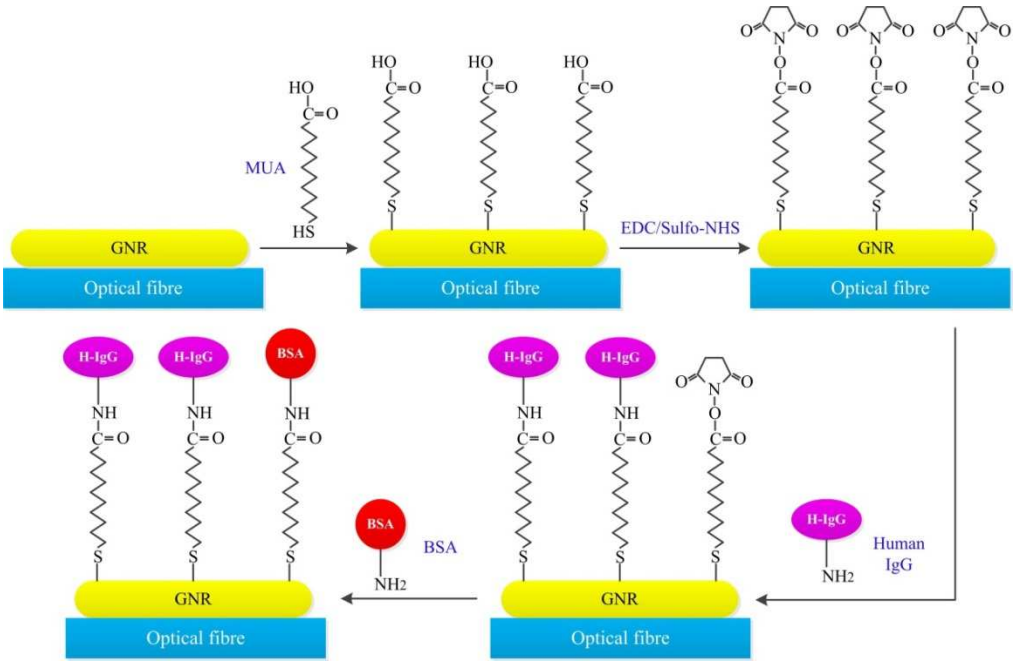

Fig. 4.3. A schematic diagram showing the process of functionalizing GNRs to create a LSPR sensor probe.

As shown in Fig. 4.3, the surfaces of the GNRs immobilized on the optical fibre were first modified with a carboxylic group-terminated thiol, MUA, by incubating the sensor probe in 10 mM MUA-ethanol solution overnight. After being thoroughly rinsed with ethanol and 0.01 M PBS buffer (with pH 7.4) respectively to remove the unbound MUA, the MUA-modified sensor probe was then immersed into a mixture of 2 mM EDC and 5 mM Sulfo-NHS for 30 minutes in 0.01M PBS buffer (with pH 5) in order to activate the carboxyl group of MUA. After the EDC/NHS activation, the fibre was then thoroughly rinsed with PBS buffer with pH 7.4 to remove the unreacted EDC/NHS, followed by being incubated in 250 µg/mL human IgG solution for 2 hours. In order to prevent any nonspecific binding, a blocking agent, BSA, was applied to block the sensing surface by immersing the PBS rinsed fibre into 2 mg/mL BSA solution for 1 hour. After being rinsed with PBS buffer with pH 7.4, finally, the sensor probe was stored in PBS buffer with pH 7.4 at 4 °C before use. Such functionalized sensor probe was then ready to detect the analyte – anti-human IgG in this case.

4.3.3 Discussions

In this experiment, MUA was applied as the cross-linker to cross-link the human IgG to the surface of GNR immobilized on the optical fibre. MUA has two terminal functional groups, with one being the thiol group and another being the carboxyl group. The thiol group of MUA works as an anchor enabling the MUA molecule to be immobilized on the GNR surface via the strong Au-S covalent bond, which results in the formation of the functional carboxyl groups on the GNR surface. The carboxyl group of MUA can be used to couple the amino group of human IgG, but not in its original form. To couple with amine, the carboxyl group of MUA needs to be activated by EDC first to form an amine-reactive *O*-acylisourea intermediate, which can react with an amine on molecule, yielding a conjugate of the two molecules joined by a stable amide bond. However, this intermediate is not stable that, if this intermediate does not encounter an amine, it will hydrolyze and regenerate the carboxyl group. The addition of Sulfo-NHS stabilizes the amine-reactive intermediate by converting it to an amine-reactive Sulfo-NHS ester, thus increasing the efficiency of EDC-mediated coupling reactions [24, 25]. As demonstrated in Fig. 4.3, the amino group of human IgG reacts with the amine-reactive Sulfo-NHS ester, binding human IgG to the surface of GNR immobilized on the optical fibre via the covalent amide bond. However, even given enough binding time, there still a chance that the not all of the Sulfo-NHS ester have reacted with human IgG, which will result in the nonspecific binding after the addition of target

molecules. Therefore, to ensure that the amine-reactive Sulfo-NHS esters binding to the GNR surface are fully occupied, a blocking agent, which has nonspecific affinity for neither human IgG nor anti-human IgG, is needed to block the sensing surface of the GNR-based LSPR optical fibre sensor. Herein, BSA with amino group was employed as the blocking agent to react with the unoccupied Sulfo-NHS ester.

4.4 Evaluation of the LSPR biosensor performance

4.4.1 Experimental set-up

As shown in Fig. 4.4, the experimental set-up used in this experiment is the same to the one used in the refractive index sensitivity study in Chapter 3.

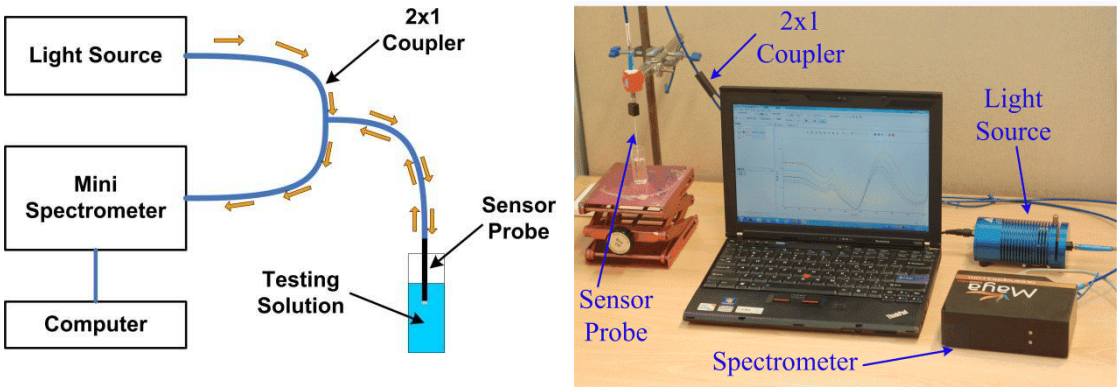

(a) (b)

Fig. 4.4. Schematic diagram (a) and photograph (b) of the experimental set-up.

4.4.2 Detection of target biomolecules

In order to evaluate the biosensing performance of the LSPR biosensor probes created above, the biosensors were then used to detect anti-human IgG with various concentrations, using the schemes illustrated in Fig. 4.5. Before the detection of the target molecules, the functionalized sensor probe was first immersed into the PBS buffer solution with pH 7.4 until a stable spectrum as the baseline was obtained and recorded. Afterwards, the sensor probe was immersed into a solution containing anti-human IgG to start the binding process and the corresponding spectrum change was monitored and recorded. The target anti-human

IgG has specific bioaffinity for human IgG immobilized on the LSPR bio-sensors, and the capture of anti-human IgG induces a refractive index change at the sensor surface, thus, the resulting signal can be captured through the LSPR effect as illustrated in Fig. 4.5.

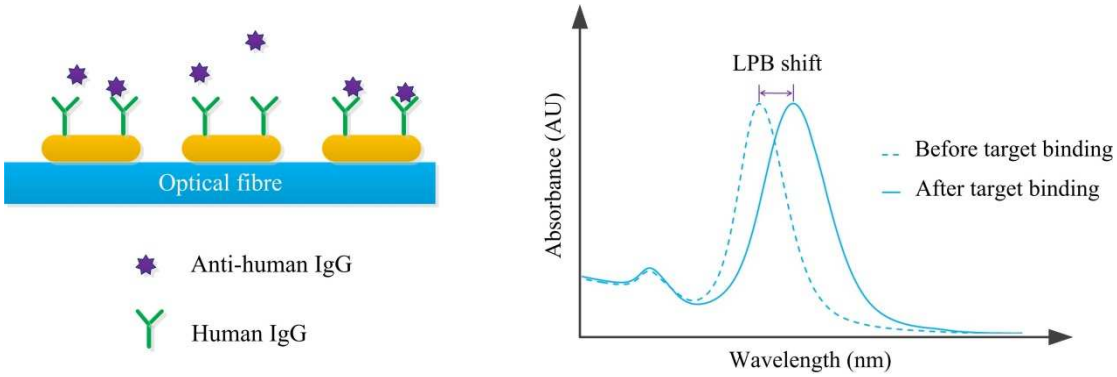

Fig. 4.5. Schematic diagram of biosensing approach using GNR-based LSPR biosensor.

4.4.3 Results and discussions

Fig. 4.6 demonstrates the target binding process monitored continuously for the GNR-based LSPR biosensors, when the sensor probe was immersed into an 8 nM anti-human IgG solution in PBS buffer with pH 7.4 for 2 h. The absorption spectra of the antibody-antigen binding process were recorded every 5 min. As shown in Fig. 4.6, a clear and gradual red shift of LPB peak wavelength was observed with the increase of the absorbance over time. As was discussed previously, before the functionalization with human IgG, when the GNR-based sensor probe was immersed into a testing solution with a particular refractive index, their absorption spectra were seen to quickly reach and stabilize at a specific spectral position (thus without that position shifting). However, when the functionalized sensor probes were dipped into the solution containing the molecules of anti-human IgG, the spectra of the sensor first reached the baseline rapidly, but then a gradual red shift of LPB and an increasing absorbance in the absorption spectra were observed as shown in Fig. 4.6. This red shift of LPB as well as the increasing absorbance was caused by the increase of refractive index at the sensing surface due to the binding taking place gradually between the human IgG immobilized on the GNPs and the anti-human IgG in the solution. The spectral shift, on the other hand, also indicates the as-prepared GNR-based LSPR biosensors are highly sensitive to the micro-refractive index change raised by the biomolecular interactions,

demonstrating the successful fabrication and functionality of the LSPR biosensors prepared in this work.

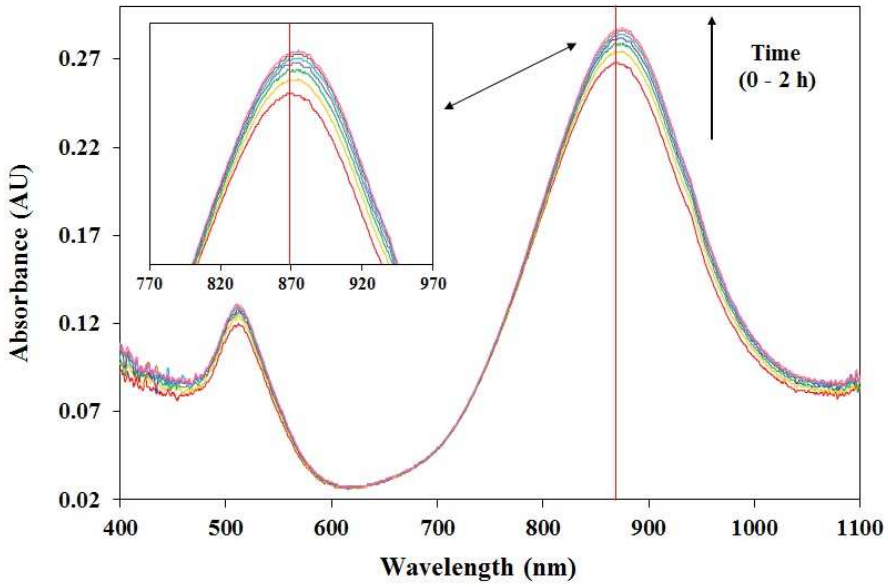

Fig. 4.6. Continuous monitoring of the process of anti-human IgG binding to human IgG immobilized on GNR-based LSPR biosensor over a period of 2 hours.

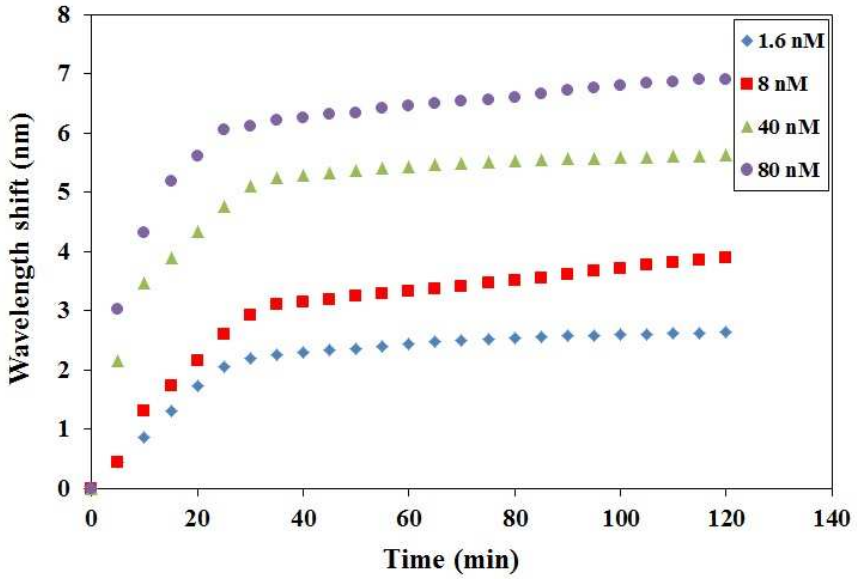

Fig. 4.7. LPB peak wavelength shift of GNR-based LSPR biosensor as a function of the incubation time at different concentrations of anti-human IgG.

Fig. 4.7 summarize the results obtained, revealing the LPB peak wavelength shift of the GNR-based LSPR biosensors, when different sensor probes were incubated in the anti-human IgG solution at concentrations of 1.6 nM, 8 nM, 40 nM and 80 nM for a period of 2 h. It was found that, despite the greater peak wavelength shift being observed at the higher concentrations of the anti-human IgG, the effective antigen-antibody binding for all concentrations nearly always took place in only the first half an hour of incubation, because, at each concentration of anti-human IgG, the peak wavelength shift increases dramatically during the first 30 min. After that, although the binding still continued during the rest of the 2 hours period of incubation, the increase of the peak wavelength shift was slowed down dramatically as shown in Fig. 4.7. The results indicate that the majority of anti-human IgG binding happened in the first half hour, therefore, at least 30 min of incubation time is required when the as-prepared LSPR optical fibre sensors operate as biosensors. It is worth to note that, the sensor response not only depends on the availability of the free binding sites on the sensor surface and the target molecules, but also depends on the biomolecular recognition rate. For biomolecules with different recognition rate, the sufficient incubation time required could be different.

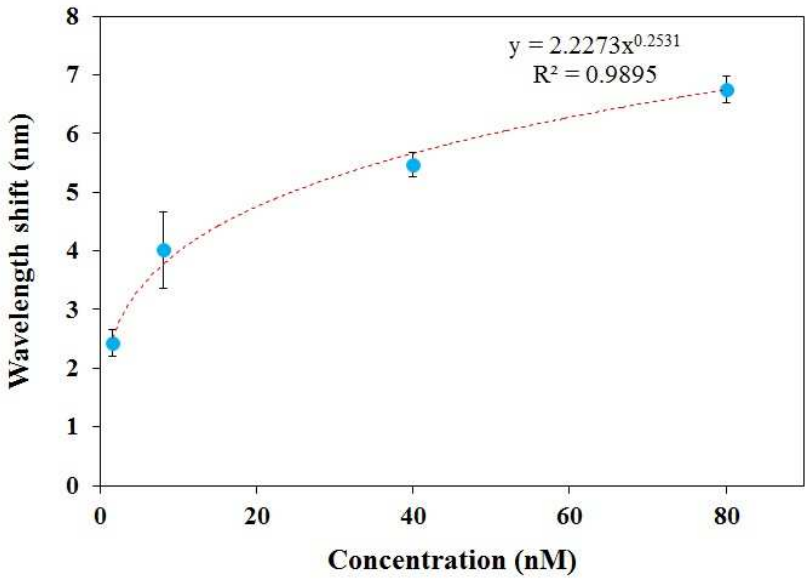

Fig. 4.8. LPB peak wavelength shift of GNR-based LSPR biosensor as a function of concentration of anti-human IgG after a 2 h period of incubation.

The sensor response (LPB peak wavelength shift) as a function of the concentration of anti-human IgG after a period of 2 hours incubation is shown in Fig. 4.8. For each concentration, at least three independent measurements from the different sensor probes were undertaken,

in order to allow the calculation of the averages and standard deviations. As demonstrated in Fig. 4.8, the higher is the concentration of anti-human IgG, the greater the LPB peak wavelength shift that can be observed. This is due to the fact that antigen-antibody binding taking place at a higher concentration of anti-human IgG results in a greater refractive index change at the surface of sensor probes. The LPB peak wavelength shifts were found to be 2.81±0.49 nm, 4.18±0.27 nm, 6.12±0.91 nm and 7.47±0.68 nm, corresponding to the incubation in anti-human IgG solutions with concentration of 1.6 nM, 8 nM, 40 nM and 80 nM, respectively. The detection limit, defined as the lowest detectable concentration, was determined to be 1.6 nM for the GNR-based LSPR biosensor, as it is difficult to recognize the wavelength shift when the concentration of anti-human IgG is below 1.6 nM.

Compared with the results of previous studies based on spherical GNPs, a slight lower detection limit (0.8 nM) for the U-bent LSPR optical fibre sensor using spherical GNPs with a mean diameter of 40 nm has been reported by Sai *et al* [8]. However, rather than interrogating the LSPR peak wavelength as was done in the work herein, the sensor reported by Sai *et al* was actually evaluated using an absorbance-based measurement, where the absorbance change was measured at a fixed wavelength. This is due to the fact that the LSPR wavelength of their sensor is insensitive to the refractive index change. As shown in Fig. 4.6, the binding of anti-human IgG resulted in both the red-shift of LPB peak wavelength and the increase of absorbance in the absorption spectra of the GNR-based LSPR biosensor created in this work. Therefore, technically, both wavelength- and absorbance-based interrogation methods can be applied measuring the LSPR response. However, the reason we prefer the wavelength-based approach to the intensity- or absorbance-based approach in this work is that, the former method allows for changes to the intensity of the light transmitted or received by the fibre – for example due to changes in alignment, variations in source intensity or fibre bending in use: all effects which in an intensity- or absorbance-based measurement regime can be mistaken for changes to the actual measurement and potentially cause errors in the final result. Therefore, compared to the intensity- and absorbance-based approaches, the wavelength-based interrogation method offers more reliable and accurate results.

On the other hand, by comparing these results with those previously reported for LSPR sensors which also use the wavelength-based measurement approach, it was found out that the defection limit of the sensor reported was close to that reported by Mayer *et al* (1 nM) [26] and higher than that of the chip based LSPR sensors reported by Marinakos *et al* (0.94 nM) [27], but much lower than that of a solution-phase based LSPR sensor reported by Yu *et*

al (10 nM) [28]. Despite a lower detection limit being achieved by the chip based LSPR sensor [27], that sensor system requires more expensive bulk components, such as a UV-Vis spectrophotometer and a greater volume of sample, compared to the optical fibre based sensor system used in our work.

The promising results obtained herein show that the GNR-based LPSR optical fibre sensors prepared in this work have the ability to be a sensitive label-free biosensor for studying the interaction between biomolecules as well as other biosening applications. In addition, the sensor performance could be further improved by optimizing the key parameters of the sensor such as the aspect ratio of the GNRs, and employing the tapered sensor probe which has shown higher refractive index sensitivity in SPR sensing.

4.5 Summary

In this chapter, a GNR-based LSPR optical fibre biosensor has been fabricated, evaluated and cross-compared. Based on the previous study, GNRs with an aspect ratio of 4.1 synthesized by the seed-mediated growth method were employed to fabricate the sensor probes, as they have demonstrated high sensitivities to refractive index change. In order to further enhance the sensor performance, the effect of sensing length on the refractive index sensitivity has also been studied and the results have shown that the GNR-based LSPR sensors with a 2 cm sensing length has the optimum refractive index sensitivities as high as 601 nm/RIU. Such sensor probe has been further functionalized with human IgG for developing a label-free LSPR biosensor. The detailed functionalization procedure has been described and discussed. The evaluation of the biosensing performance of the as-prepared LSPR biosensor has been performed by immersing the sensor probes into the anti-human IgG solution with different concentrations and measuring the absorption spectral change using a wavelength-based interrogation approach. The results show that the LPB peak wavelength of GNRs is sufficiently sensitive to detect the small refractive index changes caused by the biomolecular interaction, and a detection limit of 1.6 nM for detecting anti-human IgG was found for the as-prepared GNR-based LSPR biosensor. Compared to previously reported LSPR optical fibre biosensors, which are only based on the absorbance or intensity measurement (due to the poor wavelength sensitivity), the GNR-based LSPR biosensors demonstrated in this work are able to be interrogated based on their wavelength shifts, due to their high wavelength sensitivities to both bulk and micro-refractive index changes. The GNR-based LSPR optical fibre biosensors reported are relatively inexpensive

to produce, thus potentially disposable after single use and could be developed further for a wide range of other bio-sensing applications, especially enabling the wavelength interrogation approach shown to be successful in this work to be more widely used.

4.6 References

[1] L.S. Jung, C.T. Campbell, T.M. Chinowsky, M.N. Mar, S.S. Yee, Quantitative interpretation of the response of surface plasmon resonance sensors to adsorbed films, Langmuir : The ACS Journal Of Surfaces And Colloids, 14 (1998) 5636-5648.

[2] J. Cao, E.K. Galbraith, T. Sun, K.T.V. Grattan, Cross-comparison of surface plasmon resonance-based optical fiber sensors with different coating structures, IEEE Sensors Journal, 12 (2012) 2355-2361.

[3] A.J. Haes, R.P. Van Duyne, A unified view of propagating and localized surface plasmon resonance biosensors, Analytical and bioanalytical chemistry, 379 (2004) 920-930.

[4] K.A. Willets, R.P. Van Duyne, Localized surface plasmon resonance spectroscopy and sensing, Annual Review Of Physical Chemistry, 58 (2007) 267-297.

[5] W.H. Ni, H.J. Chen, X.S. Kou, M.H. Yeung, J.F. Wang, Optical fiber-excited surface plasmon resonance spectroscopy of single and ensemble gold nanorods, Journal of Physical Chemistry C, 112 (2008) 8105-8109.

[6] T.J. Lin, C.T. Lou, Reflection-based localized surface plasmon resonance fiber-optic probe for chemical and biochemical sensing at high-pressure conditions, Journal Of Supercritical Fluids, 41 (2007) 317-325.

[7] H.Y. Lin, C.H. Huang, G.L. Cheng, N.K. Chen, H.C. Chui, Tapered optical fiber sensor based on localized surface plasmon resonance, Optics Express, 20 (2012) 21693-21701.

[8] V.V.R. Sai, T. Kundu, S. Mukherji, Novel U-bent fiber optic probe for localized surface plasmon resonance based biosensor, Biosensors & Bioelectronics, 24 (2009) 2804-2809.

[9] K. Mitsui, Y. Handa, K. Kajikawa, Optical fiber affinity biosensor based on localized surface plasmon resonance, Applied Physics Letters, 85 (2004) 4231-4233.

[10] L.K. Chau, Y.F. Lin, S.F. Cheng, T.J. Lin, Fiber-optic chemical and biochemical probes based on localized surface plasmon resonance, Sensors And Actuators B-Chemical, 113 (2006) 100-105.

[11] N.S. Lai, C.C. Wang, H.L. Chiang, L.K. Chau, Detection of antinuclear antibodies by a colloidal gold modified optical fiber: comparison with ELISA, Analytical And Bioanalytical Chemistry, 388 (2007) 901-907.

[12] T.J. Lin, M.F. Chung, Detection of cadmium by a fiber-optic biosensor based on localized surface plasmon resonance, Biosensors & Bioelectronics, 24 (2009) 1213-1218.

[13] K.T. Huang, T.J. Lin, M.H. Hsu, Determination of cyclic GMP concentration using a gold nanoparticle-modified optical fiber, Biosensors & Bioelectronics, 26 (2010) 11-15.

[14] H.W. Liao, J.H. Hafner, Gold nanorod bioconjugates, Chemistry Of Materials, 17 (2005) 4636-4641.

[15] K. Fujiwara, H. Watarai, H. Itoh, E. Nakahama, N. Ogawa, Measurement of antibody binding to protein immobilized on gold nanoparticles by localized surface plasmon spectroscopy, Analytical And Bioanalytical Chemistry, 386 (2006) 639-644.

[16] H.H. Jeong, N. Erdene, S.K. Lee, D.H. Jeong, J.H. Park, Fabrication of fiber-optic localized surface plasmon resonance sensor and its application to detect antibody-antigen reaction of interferon-gamma, Optical Engineering, 50 (2011).

[17] B. Sepulveda, P.C. Angelome, L.M. Lechuga, L.M. Liz-Marzan, LSPR-based nanobiosensors, Nano Today, 4 (2009) 244-251.

[18] H. Huang, C.C. He, Y.L. Zeng, X.D. Xia, X.Y. Yu, P.G. Yi, Z. Chen, A novel label-free multi-throughput optical biosensor based on localized surface plasmon resonance, Biosensors & Bioelectronics, 24 (2009) 2255-2259.

[19] W. Hu, C.M. Li, H. Dong, Poly(pyrrole-co-pyrrole propylic acid) film and its application in label-free surface plasmon resonance immunosensors, Analytica Chimica Acta, 630 (2008) 67-74.

[20] A.V. Kabashin, P. Evans, S. Pastkovsky, W. Hendren, G.A. Wurtz, R. Atkinson, R. Pollard, V.A. Podolskiy, A.V. Zayats, Plasmonic nanorod metamaterials for biosensing, Nature Materials, 8 (2009) 867-871.

[21] Z. Grabarek, J. Gergely, Zero-length crosslinking procedure with the use of active esters, Analytical Biochemistry, 185 (1990) 131-135.

[22] T. Kawaguchi, D.R. Shankaran, S.J. Kim, K. Matsumoto, K. Toko, N. Miura, Surface plasmon resonance immunosensor using Au nanoparticle for detection of TNT, Sensors And Actuators B-Chemical, 133 (2008) 467-472.

[23] H.M. Hiep, T. Endo, K. Kerman, M. Chikae, D.-K. Kim, S. Yamamura, Y. Takamura, E. Tamiya, A localized surface plasmon resonance based immunosensor for the detection of casein in milk, Science And Technology Of Advanced Materials, 8 (2007) 331-338.

[24] N. Naue, R. Fedorov, A. Pich, D.J. Manstein, U. Curth, Site-directed mutagenesis of the chi subunit of DNA polymerase III and single-stranded DNA-binding protein of E-coli reveals key residues for their interaction, Nucleic Acids Research, 39 (2011) 1398-1407.

[25] T.B. Updegrove, J.J. Correia, Y.F. Chen, C. Terry, R.M. Wartell, The stoichiometry of the Escherichia coli Hfq protein bound to RNA, RNA, 17 (2011) 489-500.

[26] K.M. Mayer, S. Lee, H. Liao, B.C. Rostro, A. Fuentes, P.T. Scully, C.L. Nehl, J.H. Hafner, A label-free immunoassay based upon localized surface plasmon resonance of gold nanorods, ACS Nano, 2 (2008) 687-692.

[27] S.M. Marinakos, S. Chen, A. Chilkoti, Plasmonic detection of a model analyte in serum by a gold nanorod sensor, Analytical Chemistry, 79 (2007) 5278-5283.

[28] C. Yu, L. Varghese, J. Irudayaraj, Surface modification of cetyltrimethylammonium bromide-capped gold nanorods to make molecular probes, Langmuir : The ACS Journal Of Surfaces And Colloids, 23 (2007) 9114-9119.

Chapter 5

Surface modification of CTAB-capped GNRs for LSPR biosensor development

5.1 Introduction

The seed-mediated growth method for the synthesis of GNRs has been widely applied due to its simplicity and high yields of GNRs compared to other approaches such as electrochemical method [1], template method [2] and lithographic method [3]. The surface of GNRs synthesized using the seed-mediated growth method is fully covered by the dense bilayers of positively charged CTAB molecules, which makes the GNRs soluble in aqueous solution [4]. CTAB plays a significantly important role in the synthesis of GNRs. It not only works as a "structure-directing agent" to assemble the gold ions forming the rod-shape particles, but also works as a stabilizer to prevent the as-synthesized GNRs from aggregation [4, 5]. However, there are two main drawbacks of this CTAB bilayer limiting the CTAB-capped GNRs for further applications. First, the CTAB bilayers physisorbed onto the GNRs surface are not robust and can be easily dissociated from the GNRs surface under many circumstances such as those with high salt content, low CTAB concentration and addition of organic solvents, resulting in the irreversible aggregation of GNRs [6, 7]. This disadvantage makes the CTAB-capped GNRs difficult to be applied as a solution-phase-based LSPR biosensor for biosensing applications where the GNRs are needed to work in buffer solutions with the high salt content. Second, it has been found that free CTAB molecules show high cytotoxity in *in vitro* studies, while the bound CTAB molecules are not toxic [8]. Although the majority of free CTAB molecules in GNRs solutions can be separated by centrifugation [8], the unstable physisorption of CTAB could also result in the release of part of the bound CTAB from the GNRs surface. In addition, the complete removal of CTAB molecules also results in the irreversible aggregation of GNRs in solution. Therefore, it is necessary to apply

an appropriate approach to modify the CTAB-capped GNRs surface, in order to extend their applications for solution-phase-based LSPR biosensing, cell imaging, drug delivery and disease therapy [9, 10].

As introduced in Chapter 2, there are basically two approaches that have been applied for the surface modification of GNRs: an *indirect* approach involving the introduction of an additional layer, such as silver coating [11, 12], silicon coating [13, 14] and polyelectrolyte coating [15, 16], to cover the entire CTAB-capped GNRs surface, and a *direct* approach regarding the replacement of CTAB with the thiol-terminated ligands such as thiolated PEGs [17-20] and MUA [21-23] via ligand exchange. For the *indirect approach*, since the LSPR effect decays exponentially from the surface of GNRs, additional layer of coating will increase the distance between the GNRs surface and target molecules, thus resulting in the decrease of sensitivity when such surface modified GNRs are employed to make an LSPR biosensor. The *direct* method, on the other hand, can overcome this limitation. Compared to the thoilated PEGs, which have the large molecular size, MUA is a smaller molecule that can offer higher sensitivity and its terminal carboxyl group can be further functionalized to conjugate biomolecules. These advantages make MUA an ideal candidate as a functional linker for the preparation of biosensors. However, the common procedure of using MUA ethanolic solution to modify the surface of GNRs immobilized on a substrate, such as the example we demonstrated in Chapter 4, cannot be directly applied for the free GNRs suspending in solution. This is because that the MUA molecule has a hydrophobic property, and the CTAB molecules bound to the GNRs surface are not stable in the ethanolic solution. Therefore, protections such as constant sonication at elevated temperature [21, 22] or using an ionic exchange resin [23] are normally required to prevent the irreversible aggregation of GNRs during the ligand exchange. However, from the experience of this research, these methods either often lead to aggregation or are complicated to implement.

This chapter introduces a novel robust pH-mediated protocol for effectively modifying the surface of CTAB-capped GNRs and the demonstration of using such surface modified GNRs as a generic label-free LSPR biosensing platform. The bilayer of CTAB molecules attaching to the surface of GNRs synthesized by using the seed-mediated growth method have been replaced by MUA molecules at alkaline pH, which allows the ligand exchange between CTAB and MUA at GNRs surface to take place in an aqueous condition without additional protections. The success of the replacement of CTAB has been confirmed by the surface elemental analysis performed using an X-ray photoelectron spectroscopy (XPS). Subsequently, the MUA-modified GNRs have been further functionalized with human IgG

to develop a solution-phase-based label-free LSPR biosensor for detecting anti-human IgG, and the biosensing performances of the LSPR biosensor created have also been demonstrated.

5.2 Novel surface modification of CTAB-capped GNRs

5.2.1 Materials

Gold (III) chloride trihydrate ($HAuCl_4 \cdot 3H_2O$), ascorbic acid, silver nitrate ($AgNO_3$), cetyltrimethylammonium bromide (CTAB), sodium borohydride ($NaBH_4$), sodium hydroxide (NaOH), 11-Mercaptoundecanoic acid (MUA) and ethanol were purchased from Sigma Aldrich. Ultrapure de-ionized (DI) water (18 MΩ) was used to prepare all solutions. All chemicals and reagents were of analytical grade and used as received. All procedures were conducted at room temperature unless specified otherwise.

5.2.2 Instrumentation and characterization

The absorption spectra of the GNRs solutions were measured by using a LAMBDA 35 UV/VIS spectrophotometer (PerkinElmer Inc.) as shown in Fig. 5.1 (a), over the wavelength range from 400 nm to 1100 nm. The mean aspect ratio of the gold nanorods was determined by using a JEOL 1010 TEM. The TEM samples were prepared by placing 2 µL of diluted gold nanorods solution on a 3 mm 400-mesh Formvar coated copper grid (purchased from Agar Scientific) and evaporating the solution at room temperature. The surface elemental analyses were performed at the X-ray photoelectron spectrometer (XPS) analysis centre located within the Cardiff University, using a Kratos AXIS Ultra DLD XPS equipped with a delay-line detector and a radiation source (a monochromatic Al Kα X-ray source) as demonstrated in Fig. 5.1 (b). The XPS samples were prepared by dropping concentrated MUA-modified GNR solution on the silicon wafers. The XPS data were analyzed using CasaXPS software.

(a)

(b)

Fig. 5.1. Photographs of (a) absorption spectrum analysis system, and (b) XPS analysis system.

5.2.3 Preparation of GNRs

GNRs with three different aspect ratios were prepared by following the same procedure described in Chapter 3 using the seed-mediated growth method. The aspect ratio of GNRs was controlled by manipulating the amount of silver ions in the growth solution, with other conditions kept consistent with those mentioned in Chapter 3. In this work, the addition of

120, 200 and 300 µL of 0.02 M $AgNO_3$ solutions to three identical growth solutions resulted in the produce of GNRs with aspect ratios of 2.6 ± 0.2, 3.3 ± 0.25, 3.9 ± 0.4, respectively, which were determined by the TEM images analysis. Fig. 5.2 (a) and (b) shows both the absorption spectra and the TEM images of the as-synthesized GNR solutions with different aspect ratios. The TPB of GNRs appears at about 510 nm while the LPB has a red shift from about 685 nm to 790 nm with the increase of the aspect ratio.

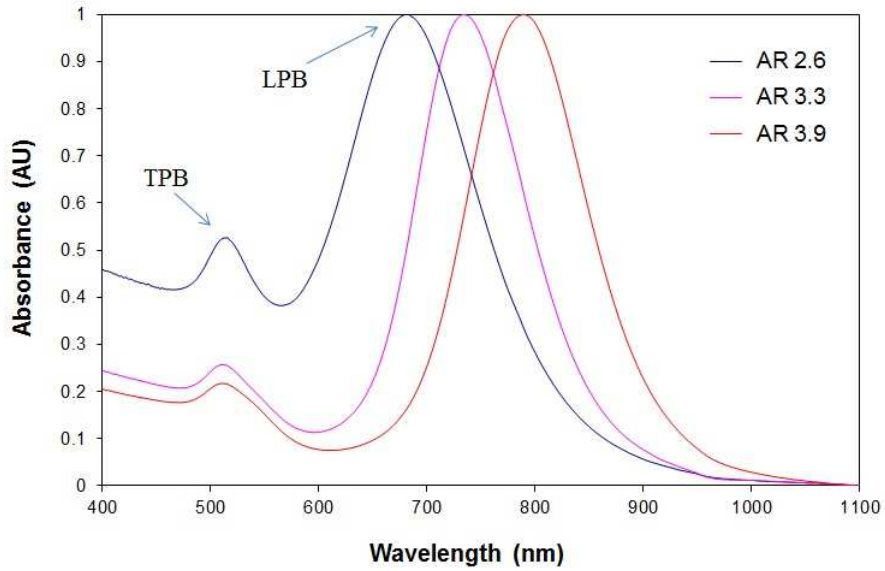

(a)

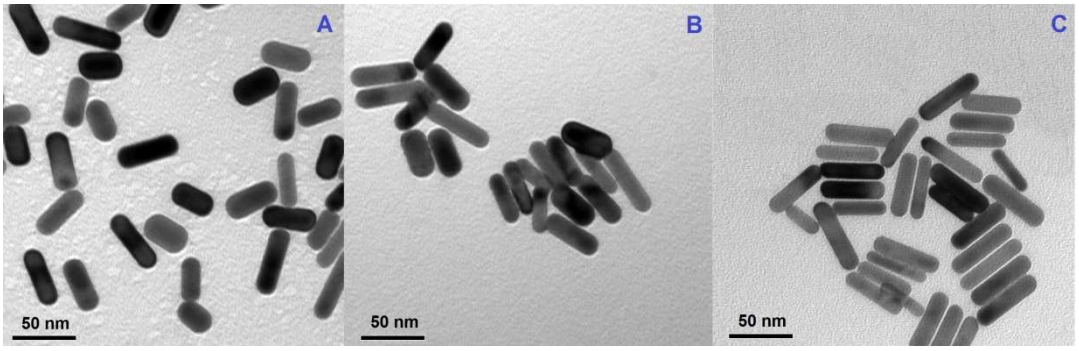

(b)

Fig. 5.2. (a) Absorption spectra of GNRs solution with different aspect ratios, (b) TEM images of GNRs with aspect ratios: A-2.6 ± 0.2, B-3.3 ± 0.25, C-3.9 ± 0.4.

5.2.4 Novel procedure of surface modification of GNRs

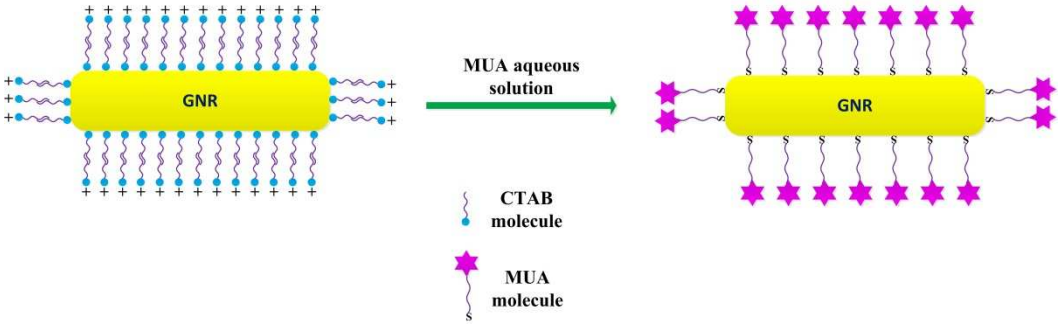

Fig. 5.3. Schematic illustration of surface modification of the CTAB-capped GNR with MUA.

A novel but simple pH-mediated method was applied in this experiment to completely replace CTAB from the surface of GNRs synthesized above. The detailed procedure used was as follows: prior to the surface modification of the GNRs, excess CTAB in the GNRs solutions with different aspect ratios synthesized as above was removed by two rounds of centrifugation at 8000 rpm for 20 min for each round. The supernate was carefully decanted and the GNRs were re-suspended in an equal amount of DI water. 20 mM MUA aqueous solution was prepared by adding 44 mg MUA to 10 mL DI water. In order to dissolve MUA, the mixture was first put under sonication for several minutes until the majority of the MUA was dispersed in water, which results in a white cloudy suspension. Subsequently, 0.2 M NaOH solution was added to the MUA solution (dropwise) with stirring and periodic sonication, until the MUA dissolves. As illustrated in Fig. 5.3, after the preparation of MUA aqueous solution, 4 mL of 20 mM MUA aqueous solution was added to each 10 mL of purified GNRs solutions with different aspect ratios prepared as above with vigorously stirring for 24 h, in order to completely replace the CTAB bound onto the GNRs surface. Finally, excess MUA was removed by another two rounds of centrifugation at 8000 rpm for 20 min each time, and the MUA-modified GNRs were then re-dispersed in 0.01 M borate buffer at pH 9.

5.2.5 Results and discussions

5.2.5.1 Surface modification of GNRs

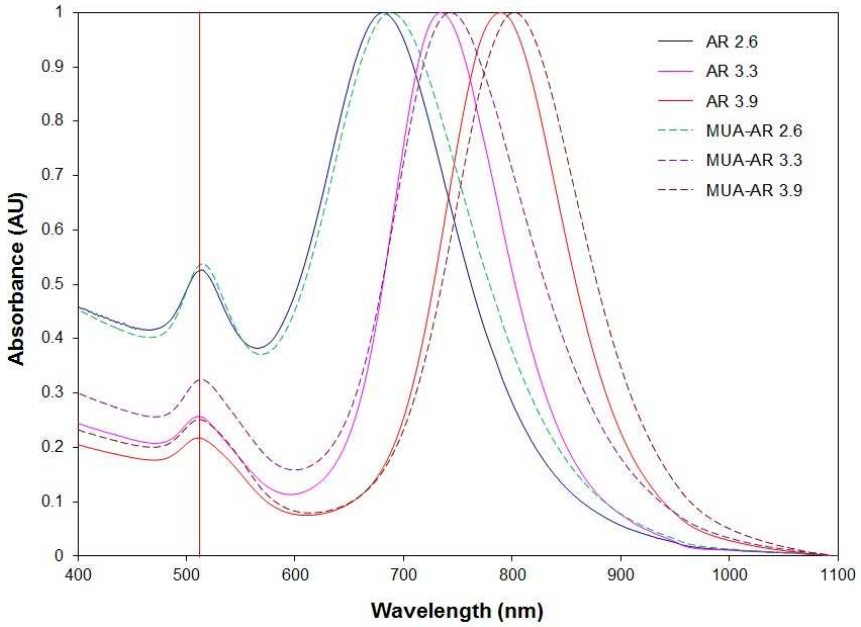

Fig. 5.4. Absorption spectra of GNRs before and after being modified with MUA.

Fig. 5.4 shows the absorption spectra of the GNRs in solution before and after being modified by MUA. The absorption spectra of GNRs before being modified by MUA shown in Fig. 5.4 were taken from the same spectra shown in Fig. 5.2 (a). As demonstrated in Fig. 5.4, after the surface modification, the spectra of the MUA-modified GNRs with different aspect ratios almost remain the same shape as the CTAB-capped GNRs, which indicated that no aggregation of GNRs occurred during the process of surface modification. After the ligand exchange with the MUA, the resonance peak of TPB almost still stays at 510 nm with no significant wavelength shift observed. However, a clear red shift in the LPB of GNRs with different aspect ratios was observed after the surface modification. The red shift could be attributed to the refractive index change at the surface of GNRs due to the ligand exchange. It has been reported that the LPB of GNRs in solution is more sensitive to the refractive index change of the environment surrounding the GNRs surface than TPB [24]. Table 2 summarises the change of LPW of GNRs before and after the modification with MUA. For the GNRs with aspect ratios of 2.6 ± 0.2, 3.3 ± 0.25, 3.9 ± 0.4, the resonance peak of LPB shifted about 4, 7 and 10 nm, respectively. The results obtained are in a good

agreement with those reported, confirming that the sensitivity of GNRs increases with the increase of aspect ratios [25].

Table 2. Resonance peak of LPB of GNRs before and after being modified with MUA[a].

	AR 2.6 ± 0.2	AR 3.3 ± 0.25	AR 3.9 ± 0.4
CTAB-GNRs	684.84±0.02	734.09±0.02	790.5±0.01
MUA-GNRs	688.95±0.1	741.69±0.32	801.33±0.35

[a]For each aspect ratio, the resonance peak of LPB before and after being modified with MUA was obtained from three independent measurements in order to calculate the averages and standard deviations.

In this work, the surface modification of CTAB-capped GNRs involves the efficient replacement of CTAB with MUA. The ligand exchange is realized by simply mixing the MUA aqueous solution with GNRs solution over a certain period of time. Normally, when MUA is used for the surface modification of gold film or GNPs coated on a substrate, the surface modification is carried out by immersing gold film or GNPs coated substrate in the MUA solution prepared by dissolving MUA in ethanol or an ethanol-water mixture, due to the fact that MUA has the hydrophobic character. Such an example can be found in the preparation of GNR-based LSPR optical fibre biosensor as demonstrated in Chapter 4. However, as CTAB molecules are very soluble in polar solvents like ethanol, when the CTAB-capped GNRs are in the presence of ethanol or an ethanol-water mixture, the CTAB molecules bound onto the GNRs surface become unstable and will strip off eventually. It is not a problem for the GNRs immobilized on a substrate. However, for those GNRs suspending in solution, the loss of CTAB protection due to the addition of MUA-ethanol solution will result in a serious and irreversible aggregation of GNRs. Fig. 5.5 shows the results before and after a small amount of ethanol was added to the GNRs solution. The shape of the spectrum completely changed after one hour, indicating that the GNRs have lost the protective bilayer of CTAB. That's the reason why protections such as consistent sonication at elevated temperature [21, 22] or using an ionic exchange resin [23] are necessarily needed to prevent the GNRs from aggregation in the previously reported approaches. In addition, these published approaches normally require several steps to complete. The novel methodology for surface modification of CTAB-capped GNRs in solution proposed in this work exploits the carboxylic acid group present in MUA by operation in basic aqueous solution, which can overcome the drawbacks appeared in the use of MUA ethanolic solution. In the carboxylate form, the MUA is still able to displace the CTAB molecules and prevent aggregation of the GNRs, avoiding the use of an ethanolic

solution entirely. In addition, the procedure of surface modification of GNRs demonstrated here is much simpler than that of previously reported approaches involving the use of MUA. Thus, a novel pH-mediated protocol of surface modification using MUA carboxylate is proposed in this work that removes CTAB from the GNRs surface without aggregation and simplifies the procedure to produce functionalizable GNRs in aqueous solution.

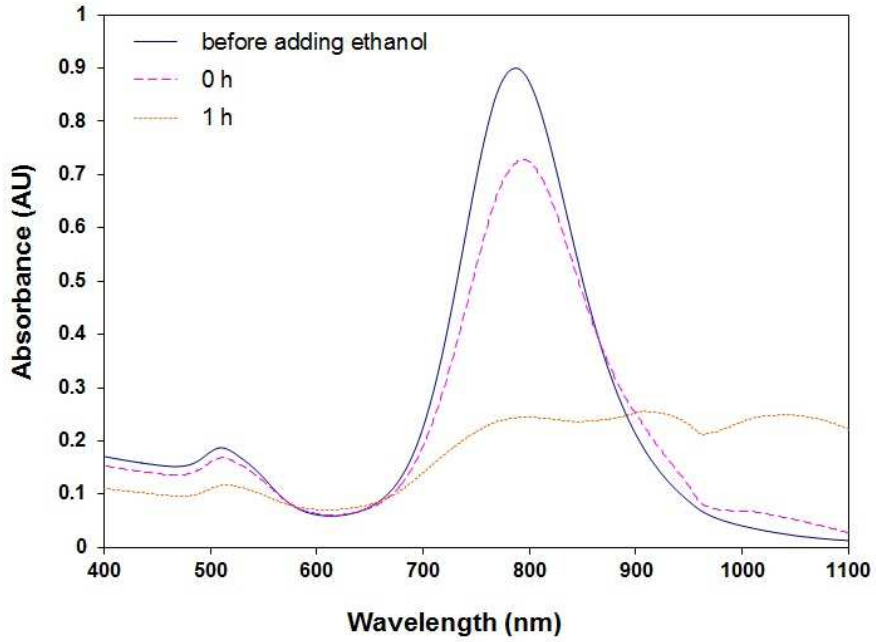

Fig. 5.5. Absorption spectra of GNRs solutions with the addition of ethanol over time.

To further confirm the success of the complete replacement of CTAB with MUA, a surface elemental analysis of the GNRs surface was carried out using XPS. Fig. 5.6 (a) and (b) shows the XPS spectra of CTAB-protected GNRs and MUA-modified GNRs, respectively. In the XPS spectrum of CTAB-capped GNRs as shown in Fig. 5.6 (a), the bromine signal was found with no sulfur signal observed, indicating the presence of CTAB before the surface modification. On the contrary, as shown in Fig. 5.6 (b), the bromine signal is absent from the XPS spectrum of MUA-modified GNRs, but a clear sulfur signal can be observed, indicating that CTAB molecules attaching to the GNRs surface have been replaced by MUA molecules after the surface modification. The results obtained from the surface elemental analysis of GNRs confirm the complete removal of CTAB and a replacement with MUA. As a silica wafer was used as the supporting substrate, the presence of the Au signal was observed in both of the XPS spectra of the CTAB-GNRs and the MUA-GNRs (inset in Fig. 5.6 (a) and (b)), verifying that the results are acquired from the GNRs indeed, rather than

from solution and this confirms further the success of the ligand exchange on the GNRs surface.

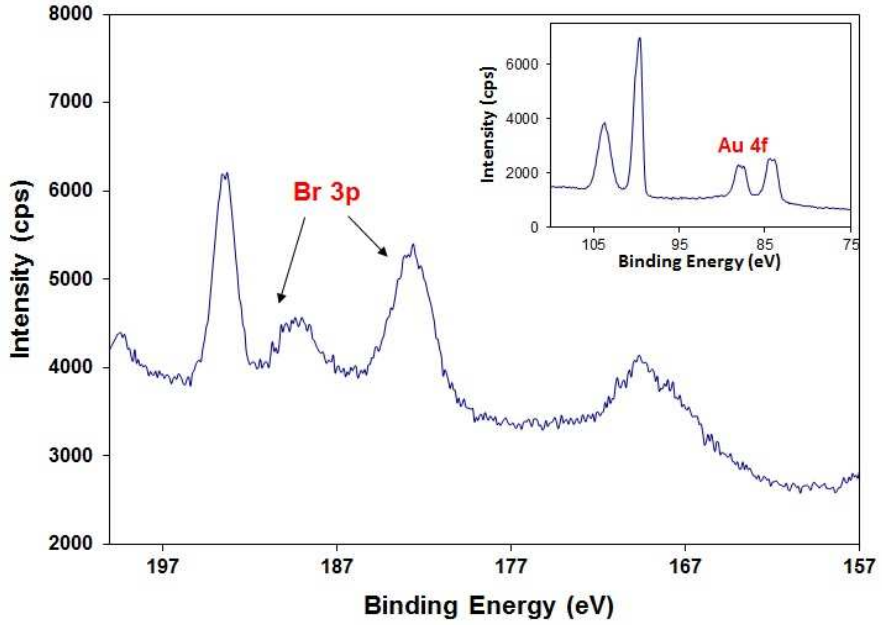

(a)

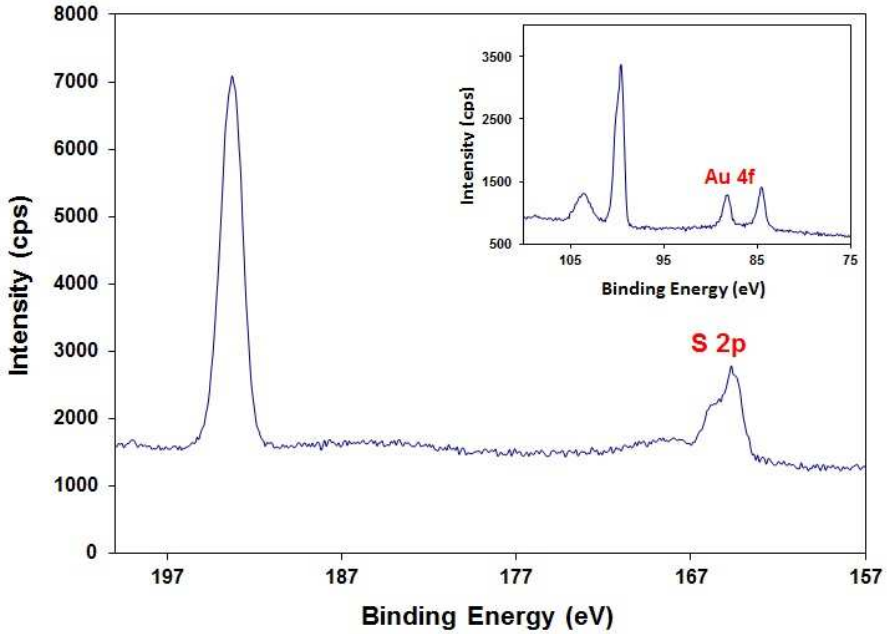

(b)

Fig. 5.6. XPS spectra of (a) CTAB-capped GNRs, and (b) MUA-modified GNRs.

5.2.5.2 Stability of MUA-modified GNRs

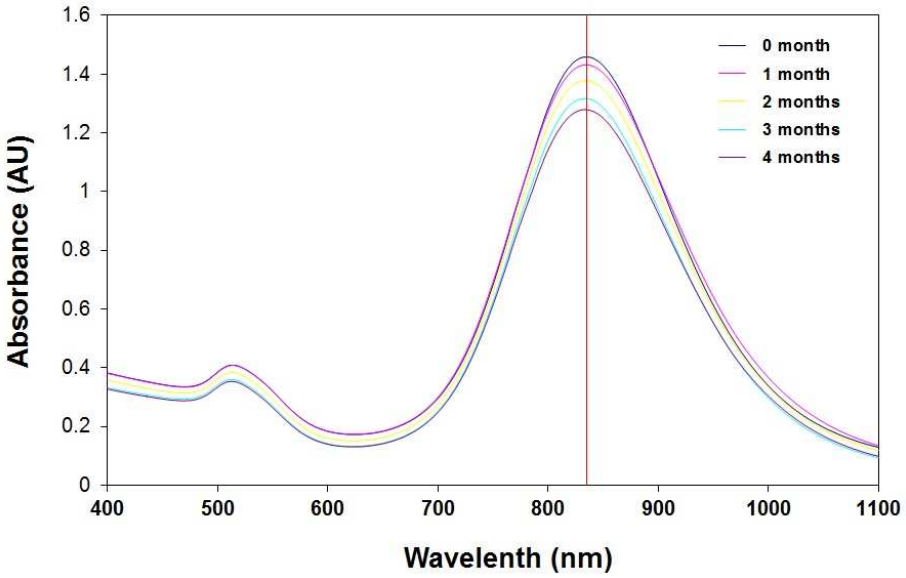

(a)

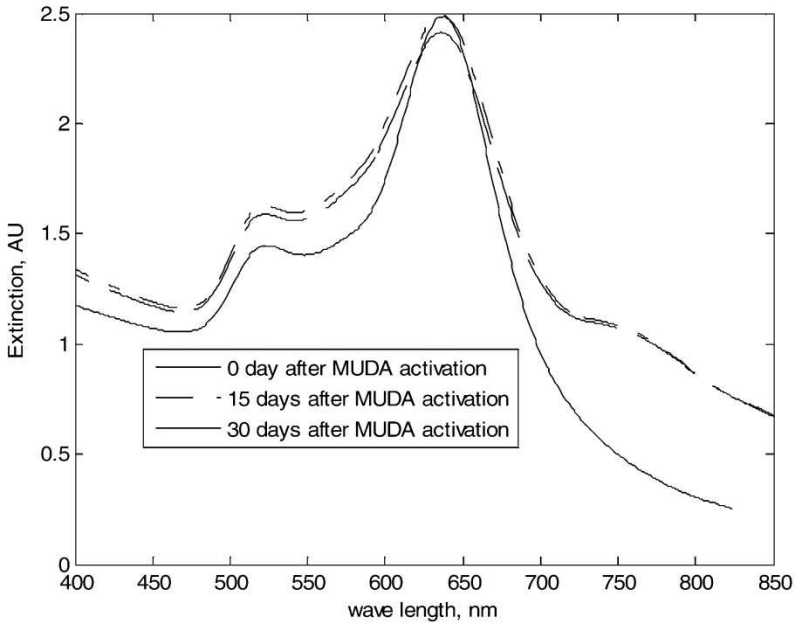

(b)

Fig. 5.7. (a) Absorption spectra of MUA-modified GNRs in borate buffer at pH 9 during 4 months storage at 4°C, (b) Stability of MUA-modified GNRs prepared and reported by other researchers [21].

After the surface modification, the MUA-modified GNRs were purified by centrifugation, followed by being resuspended in 0.01 M borate buffer at pH 9 and stored at 4°C. The stability of the MUA-modified GNRs was monitored for a period of 4 months and the absorption spectra of the GNRs solution recorded during the 4 months are shown in Fig. 5.7 (a). As can be observed in Fig. 5.7 (a), the absorbance in the absorption spectrum decreased slightly in each month, which could be due to the deposition of a small amount of GNRs. However, the majority of GNRs were still suspended in the buffer solution and no significant change in the absorption spectra was observed, such as the broadening of the spectrum or resonance peak shift of LPB, as found in Fig. 5.5. Even after 4 months storage, the absorption spectrum still remained its original shape without any deformation, indicating the MUA-modified GNRs developed in this work are of high stability, for up to 4 months at least. Compared to the stability of MUA-modified GNRs in the previously reported work as shown in Fig. 5.7 (b) [21], where the surface modification with MUA was carried out under constant sonication at elevated temperature, the spectrum of such surface modified GNRs not only became broader but also a slight red-shift of peak wavelength in LPB can be observed in Fig. 5.7 (b) after only 15 days of preparation, indicating the poor stability of the MUA-modified GNRs produced in their work.

In addition, the stability of the MUA-modified GNRs was also evaluated under various pH conditions. When the MUA-modified GNRs were suspended in a pH 3 solution, an immediate aggregation of the GNRs was observed. The absorption spectra of MUA-modified GNRs suspended in the pH 3 solution is shown in Fig. 5.8. As can be seen in Fig. 5.8, after only 2 min, the absorption spectrum of GNRs had already become broadening and the LPB almost disappeared. After half-hour, the spectrum had completely changed from its original shape and nearly all the GNRs had deposited at the bottom of the container. However, when the pH value of the same GNRs solution was adjusted to a higher value (pH >7), the MUA-modified GNRs were observed to start disaggregating and return to the suspension form eventually. This reversible aggregation phenomenon can be attributed to the simple acid-base character, as the solubility of the MUA-capped GNRs will change accordingly. The stability of the MUA-modified GNRs was also verified in a neutral pH environment, where the MUA-modified GNRs were suspended in DI water at pH 7, and again the aggregation occurred over time. The results shown in Fig. 5.9 confirm that GNRs start to aggregate gradually after a few hours and eventually deposit completely at the bottom after 24 h. A similar reversible aggregation phenomenon such as that was seen in the case of pH 3 was also observed, where the GNRs separated from each other and dispersed in the solution again after the pH value was readjusted to the high level (pH >7). This reversible

aggregation property could be useful for some particular applications. Stable performance of the MUA-modified GNRs had been observed when the pH level is equal or greater than pH 9. Therefore, in this work, the MUA-modified GNRs were stored in the borate buffer at pH 9 after the surface modification.

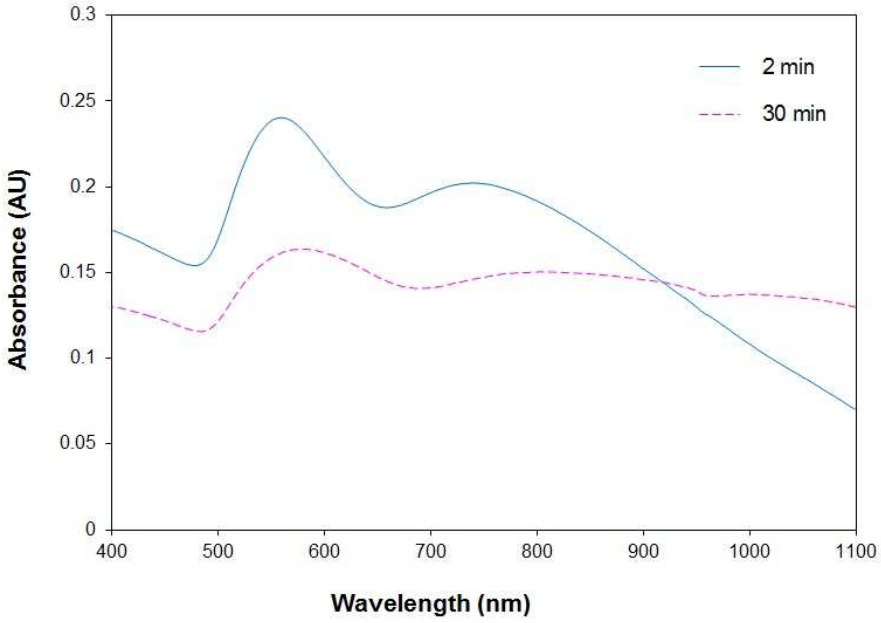

Fig. 5.8. Absorption spectra of the MUA modified GNRs in PBS buffer at pH 3.

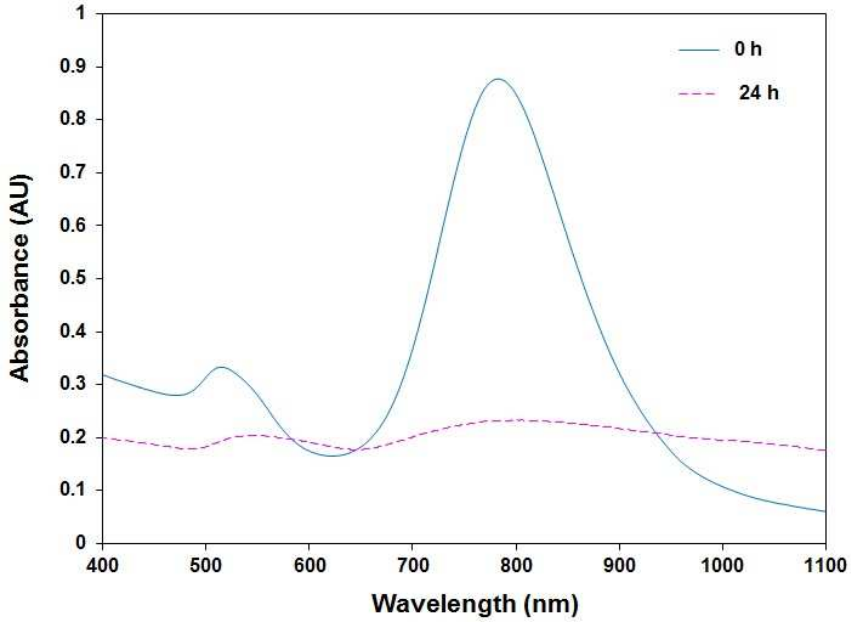

Fig. 5.9. Absorption spectra of the MUA-modified GNRs in DI water at pH 7.

A different and opposite phenomenon had also been observed for the CTAB-capped GNRs. The CTAB-capped GNRs had shown a good stability when they were suspended in water and slightly acidic solutions. However, when they were suspended in an alkaline solution with pH level greater than 7, an irreversible aggregation of GNRs occurred. This is due to the reason that the cationic molecules of CTAB on the GNRs surface are unstable in the high anionic density environment so that the GNRs lose the protection of the CTAB stabilizer, which can keep the GNRs away from each other by the repulsive force. This aggregation difference between the CTAB-capped and MUA-modified GNRs indirectly proves the success of the surface modification in this experiment carried out.

5.3 Development of solution-phase-based LSPR biosensor using the MUA-modified GNRs

5.3.1 Materials

Human IgG (purified immunoglobulin, reagent grade), anti-humanIgG (whole molecule, produced in goat), bovine serum albumin (BSA), N-(3-Dimethylaminopropyl)-N′-ethylcarbodiimide hydrochloride (EDC) and *N*-hydroxysulfosuccinimide (Sulfo-NHS) were purchased from Sigma Aldrich. Ultrapure de-ionized (DI) water (18 MΩ) was used to prepare all solutions.

5.3.2 Functionalization of MUA-modified GNRs to develop LSPR biosensor

After the surface modification, the MUA-modified GNRs were functionalized with the human IgG via the EDC/NHS protocol [26], in order to fabricate a solution-phase-based LSPR biosensor for detecting anti-human IgG. The detailed procedure is as follows: 20 µL of freshly prepared EDC (0.05 M) /Sulfo-NHS (0.1 M) solution was added to 1 mL of MUA-modified GNRs solution with aspect ratio 3.9 in a 1.5 mL micro centrifuge tube to activate the carboxyl group of the MUA. The mixture was then gently vortexed for 25 min, followed by the addition of 50 µL of 1 mg/mL human IgG into the same tube with gentle vortex. After 1 h of incubation, the human IgG-functionalized GNRs were purified by centrifugation at 8000 rpm for 20 min and washed twice using a washing buffer (1% BSA in 0.01 M borate buffer at pH 9). Here, the washing buffer also works as a blocking agent to block the sensing

surface of the functionalized GNRs in order to prevent the unspecific binding. Finally, the human IgG conjugated GNRs were resuspended and dispersed in the washing buffer and stored at 4 °C before use.

5.3.3 Detection of target molecule

Further to the above successful functionalization of the MUA-modified GNRs, a solution-phase-based LSPR biosensor platform had been established and was ready for further tests. In this work, anti-human IgG was employed as the target molecule to evaluate the biosensing performance of the LSPR biosensor created. This was conducted by adding a known amount of anti-human IgG into 1 mL of the as-prepared GNRs biosensor solution, followed by gently shaking the mixture for a few seconds. In order to observe the dependence of the sensor response on incubation time, the mixture was incubated for a period of 1 h and the absorption spectrum was collected every 5 min during the period of incubation, using the LAMBDA 35 UV/VIS spectrophotometer.

5.3.4 Results and discussions

5.3.4.1 Functionalization of MUA-modified GNRs

As the sensitivity of GNRs increases with the increase of their aspect ratios [25], in order to enhance the sensitivity of the biosensor probe, GNRs with a mean aspect ratio of 3.9 were chosen in this work to be further functionalized as a LSPR biosensor probe. The carboxyl groups of the MUA immobilized on the GNRs surface were first activated by EDC to form an intermediate, which was further coupled with the water soluble Sulfo-NHS, resulting in the formation of a stable amine-reactive Sulfo-NHS ester. The activated Sulfo-NHS ester crosslinker then reacted with the amine groups of the human IgG, yielding stable amide bonds, which enable the human IgG to be covalently immobilized on the GNRs surfaces. As shown in Fig. 5.10, after the MUA-modified GNRs were conjugated with human IgG, a clear 17 nm red shift of the resonance peak of LPB was observed in the absorption spectra. This red shift is caused by the refractive index change at the GNRs surface due to the binding of human IgG. On the other hand, the resonance peak of TPB almost still remained at 510 nm without any significant shift. After the successful binding of human IgG, the unoccupied

Sulfo-NHS esters were blocked by BSA in the washing buffer to avoid any nonspecific recognition, creating an immunosensor which is specific for anti-human IgG.

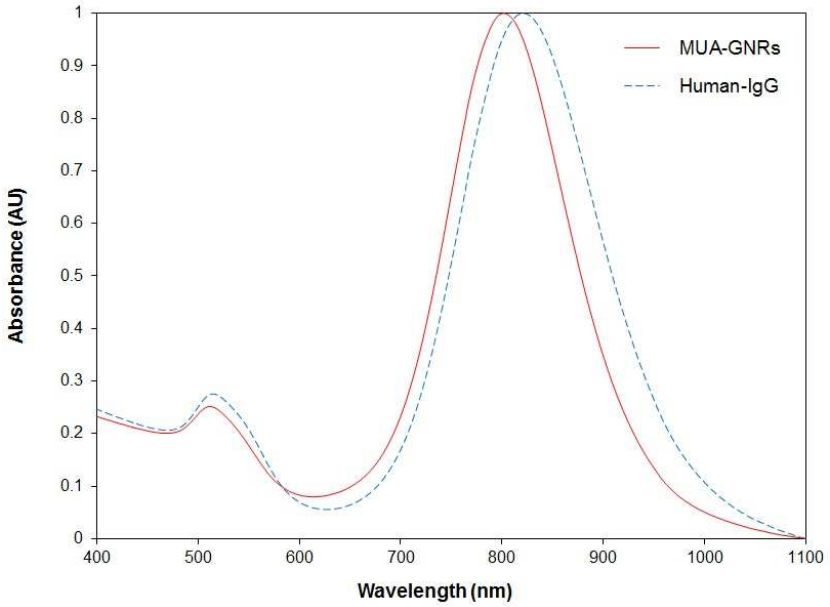

Fig. 5.10. Absorption spectra of MUA-modified GNRs before and after being functionalized with human IgG.

5.3.4.2 Evaluation of biosensing performance

The dependence of sensor response on incubation time was first evaluated by adding anti-human IgG with different concentrations into different sensor probe solutions, and the absorption spectra of the mixtures were kept under monitoring for 1 h incubation time. The resonance peak of LPB, due to its high sensitivity to the refractive index change, was employed as an indicator to observe the sensor response. Fig. 5.11 shows the resonance peak shift of LPB as a function of time for the binding of anti-human IgG with different concentrations. As demonstrated in Fig. 5.11, the majority of LPB peak wavelength shifts corresponding to the different concentrations of anti-human IgG almost all occurred in the first 10 min, indicating the biosensor created has a fast response to the target binding. Despite the binding of anti-human IgG was continuously taking place over 1 h incubation, no significant resonance peak shift of LPB had been observed after the first 10 min, indicating the antigen-antibody reaction nearly reached equilibrium, thus the anti-human IgG incubation time could be shortened to 10 min.

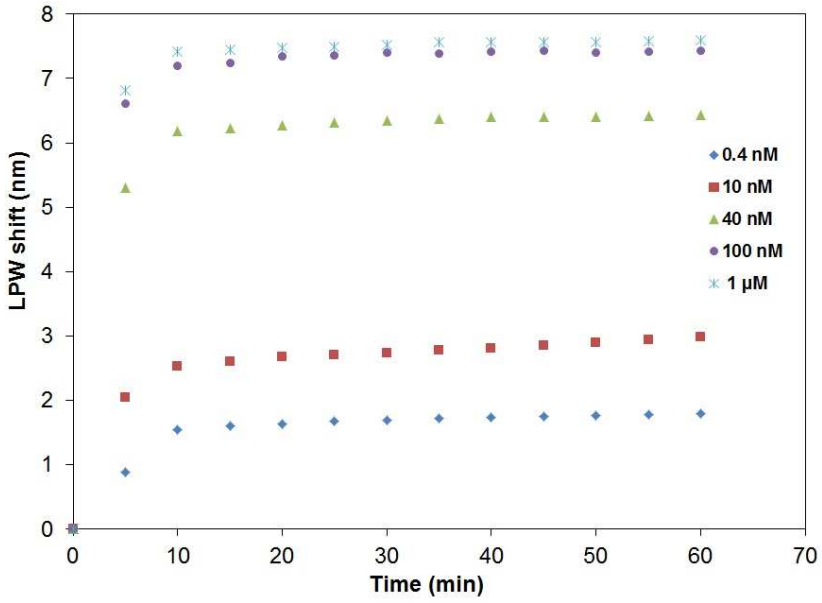

Fig. 5.11. Resonance peak shift of LPB vs. incubation time of anti-human IgG with different concentrations.

In order to determine the detection limit of the as-prepared LSPR biosensor and observe the sensor response to the different concentrations of anti-human IgG, one experiment had been conducted by gradually increasing the concentration of anti-human IgG in the same sensor probe solution. For each concentration, the mixture was incubated for 10 min and the corresponding spectra, as shown in Fig. 5.12, were collected accordingly. When the concentration of anti-human IgG is below 0.4 nM, no significant resonance peak shift of LPB was observed. However, when the concentration was adjusted to a value greater than 0.4 nM, a constant red-shift of LPB peak wavelength was observed in the absorption spectra as illustrated in Fig. 5.12, showing a typical LSPR sensor response to the surrounding refractive index change (due to the antigen-antibody recognition in this case). For the concentrations of anti-human IgG greater than 100 nM, no significant additional peak wavelength shift of LPB could be observed even when the concentration reached 1 µM, indicating the saturation of the biosensor for binding anti-human IgG. Therefore, the detection limit of the as-created LSPR biosensor for detecting anti-human IgG is determined as 0.4 nM, as no wavelength shift could be easily recognized when the concentration is below this value.

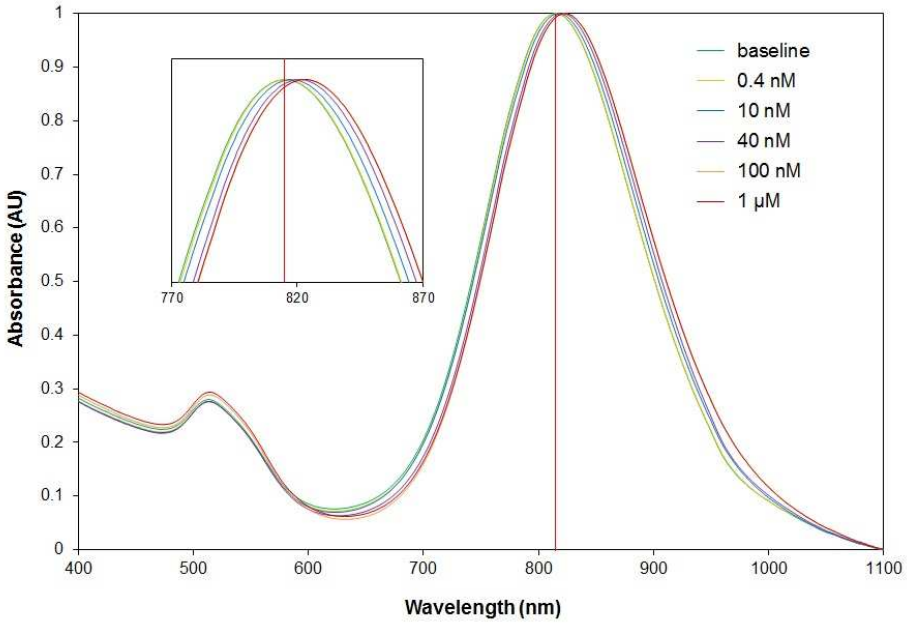

Fig. 5.12. LSPR sensor response to anti-human IgG with different concentrations.

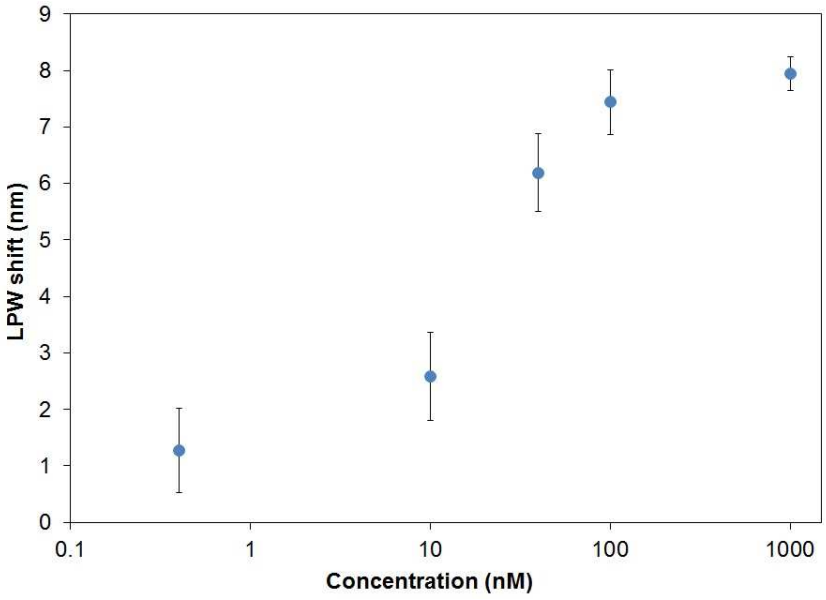

Fig. 5.13. Resonance peak shift of LPB vs. anti-human IgG concentration.

As shown in Fig. 5.13, the sensitivity of the LSPR biosensor fabricated was evaluated by measuring the resonance peak shift of LPB as a function of concentration of anti-human IgG. For each concentration, at least three independent measurements from different samples were undertaken, in order to calculate the averages and standard deviations. As demonstrated

in Fig. 5.13, the greater the concentration of anti-human IgG, the more LPB peak wavelength shift can be observed. The resonance peak of LPB didn't shift much until the concentration of anti-human IgG increased to 40 nM, indicating the effective binding of anti-human IgG happened at the concentration above 10 nM. However, when the concentration reached 1 μM, only about 0.5 nm additional shift was observed compared to the LPB peak wavelength shift obtained at 100 nM, which indicates the as-prepared LSPR biosensor nearly saturates at 100 nM.

The results shown above demonstrate that a label-free LSPR biosensor for detecting the interaction between an antigen and antibody has been successfully fabricated using the MUA-modified GNRs prepared by the pH-mediated method introduced in this work. The resonance peak shift of LPB caused by the antigen-antibody recognition only can be observed in the presence of anti-human IgG. No such wavelength shift was observed when the same experiment was carried out on the GNRs without being functionalized with human IgG. The detection limit of the as-prepared LSPR sensor probe for detecting anti-human IgG is as low as 0.4 nM, which is 25 times lower than that reported in a previously published similar work (10 nM), in which the surface modification of GNRs was carried out with the MUA ethanolic solution under protections [21], rather than with the MUA aqueous solution without any protection as we did in this work. The low detection limit obtained could be attributed to the efficient surface modification of GNRs by employing the pH-mediated method developed in this work. However, we noticed that the sensitivity of the sensor prepared in this work is not as high as that of previously published work [21], because the resonance peak of LPB did not shift as much as that reported at the same concentration of the targeting molecules. As the binding of biomolecules was taken place in a neutral pH environment in the previously reported work, considering the alkaline conditions (pH 9) applied in preparing the GNRs-based sensor probe solution in this experiment and the EDC cross-linking is more efficient in acidic environment (~ pH 5) [27, 28], the sensitivity of the sensor developed in this work could be improved by approaches such as increasing the concentration of the EDC, which may compensate for the reduced coupling efficiency. In addition, as the sensitivity of the GNRs increases with the increase of aspect ratio, the sensitivity of the LSPR biosensor could be further improved by employing GNRs with higher aspect ratio.

5.4 Summary

In this chapter, a simple, yet robust method to completely replace the CTAB surfactant from the surface of seed-mediated grown GNRs with MUA by controlling the pH has been demonstrated. This method allows the ligand exchange between the CTAB and the MUA to proceed in a total aqueous environment and no irreversible aggregation of GNRs was observed during the surface modification process or subsequently during further manipulation. Compared to the previously reported methods using MUA ethanolic solution, this new approach enables the operational process to be free from additional protections, such as sonication at elevated temperatures or using ionic exchange resin. The MUA-modified GNRs produced in this work are of high stability, shown here to be up to 4 months (at least) in a buffer solution at pH 9. The introduction of a carboxyl group of MUA at the GNRs surface allows ease of the further functionalization of GNRs to form a solution-phase-based label-free LSPR biosensor for the detection of biomolecular interaction. The detection limit of the LSPR biosensor created for detecting anti-human IgG was found as low as 0.4 nM. The promising results show the ability of the MUA-modified GNRs prepared in this work to be used as a label-free biosensor platform. The novel pH-mediated protocol of surface modification of GNRs proposed in this work is also generic and thus could be beneficial to other biochemical applications, such as cell imaging, drug delivery and disease therapy.

5.5 References

[1] S.S. Chang, C.W. Shih, C.D. Chen, W.C. Lai, C.R.C. Wang, The shape transition of gold nanorods, Langmuir : The ACS Journal Of Surfaces And Colloids, 15 (1999) 701-709.

[2] C.R. Martin, Nanomaterials: a membrane-based synthetic approach, Science, 266 (1994) 1961-1966.

[3] L. Billot, M.L. de la Chapelle, A.S. Grimault, A. Vial, D. Barchiesi, J.L. Bijeon, P.M. Adam, P. Royer, Surface enhanced Raman scattering on gold nanowire arrays: Evidence of strong multipolar surface plasmon resonance enhancement, Chemical Physics Letters, 422 (2006) 303-307.

[4] B. Nikoobakht, M.A. El-Sayed, Evidence for bilayer assembly of cationic surfactants on the surface of gold nanorods, Langmuir : The ACS Journal Of Surfaces And Colloids, 17 (2001) 6368-6374.

[5] C.J. Murphy, L.B. Thompson, D.J. Chernak, J.A. Yang, S.T. Sivapalan, S.P. Boulos, J. Huang, A.M. Alkilany, P.N. Sisco, Gold nanorod crystal growth: From seed-mediated synthesis to nanoscale sculpting, Current Opinion In Colloid & Interface Science, 16 (2011) 128-134.

[6] B.C. Rostro-Kohanloo, L.R. Bickford, C.M. Payne, E.S. Day, L.J.E. Anderson, M. Zhong, S. Lee, K.M. Mayer, T. Zal, L. Adam, C.P.N. Dinney, R.A. Drezek, J.L. West, J.H. Hafner, The stabilization and targeting of surfactant-synthesized gold nanorods, Nanotechnology, 20 (2009).

[7] A.P. Leonov, J. Zheng, J.D. Clogston, S.T. Stern, A.K. Patri, A. Wei, Detoxification of Gold Nanorods by Treatment with Polystyrenesulfonate, ACS Nano, 2 (2008) 2481-2488.

[8] E.E. Connor, J. Mwamuka, A. Gole, C.J. Murphy, M.D. Wyatt, Gold nanoparticles are taken up by human cells but do not cause acute cytotoxicity, Small, 1 (2005) 325-327.

[9] X. Huang, I.H. El-Sayed, W. Qian, M.A. El-Sayed, Cancer cell imaging and photothermal therapy in the near-infrared region by using gold nanorods, Journal Of The American Chemical Society, 128 (2006) 2115-2120.

[10] X. Huang, S. Neretina, M.A. El-Sayed, Gold Nanorods: From synthesis and properties to biological and biomedical applications, Advanced Materials, 21 (2009) 4880-4910.

[11] C.S. Ah, S. Do Hong, D.J. Jang, Preparation of AucoreAgshell nanorods and characterization of their surface plasmon resonances, Jounal Of Physical Chemistry B, 105 (2001) 7871-7873.

[12] M.Z. Liu, P. Guyot-Sionnest, Synthesis and optical characterization of Au/Ag core/shell nanorods, Jounal Of Physical Chemistry B, 108 (2004) 5882-5888.

[13] C. Wang, Z. Ma, T. Wang, Z. Su, Synthesis, assembly, and biofunctionalization of silica-coated gold nanorods for colorimetric biosensing, Advanced Functional Materials, 16 (2006) 1673-1678.

[14] I.E. Sendroiu, M.E. Warner, R.M. Corn, Fabrication of silica-coated gold nanorods functionalized with DNA for enhanced surface plasmon resonance imaging biosensing applications, Langmuir : The ACS Journal Of Surfaces And Colloids, 25 (2009) 11282-11284.

[15] A. Gole, C.J. Murphy, Biotin-streptavidin-induced aggregation of gold nanorods: Tuning rod-rod orientation Langmuir : The ACS Journal Of Surfaces And Colloids, 21 (2005) 10756-10762.

[16] A. Gole, C.J. Murphy, Polyelectrolyte-coated gold nanorods: synthesis, characterization and immobilization, Chemistry Of Materials, 17 (2005) 1325-1330.

[17] S. Pierrat, I. Zins, A. Breivogel, C. Sonnichsen, Self-assembly of small gold colloids with functionalized gold nanorods, Nano Letters, 7 (2007) 259-263.

[18] H.W. Liao, J.H. Hafner, Gold nanorod bioconjugates, Chemistry Of Materials, 17 (2005) 4636-4641.

[19] T. Niidome, Y. Akiyama, K. Shimoda, T. Kawano, T. Mori, Y. Katayama, Y. Niidome, In vivo monitoring of intravenously injected gold nanorods using near-infrared light, Small, 4 (2008) 1001-1007.

[20] T. Niidome, M. Yamagata, Y. Okamoto, Y. Akiyama, H. Takahashi, T. Kawano, Y. Katayama, Y. Niidome, PEG-modified gold nanorods with a stealth character for in vivo applications, Journal Of Controlled Release, 114 (2006) 343-347.

[21] C. Yu, L. Varghese, J. Irudayaraj, Surface modification of cetyltrimethylammonium bromide-capped gold nanorods to make molecular probes, Langmuir : The ACS Journal Of Surfaces And Colloids, 23 (2007) 9114-9119.

[22] B. Thierry, J. Ng, T. Krieg, H.J. Griesser, A robust procedure for the functionalization of gold nanorods and noble metal nanoparticles, Chemical Communications, (2009) 1724-1726.

[23] Q. Dai, J. Coutts, J. Zou, Q. Huo, Surface modification of gold nanorods through a place exchange reaction inside an ionic exchange resin, Chemical Communications, (2008) 2858-2860.

[24] P.K. Jain, S. Eustis, M.A. El-Sayed, Plasmon coupling in nanorod assemblies: optical absorption, discrete dipole approximation simulation, and exciton-coupling model, Journal Of Physical Chemistry B, 110 (2006) 18243-18253.

[25] H.J. Chen, X.S. Kou, Z. Yang, W.H. Ni, J.F. Wang, Shape- and size-dependent refractive index sensitivity of gold nanoparticles Langmuir : The ACS Journal Of Surfaces And Colloids, 24 (2008) 5233-5237.

[26] Z. Grabarek, J. Gergely, Zero-length crosslinking procedure with the use of active esters, Analytical Biochemistry, 185 (1990) 131-135.

[27] M.J.B. Wissink, R. Beernink, J.S. Pieper, A.A. Poot, G.H.M. Engbers, T. Beugeling, W.G. van Aken, J. Feijen, Immobilization of heparin to EDC/NHS-crosslinked collagen. Characterization and in vitro evaluation, Biomaterials, 22 (2001) 151-163.

[28] A. Tiraferri, C.D. Vecitis, M. Elimelech, Covalent binding of single-walled carbon nanotubes to polyamide membranes for antimicrobial surface properties, ACS Applied Materials & Interfaces, 3 (2011) 2869-2877.

Chapter 6

Conclusions and future work

6.1 Conclusions of the work carried out

The work carried out in this thesis mainly aimed to develop a novel, sensitive GNR-based LSPR optical fibre sensor for the label-free biosensing applications, and to develop a simple, robust method for effectively modifying the surface of CTAB-capped GNRs which can be applied as a generic platform for label-free LSPR biosensing as well as other biomedical applications. Based on the results obtained from this research and the achievements attained, the conclusions of the work carried out in this thesis are drawn below:

- A brief yet comprehensive review on the subjects of SPR and LSPR sensors was given in Chapter 2, based on a large number of related references. The background, sensing principle, sensor system, fabrication techniques, applications, as well as other aspects with regard to the SPR and LSPR sensors were systematically introduced in this review along with appropriate comparisons and discussions, which formed the basis of this work and provided sufficient information for supporting the work to be carried out.

- Based on the review of previously reported work regarding the LSPR sensors, it was found that optical fibre based LSPR sensors showed many advantages, such as small sample volume requirement, a miniaturized and simplified optical design, immunity to electromagnetic interference and capability for remote sensing, over the LSPR sensors based on other configurations. However, the majority of the previously reported LSPR optical fibre sensors were based on the conventional spherical GNPs. No research had been reported on the LSPR optical fibre sensor using the rod-shaped GNPs — GNRs, which had shown unique and intriguing optical properties and had

been found to possess refractive index sensitivity higher than that of spherical GNPs in the studies of LSPR sensors based on other configurations. Therefore, the exploration of developing a GNR-based LSPR optical fibre sensor was carried out as demonstrated in Chapter 3.

- In order to fabricate the GNR-based LSPR optical fibre sensor, GNRs with various aspect ratios were first synthesized using a seed-meditated growth method due to the ease of preparation and a high yield of GNRs compared to other GNRs synthesis approaches. Factors that may affect the quality of the GNRs during the synthesis process, such as ageing time and temperature, were discussed in detail based on the phenomena observed in numerous experiments carried out to synthesize GNRs in this work. According to these findings, the optimum conditions for synthesizing GNRs were determined, resulting in a yield of GNRs as high as ~ 90%. Two plasmon resonance bands — TPB and LPB, corresponding to electron oscillations along the short and long axes of the rod, respectively, were observed in the absorption spectra of the as-synthesized GNRs solutions. To fabricate the LSPR sensor probes, GNRs with different aspect ratios were covalently immobilized onto the MPTMS-modified, decladded surfaces of several pieces of multimode optical fibres, respectively, using a dip-coating method. In order to enable the sensor probe to be operated as a reflective sensor, a silver mirror was chemically attached to one distal end of the optical fibre through a silver reaction technique. Thus, the GNR-based LSPR optical fibre sensors were successfully created.

- The LSPR sensor system, including several sensor probes, a white light source, a mini-spectrometer, a 2x1 fibre coupler and a computer, was set up for the evaluation of the performances of the GNR-based LSPR optical fibre sensors prepared in this work. By immersing the sensor probes into the testing solutions with different refractive indexes ranging from 1.34 to 1.41, the LPB of each sensor was found to be much more sensitive to the surrounding refractive index change than the TPB. By monitoring the resonance peak shift of the LPB with refractive index change, it was found that the LSPR optical fibre sensors based on GNRs with aspect ratios of 2.6, 3.1, 3.7 and 4.3 had refractive index sensitivities of 269, 401, 506 and 766 nm/RIU, respectively, indicating that the sensitivity of the GNR-based LSPR optical fibre sensor increases with the increase of the aspect ratio of GNRs, which is in a good agreement with the previously reported results obtained from the GNR-based LSPR sensors with other configurations. In addition to the high stability, the GNR-based

LSPR optical fibre sensors also demonstrated higher refractive index sensitivities with better linearity in comparison with those of LSPR optical fibre sensors based on spherical GNPs. The promising results indicate that the GNR-based LSPR optical fibre sensors prepared in this work could offer improved performance for the applications in which the conventional spherical GNP-based LSPR optical fibre sensors have been employed.

- The development and evaluation of the GNR-based LSPR optical fibre biosensors for label-free biosensing were carried out and reported in Chapter 4. In order to enhance the sensor performance, a LSPR optical fibre sensor probe with a 2 cm sensing length, immobilized with GNRs with mean aspect ratios of 4.1, was chosen to be fabricated and it showed a refractive index sensitivity as high as 601 nm/RIU. The GNRs immobilized on sensor probe were further functionalized with human IgG via the EDC/NHS coupling approach to develop a LSPR biosensor for detecting the specific target — anti-human IgG. A wavelength-based interrogation method was employed for the evaluation of the biosensing performance of the as-prepared LSPR biosensor, and a detection limit of 1.6 nM for detecting anti-human IgG was achieved. Compared to the previously reported LSPR optical fibre biosensors which are based on the absorbance or intensity measurement due to their poor wavelength sensitivity to micro-refractive index change, the GNR-based LSPR optical fibre biosensors prepared here are of high wavelength sensitivities to both bulk and micro-refractive index changes. The results obtained from this work show that the GNR-based LSPR optical fibre sensors created have the ability to work as a sensitive label-free biosensing platform, which offers better sensing performance for a wide range of biosensing applications compared to the GNP-based sensing platform.

- A novel, simple yet robust pH-mediated method for effectively modifying the surface of CTAB-capped GNRs with MUA was reported in Chapter 5. This method involves the dissolution of the hydrophobic MUA molecules in aqueous solution by controlling the pH of the solution, which allows the ligand exchange between the CTAB molecules attached on the GNRs surface and the MUA molecules dissolved in aqueous solution to take place in a total aqueous environment. No irreversible aggregation of GNRs was observed during the process of surface modification, and the success of the complete replacement of CTAB with MUA was confirmed by the surface elemental analysis using XPS. Such MUA-modified GNRs produced in this work also showed a high stability up to 4 months at least when stored in a buffer

solution at pH 9 at 4°C. Compared to the previously reported surface modification approaches using the MUA ethanolic solution, the pH-mediated method proposed in this work overcomes the limitations of the previous methods for the need of additional protections, such as sonication at elevated temperatures or using ionic exchange resin, in order to prevent the aggregation of GNRs during the process of surface modification, thus simplifying the experimental procedure.

- The MUA-modified GNRs with a mean aspect ratio of 3.9 were further functionalized with human IgG to develop a solution-phase-based LSPR biosensor. The detection limit of the LSPR biosensor for detecting anti-human IgG was found to be as low as 0.4 nM. The results show that the MUA-modified GNRs created in this work have the ability to be used as a generic label-free biosensor platform, and the novel pH-mediated protocol proposed in this work could be also beneficial to other biochemical applications, such as cell imaging, drug delivery and disease therapy.

6.2 Future work

Based on the results obtained from the work reported in this thesis and the trend in the field of LSPR sensing, the future work could be carried out towards following directions:

- Despite the high refractive index sensitivities have been achieved in this work for the GNR-based optical fibre sensors created, further improvement in sensitivity is still possible. As demonstrated in Chapter 3, the refractive index sensitivity of GNR-based LSPR sensor was found to increase with the increase of aspect ratio. Thus, it is possible to further improve the sensitivity by employing GNRs with greater aspect ratios. However, this is not an ultimate solution. As the LPB of GNRs red shifts with the increase of aspect ratio, for GNRs with large aspect ratios, their LPBs may locate at a wavelength beyond the detectable range of the spectrometer, making the detection impossible to be carried out. Therefore, the detectable range of the spectrometer should be taken into consideration when choosing the size of GNRs. Other means include the use of tapered optical fibre and gold-silver alloyed nanoparticles. The tapered optical fibre based sensors have demonstrated higher sensitivities than those of optical fibre sensors with uniform geometry when using the evanescent field to directly interact with the analyte [1-3]. Therefore, by

replacing the conventional multimode fibre applied in this work with the tapered optical fibre, the refractive index sensitivity is expected to be further improved. In addition, silver has shown higher sensitivity to refractive index change than gold [4]. However, one major disadvantage of silver is that silver can be easily oxidized when exposed in air. The introduction of a gold layer to the surface of sliver nanoparticle forms a gold/silver, shell/core alloyed nanoparticle, which can overcome the drawback of using silver alone. By this way, the silver core can enhance the refractive index sensitivity, and the gold shell can offer not only high stability but also easy modification with cross-linker for the conjugation of biomolecules.

- As the LPB of GNRs has a red-shift with increase of aspect ratio, when GNRs with different aspect ratios are integrated, a multiplexed sensing system can be realised. Such an example has also been demonstrated by a solution-phase based LSPR biosensor for detecting multiple target biomolecules [5]. However, no similar work has been reported on the optical fibre based LSPR sensor yet. Therefore, to fully take the advantages of GNRs, the development of a multiplexed optical fibre based LSPR sensor system/network could be carried out in the future.

- Although LSPR sensing technique has been applied in the development of a label-free biosensor for detecting the specific target molecules, LSPR technique itself is non-specific sensing technique. This is because that the LSPR response is only dependent on the refractive index surrounding the nanoparticles, and the specificity is only achieved through the molecular recognition such as antigen-antibody recognition [6, 7]. Therefore, LSPR is not very suitable for the identification of unknown molecules. The combination of LSPR technique with other identification techniques such as SERS allows the unknown molecules to be first characterized with LSPR and then identified with the identification technique [7] and this will greatly expand the range of applications of LSPR technique and will become a trend in LSPR sensing in the future.

6.3 References

[1] A.G. Mignani, R. Falciai, L. Ciaccheri, Evanescent wave absorption spectroscopy by means of bi-tapered multimode optical fibers, Applied Spectroscopy, 52 (1998) 546-551.

[2] J. Villatoro, D. Luna-Moreno, D. Monzon-Hernandez, Optical fiber hydrogen sensor for concentrations below the lower explosive limit, Sensors And Actuators B-Chemical, 110 (2005) 23-27.

[3] N. Diaz-Herrera, M.C. Navarrete, O. Esteban, A. Gonzalez-Cano, A fibre-optic temperature sensor based on the deposition of a thermochromic material on an adiabatic taper, Measurement Science And Technology, 15 (2004) 353-358.

[4] J. Homola, S.S. Yee, G. Gauglitz, Surface plasmon resonance sensors: review, Sensors And Actuators B-Chemical, 54 (1999) 3-15.

[5] C. Yu, J. Irudayaraj, Multiplex biosensor using gold nanorods, Analytical Chemistry, 79 (2007) 572-579.

[6] J.N. Anker, W.P. Hall, O. Lyandres, N.C. Shah, J. Zhao, R.P. Van Duyne, Biosensing with plasmonic nanosensors, Nature Materials, 7 (2008) 442-453.

[7] B. Sepulveda, P.C. Angelome, L.M. Lechuga, L.M. Liz-Marzan, LSPR-based nanobiosensors, Nano Today, 4 (2009) 244-251.

List of publications by the author

Journals:

1. **J. Cao**, E.K. Galbraith, T. Sun, K.T.V. Grattan, Cross-Comparison of Surface Plasmon Resonance-Based Optical Fiber Sensors With Different Coating Structures, IEEE Sens. J., 12 (2012) 2355-2361.

2. **J. Cao**, E.K. Galbraith, T. Sun, K.T.V. Grattan, Effective surface modification of gold nanorods for localized surface plasmon resonance-based biosensors, Sensors and Actuators B-Chemical, 169 (2012) 360-367.

3. **J. Cao**, M.H. Tu, T. Sun, K.T.V. Grattan, Wavelength-based localized surface plasmon resonance optical fiber biosensor, Sensors and Actuators B: Chemical, 181 (2013) 611-619.

Conferences:

1. **J. Cao**, E.K. Galbraith, T. Sun, K.T.V. Grattan, Comparison of Surface Plasmon Resonance and Localized Surface Plasmon Resonance-based optical fibre sensors, Sensors & Their Applications Xvi, 12-14 September, 2011, Cork, Ireland, Journal of Physics Conference Series, Volume 304, Article Number 012050.

2. **J. Cao**, E.K. Galbraith, T. Sun, K.T.V. Grattan, Development and sensitivity studies of a gold nanorod platform for a localized surface plasmon resonance based optical fibre biosensor, 21st International Conference on Optical Fiber Sensors, 15-19 May, 2011, Ottawa, Canada, Proceeding of SPIE, Volume 7753, Article Number 775311.

3. **J. Cao**, T. Sun, K.T.V. Grattan, Development of gold nanorod-based localized surface plasmon resonance optical fiber biosensor, Presented at 22nd International Conference on Optical Fiber Sensors, 15-19 October, 2012, Beijing, P. R. China, Proceedings of SPIE, Volume 8421, Article Number 84211X.